USDRIVE

DRIVING RESEARCH AND INNOVATION FOR VEHICLE EFFICIENCY AND ENERGY SUSTAINABILITY

U.S. DRIVE Highlights of Technical Accomplishments

2021

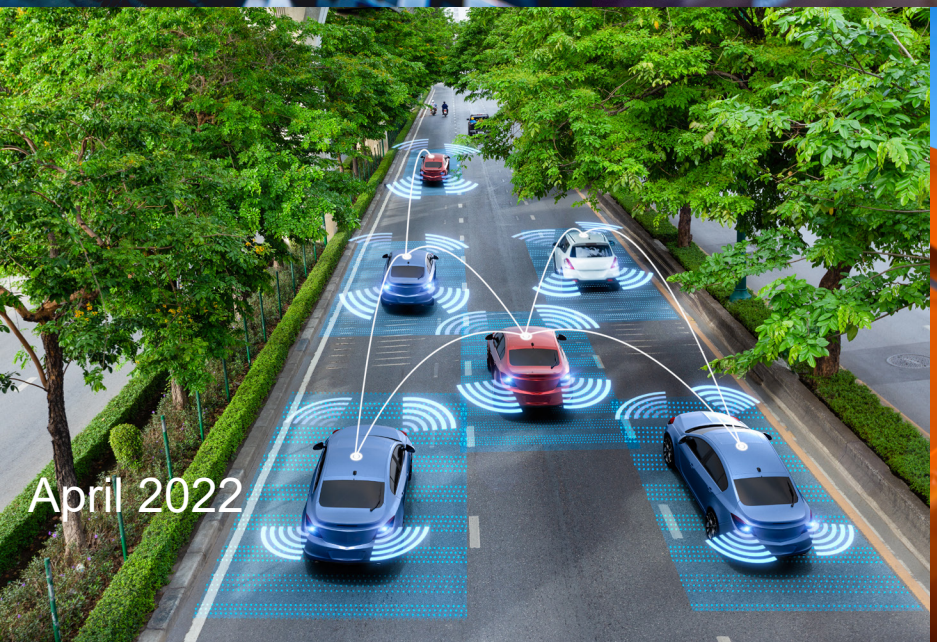

April 2022

U.S. DRIVE
Highlights of Technical Accomplishments Overview

Through precompetitive collaboration and technical exchange, U.S. DRIVE accelerates the development of energy-efficient advanced automotive and energy infrastructure technologies.

U.S. DRIVE (*Driving Research for Vehicle efficiency and Energy sustainability*) is a voluntary government-industry partnership focused on precompetitive, advanced automotive and related infrastructure technology research and development. Partners are the United States Department of Energy (DOE) and leaders in the automotive industry (United States Council for Automotive Research LLC, the collaborative technology company of Ford Motor Company, General Motors, and Stellantis); energy industry (BP, Chevron, Phillips 66, ExxonMobil, and Shell); and electric utility industry (American Electric Power, DTE Energy, Duke Energy, Southern California Edison, and the Electric Power Research Institute).

The Partnership benefits from a history of successful collaboration across multiple technical areas, each focused on a key area of the U.S. DRIVE portfolio (see below). These teams convene the best and brightest scientists and engineers from across the Partnership to discuss key technical challenges, identify possible solutions, and evaluate progress toward goals and targets published in technology roadmaps. By providing a framework for frequent and regular interaction among technical experts in common areas of expertise, U.S. DRIVE accelerates technical progress, helps to avoid duplication of efforts, ensures that publicly-funded research delivers high-value results, and overcomes high-risk barriers to technology commercialization.

U.S. DRIVE teams selected the highlights in this document from many hundreds of DOE-funded projects conducted by some of the nation's top research organizations. Each one-page summary represents what Partnership experts collectively consider to be significant progress in the development of advanced automotive and infrastructure technologies. The report features technical highlights in two general categories:

Vehicles

- Advanced Combustion and Emission Control
- Electrical and Electronics
- Electrochemical Energy Storage
- Fuel Cells
- Materials
- Vehicle and Mobility Systems Analysis

Infrastructure and Integration

- Grid Integration
- Hydrogen Codes and Standards
- Hydrogen Delivery and Storage
- Hydrogen Production
- Integrated Systems Analysis
- Net-Zero Carbon Fuels

More information about U.S. DRIVE, including prior-year accomplishments reports and technology roadmaps, is available on the DOE (https://www.energy.gov/eere/vehicles/us-drive) and USCAR (www.uscar.org) web sites.

Contents

VEHICLES

Advanced Combustion and Emission Control

2021 U.S. DRIVE Highlight

Active Machine Learning Software Tool Speeds up Engine Design Optimization by an Order of Magnitude

Novel optimization algorithm combining ensemble machine learning-based surrogate models and adaptive sampling significantly shrink industrial design cycles for advanced engines.

Argonne National Laboratory

The traditional approach to industrial design optimization of automotive engines involves a lot of experimental testing, prototype evaluation, and undergoing multiple design iterations. In this context, virtual design optimization, coupling engine simulations and optimization algorithms, has played a prominent role in narrowing down from large design spaces to the most promising designs. Nevertheless, the design of experiments and evolutionary optimization techniques typically used by the industry suffer from the issues of low accuracy, lack of robustness, and slow convergence. This results in long time-to-design (of the order of months) and high cost. More recently, machine learning (ML)-based surrogate models have been employed to speed up optimization. However, the size of initial datasets needed for generating accurate ML surrogate models is usually not known *a priori*.

Researchers at Argonne National Laboratory developed a novel active ML-based optimization technique, known as ActivO, to circumvent these major limitations. ActivO successively builds and updates the ML models in a dynamic "on-the-fly" manner by running sequential batches of only a small number of simulations (~5-10), which obviates the need for heavy computational resources, such as supercomputers. ML guides the optimization by indicating which design points to simulate in the next iteration, and the new simulations are used to re-train the ML surrogate models. ActivO combines two disparate ML models known as "weak" and "strong" learners (Figure 1). The weak learner "explores" the design space to look for promising regions that are likely to exhibit high objective values, while the strong learner seeks to "exploit" those promising regions by performing a more local search. While the weak learner prevents premature convergence to a suboptimal design, strong learner helps the optimization scheme to converge rapidly once in the neighborhood of the global optimum.

Argonne researchers recently applied ActivO to computational fluid dynamics (CFD)-driven engine design, demonstrating 7-10x speedup compared to traditional methods and 2x computational savings relative to state-of-the-art ML approaches. The ActivO software (patent pending), developed under a DOE Technology Commercialization Fund project, is a generic tool that can be leveraged for a wide variety of industrial design optimization tasks relevant to internal combustion engines (ICEs), aftertreatment systems, vehicle aerodynamics, etc.

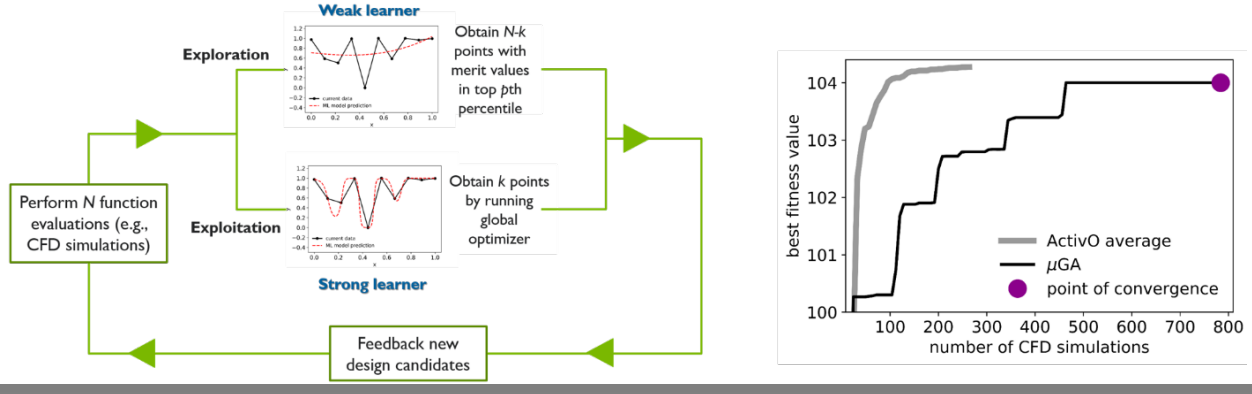

Figure 1. A schematic of ActivO workflow (left) and comparison between ActivO and GA for an ICE design optimization case (right).

2021 U.S. DRIVE Highlight

New Computational Models Predict Spray Development and Film Formation in Gasoline Direct Injection Engines

New simulation best practices and a novel spray-wall interaction model lay out a clear path towards accurate predictions of free-spray behavior, wall impingement, and fuel film evolution.

Argonne and Sandia National Laboratories within PACE Consortium

Accurate knowledge of fuel sprays, mixture formation, and spray-wall interaction (SWI) is of utmost relevance to enable targeted injection strategies in gasoline direct injection (GDI) internal combustion engines (ICE). This can in turn unlock high efficiency of conventional and dilute engine combustion, as well as minimize unburnt hydrocarbons and particulate matter tailpipe emissions, especially during cold-start operation. These are goals that warrant a need for predictive and accurate free-spray and SWI computational fluid dynamics (CFD) models that do not rely on extensive calibration and are valid across wide ranges of ICE operations.

A synergistic effort of experiments and CFD led to improved predictions of free-spray behavior and fuel film formation, a steppingstone toward accurate assessments of combustion behavior and emissions, and more effective ICE design optimization. X-ray measurements at Argonne provided quantitative, spatio-temporally resolved distributions of projected fuel mass for a multi-hole GDI injector. Sandia's imaging of a GDI spark-ignition optical ICE showed evidence of spray plume merging during both the intake and compression strokes, as a result of thermodynamics- and aerodynamics-induced spray collapse, respectively.

By means of new best practices, Argonne's large-eddy simulations of early intake injections successfully captured transitional spray morphology changes in response to injected fuel temperature and engine speed variations. Furthermore, researchers successfully validated a new SWI model developed at Argonne in simulations of late injection strategies using optical and X-ray data of free-spray and wall-film evolution (Figure 1). CFD simulations successfully integrated every spray model developed within the Partnership to Advance Combustion Engines (PACE) consortium, and seamlessly coupled them with those available in the default CFD solver. All the best practices have been shared within PACE and the new SWI model is now available as a "plug-and-play", user-defined function. Researchers at Sandia and Oak Ridge National Laboratories have successfully used the new model, showing further validation against experiments. The best practices and spray models developed in PACE can be employed for a variety of speed-load conditions and will positively impact the predictivity of engine simulations under various regimes and cold-start operations.

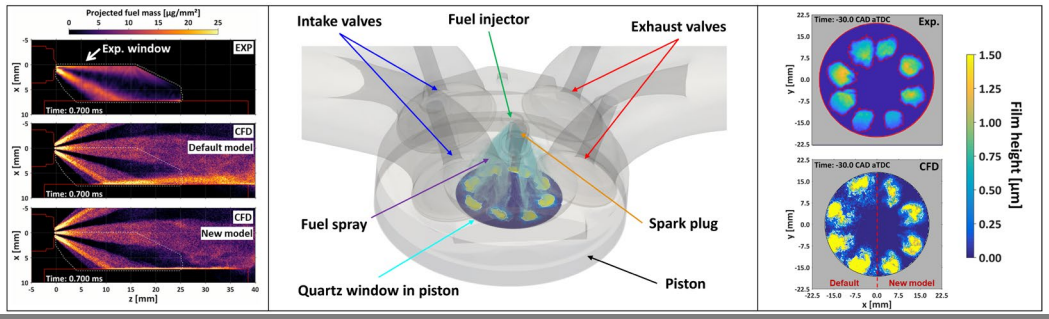

Figure 1. Left: validation of predicted projected fuel mass during SWI. X-ray experiments (top), default spray-wall interaction model (middle), and new spray-wall interaction model developed at Argonne (bottom). Middle: schematic of the Sandia optical engine model. Right: validation of the fuel film footprint on the window of Sandia's optical engine for a late-injection case.

2021 U.S. DRIVE Highlight

Novel Computational Model Successfully Captures Observed Low-Temperature Plasma Ignition Processes

Developed computational methodology provides OEMs with the ability to accurately model non-equilibrium ignition processes of different fuels at engine relevant conditions.

Argonne and Sandia National Laboratories within PACE Consortium

Relative to conventional spark ignition systems, low-temperature plasma (LTP) ignition offers the potential for faster burn rates, lower sensitivity to dilution, and reduced electrode wear through a combination of more distributed ignition volumes and lower energy streamers. These features have led to demonstrated extension of part-load dilution tolerance limits and increased resistance to high-load knock. However, a central challenge has been the development of computational fluid dynamics (CFD) modeling approaches that enable rapid optimization of electrical discharge characteristics and electrode configurations due to the complexity of involved plasma physics.

Argonne National Laboratory researchers developed a novel energy deposition CFD approach that lumped the chemical and thermal characteristics of the plasma streamer discharge into an equivalent source term for the energy equation. The development of this new CFD model was guided by canonical ignition experiments performed at Sandia National Laboratories and by previous high-fidelity non-equilibrium plasma simulations performed at Argonne National Laboratory using the commercial plasma solver Vizglow. The new energy deposition model was implemented into the commercial solver CONVERGE CFD through a dedicated User Defined Function. High-fidelity large eddy simulations (LES) employing such a novel approach successfully captured the impact of discharge strategies (single- or multi-pulse) on the LTP ignition process for different fuels across a range of operating conditions. Experiments and simulations were compared for a 3 mm gap and density values that are consistent with in-cylinder densities at part-load engine operation. Simulations accurately described the impact of the pulsing strategy (i.e., single- or multi-pulse, with 0.7 mJ delivered per pulse) on the ignition of ethylene (C_2H_4) and methane (CH_4). As can be seen in Figure 1 (top), simulations predicted the single-pulse ignition of an ethylene/air mixture. Simulations also predicted that the same single pulse would not ignite a methane/air mixture at the same conditions (Figure 1, bottom). For methane, a second pulse was needed to ignite the mixture, which matched the experimental observations (Figure 1, bottom). This is a first-of-its-kind capability for modeling LTP ignition processes using engine CFD codes.

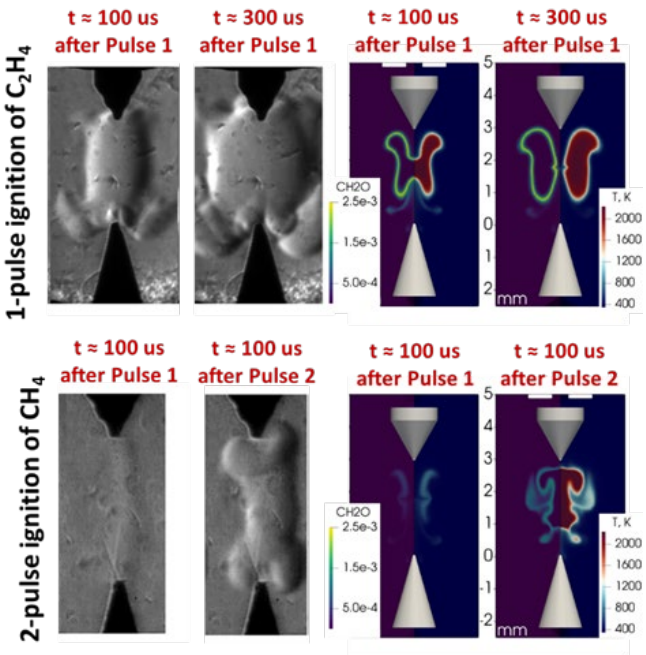

Figure 1. Simulations (right) capturing experiments (left) for different pulsing strategies and fuels (top: C_2H_4; bottom: CH_4).

2021 U.S. DRIVE Highlight

Diesel Kinetic Mechanism for Practical Engine Simulations

Researchers developed computationally efficient diesel mechanism for computational fluid dynamic simulations to predict fuel effects and emissions.

Lawrence Livermore, Oak Ridge, Sandia, and Argonne National Laboratories

Simulations have become an integral part of the engine design cycle and a key component of this framework are the chemical kinetic models used. Computational fluid dynamics (CFD) simulations of diesel engines require reduced kinetic mechanisms to simulate the effect of fuel properties on engine performance and criteria emissions in a tractable manner. A 343-species and 1,941-reactions reduced mechanism has been developed for use in CFD.

The reduced mechanism is suitable for multi-component diesel surrogate fuels that utilize a palette of C10-C20 components, including trans-decalin, a-methylnaphthalene, n-dodecane, n-cetane, iso-cetane, n-octadecane, and n-eicosane. The diesel chemistry is built hierarchically, and in a modular fashion on a gasoline ETPRF surrogate mechanism (ethanol, toluene, iso-octane and n-heptane). Reduced mechanisms for the neat components were developed separately and then merged into a single mechanism. This approach ensures different surrogate fuel compositions can be modeled with a single mechanism and allows components to be added or removed as needed.

The mechanism includes oxides of nitrogen (NO_X) and polyaromatic hydrocarbon chemistry (up to 4-rings) to simulate emissions.

The reduced mechanism was validated against ignition data of a 4-component diesel surrogate fuel from the Sandia National Laboratories' constant-volume spray chamber as shown in the first column of Figure 1 Right. The second column of Figure 1 Right shows comparisons with engine data for two different diesel fuels taken at Argonne and Oak Ridge National Laboratories. The ignition delay times (IDT) spray and engine simulations were found to be within 10% and 0.2 crank angle degrees (CAD) of the experimental measurements, respectively. UHC, NO_X, and CO emissions from the engine simulations were within a factor of two of measured values. A larger difference, up to a factor of 10, was observed for soot mass. The simulated soot mass was found to be sensitive to the soot model used. Future work will focus on developing improved soot models. The mechanism is available upon request and should be published shortly.

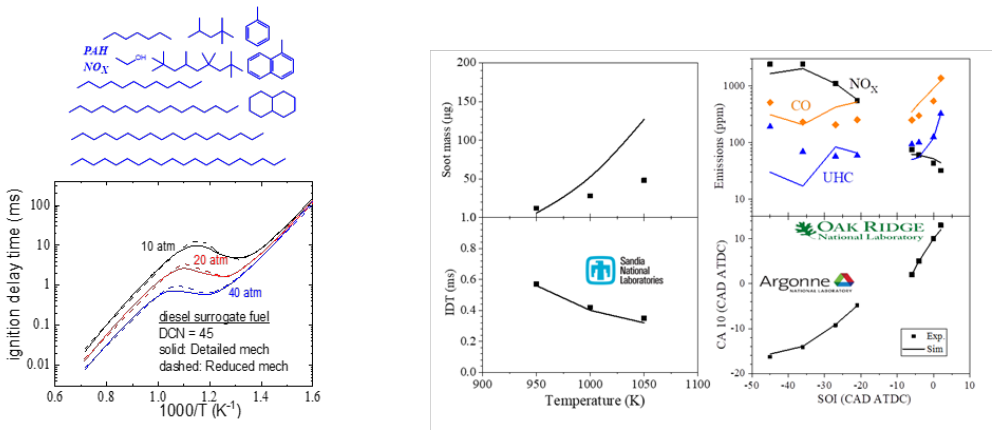

Figure 1. Left. Sub-mechanisms in the reduced mechanism and comparison of ignition delays predicted by the reduced and detailed mechanism. Right. The reduced mechanism reasonably captures the ignition delay and emissions during combustion of diesel fuels in constant-volume spray chambers and engines.

2021 U.S. DRIVE Highlight

Co-Optima Model Utilized to Predict Blending RON and Understand Mechanism of Synergistic Blending

Model accurately predicts RON and provides information about the impact of the structural composition (functional group) on the synergistic blending effects of blendstocks in gasoline.

National Renewable Energy Laboratory and Lawrence Livermore National Laboratory within Co-Optima Initiative

Research octane number (RON) is an important fuel property that is used to measure the resistance to autoignition in spark-ignition engines. Many blendstocks are known to blend synergistically for RON which means that they do not blend according to a linear blending model and produce higher RON values than are predicted according to linear models. Understanding the kinetics that dictate non-linear, synergistic blending can help original equipment manufacturers (OEMs) to predict fuel blend performance more accurately in simulations.

Researchers blended five synergistic blending components (ethanol, 2,5-dimethylfuran [DMF], 2-methylfuran [2MF], prenol, and 2-methyl-2-butene [2M2B]) into a four-component surrogate gasoline mixture (n-heptane, isooctane, 1-hexene, and toluene) and measured and predicted their RON using the Co-Optima mechanism. Figure 1 shows the octane number increase (ON_{int}), (calculated as the measured RON minus the RON predicted from a linear blending model) versus the mole percent blendstock results for RON measurements. DMF demonstrates superior RON increase when compared to the other blendstocks investigated.

RON predictions were in excellent agreement with measured values for DMF (Figure 2) and ethanol (within 2 RON units, not shown), with less satisfying results for 2MF and 2M2B (as much as 6 and 12 RON units off respectively). Predictions for prenol did not capture the synergistic blending behavior observed experimentally, reflecting the fact that the kinetic model for prenol does not include sufficiently accurate low-temperature chemistry and updates to the model are warranted. The team employed kinetic simulations to reveal the mechanism of synergistic blending by identifying the top reactions consuming the blendstock. The kinetics were then interrogated to understand the reactions responsible for the synergistic blending behavior. Reactions that scavenge hydroxyl (OH) radicals in the low temperature autoignition region were identified as

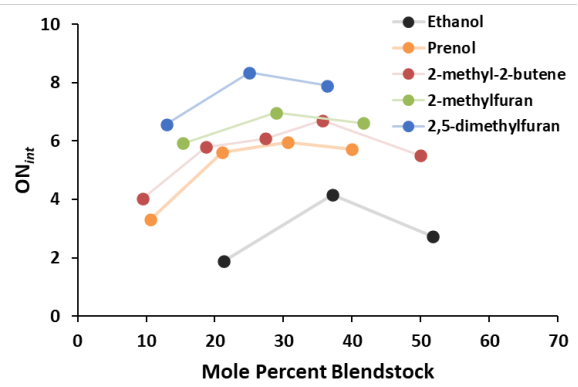

Figure 1. Octane Number increase (ONint) vs. mole percent blendstock in four-component gasoline surrogate. From Fioroni et al. https://doi.org/10.1016/j.fuel.2021.121865.

responsible for synergistic blending. It was also noted that those reactions scavenging radicals by OH addition to form resonance stabilized products were most effective. Additionally, researchers found that DMF can undergo a rapid ring-opening reaction (Figure 2) that drives the reaction equilibrium towards less reactive products and reduces the concentration of the OH radical pool, thus providing a higher octane increase.

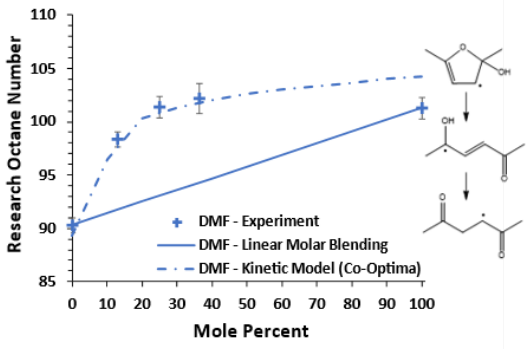

Figure 2. Predicted vs. measured RON blending results for DMF and ring-opening reaction for DMF via OH radical addition. From Fioroni et al. https://doi.org/10.1016/j.fuel.2021.121865.

2021 U.S. DRIVE Highlight

Novel Pt-Only Three-Way Catalyst Developed with Lower Light-Off Temperatures than Pd-Based Catalysts

A TWC based on a novel alumina nano-sheet with islands of dispersed ceria to anchor Pt shows excellent reactivity and durability compared to Pd-based catalysts.

Oak Ridge National Laboratory, University at Buffalo

Due to the recent rapid increases in palladium (Pd) and rhodium (Rh) prices, new three-way catalyst (TWC) formulations are needed to achieve cost effective emissions compliance for stoichiometric spark ignition (SI) engines. Additionally, these formulations should operate at temperatures as low as possible to address cold start emissions challenges associated with increasingly stringent emissions regulations and hybrid powertrains that can generate multiple cold start/re-start events during normal driving. Oak Ridge National Laboratory (ORNL) is developing catalyst supports that enhance the activity of precious metal catalysts at low temperatures while also maintaining this activity after high temperature aging. A novel platinum (Pt)-only TWC based on one of these supports shows promising low temperature performance and durability.

ORNL and the University at Buffalo developed a new Pt-only TWC formulation based on alumina nanosheets (Al_2O_3 NS) with islands of ceria (CeO_2). Pt (1 wt%) is dispersed on these materials and preferentially deposits on the ceria phase (Figure 1). Researchers synthesized a full range of ceria additions (0%-100%) to determine which loading provided the best activity and durability using the U.S. DRIVE TWC evaluation and aging protocols as guidelines. The materials were hydrothermally aged at 800°C for up to 10 hours while cycling between lean and rich conditions.

Figure 1 compares the best performing $Pt/CeO_2/Al_2O_3$ (NS) TWC (60% ceria) to other relevant TWCs. Using the temperature of 90% conversion (T_{90}) of CO, total hydrocarbons (THC), and NO_x as the figure of merit (lower T_{90} means better activity), this 1 wt% Pt-only catalyst is significantly more active than a traditional Pd/Al_2O_3 catalyst and compares favorably with one of the most active catalysts in the literature, 0.5% $Rh/12\%TiO_2/Al_2O_3$, without using any Pd or Rh. Additionally, when compared to its base components, $Pt\text{-}CeO_2$ and $Pt\text{-}Al_2O_3$ (NS), this new material has much better activity, illustrating an important synergistic behavior between these three materials. These results show a pathway to Pd and Rh substitution and lower costs while also improving low temperature activity.

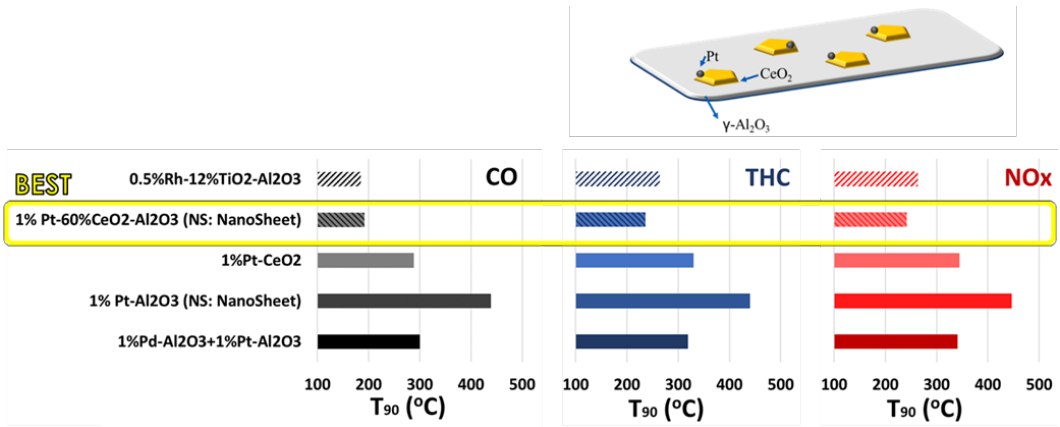

Figure 1. Novel alumina nanosheet (Al_2O_3 NS) with ceria (CeO_2) islands is utilized to anchor Pt and provide a Pd+Rh-free TWC that is more active than its base components, $Pt\text{-}CeO_2$ and $Pt\text{-}Al_2O_3$ (NS), and relevant Pd/Rh TWCs after lean/rich aging at 800 °C for 10 h.

2021 U.S. DRIVE Highlight

Conjugate Heat Transfer Modeling Provides Pathway to Improved Cold-Start Combustion Simulations

Model provides insight into crucial but difficult to measure parameter inputs for accurate simulation of cold-start emissions.

Oak Ridge National Laboratory within PACE Consortium

In support of the DOE-Vehicle Technologies Office's Partnership to Advance Combustion Engines (PACE) consortium, researchers at Oak Ridge National Laboratory (ORNL) used DOE's leadership computing resources and a coupled computational fluid dynamics (CFD) and conjugate heat transfer (CHT) engine model to evaluate engine-cylinder wall temperatures under cold-start relevant conditions. The extreme sensitivity of spray-wall interaction models to thermal boundary conditions and the difficulty in measuring surface temperatures throughout the combustion chamber during engine operation are a significant barrier to accurate simulation of engine operation during cold-start when the majority of drive-cycle emissions are produced.

The engine model was created in CONVERGE™ v3.0 based on scanned production hardware for a General Motors 2.0-L Ecotec LNF engine and calibrated with experimental data collected at ORNL using the ACEC Technical Team Cold-start Protocol for steady-state operation with intake air, coolant, and oil maintained at 20°C. Researchers used a 3-D CHT model for the engine head, valves, and piston with 1-D CHT applied to the cylinder liner. The team performed simulations on Eagle, DOE's high-performance computing machine at the National Renewable Energy Laboratory, using the PACE gasoline surrogate fuel.

Model results predict a spatio-temporally averaged cylinder wall temperature of approximately 60°C for steady-state operation under the Cold-start Protocol despite the 20°C soaking temperature (Figure 1). Head temperatures showed significant spatial variability with ~40°C difference between the intake and exhaust sides. Temporal differences were small with only a slight increase in piston temperature noted during combustion.

The team also examined the sensitivity of the CHT solution to uncertainty in back-side boundary conditions with the predicted head temperatures found to be rather insensitive. However, the piston was found to exhibit moderate sensitivity to boundary conditions on the skirt and gallery with a 40°C difference producing a 30°C difference in piston face temperature.

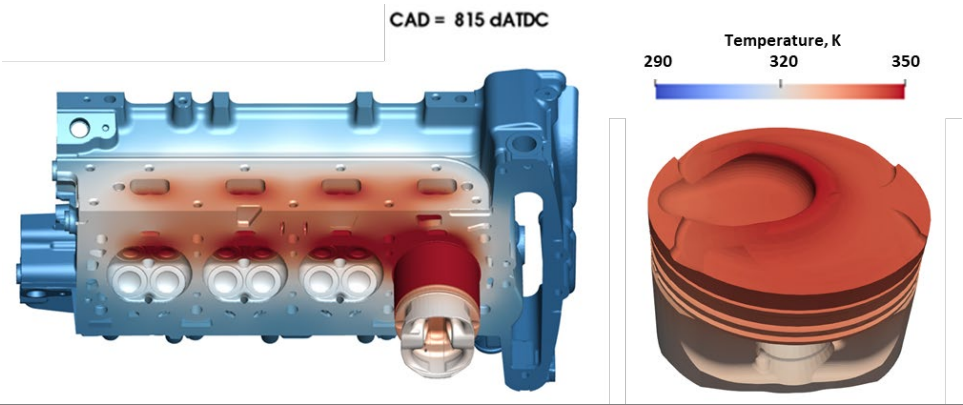

Figure 1. Surface temperatures (in K) of the metal engine components predicted by the coupled CFD/CHT engine model operating under the ACEC Technical Team Cold-start Protocols.

2021 U.S. DRIVE Highlight

New Insights Help Explain Stochastic Pre-Ignition Events and Could Lead to More Predictive Models

Real-time fuel dilution measurements highlight fuel impingement and retention as critical steps influencing stochastic pre-ignition event probability.

Oak Ridge National Laboratory within PACE Consortium

Stochastic pre-ignition (SPI) continues to present technical barriers in maximizing the fuel efficiency potential of downsized boosted engines. Although there have been several studies to understand SPI sources and relations, the fundamentals of SPI have remained elusive because of complex dependencies between fuel and lubricant properties and engine operating conditions.

A new approach being pioneered by Oak Ridge National Laboratory (ORNL) has implemented a laser induced fluorescence (LIF) diagnostic to measure fuel wall impingement and associated fuel retention in the engine during SPI prone conditions. This methodology is being used to help develop a phenomenological model of SPI to understand the fundamentals of SPI more clearly, and to identify the associated mitigation pathways.

A key feature of this phenomenological model is the importance of fuel wall impingement and associated fuel retention in the top ring zone (TRZ). The ability to measure and correlate SPI event propensity with fuel retention has provided clear and defined insights into a suspected mechanism of SPI. Figure 1 shows results from the LIF approach where the fuel retained in the top ring zone of the engine was calculated from the combination of the LIF measurement and the carbon balance of the engine.

The data gathered from this novel approach clearly highlights that SPI event propensity is proportional with the fuel retained in the TRZ (Figure 1). Operating conditions and fuels that are more radially retained in the TRZ increase SPI and SPI cluster event counts. Likewise, the composition of retained fuel in the TRZ is suspected to be chemically unique, resulting in decreased ignition delay species formed through thermal decomposition and reactions, and leading to chemically active ignition sources beyond those typically present in mixtures of neat fuel or lubricant.

These insights provided a framework to correlate existing working theories of SPI with measurements and quantification. This data is accelerating the identification and development of technologies needed for accurate modeling of spray, mixture formation, and ignition processes to permit SPI-free designs of appropriate fuel injection equipment and injection strategies, ultimately reducing fuel consumption and CO_2 emissions.

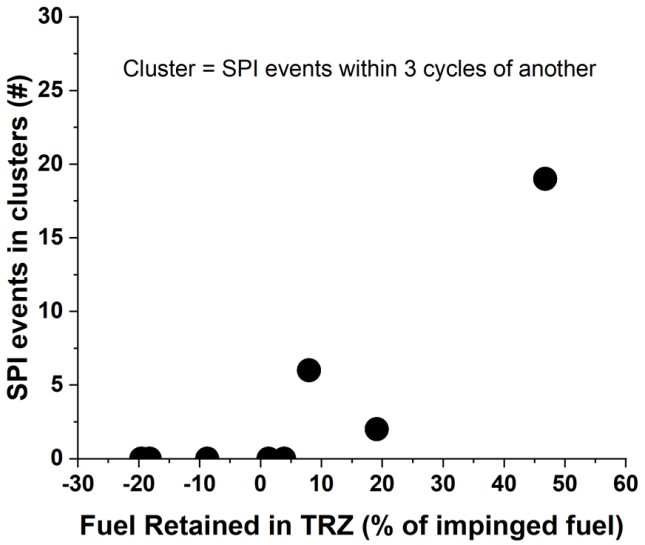

Figure 1. SPI events occurring in clusters as a function of measured fuel retained in the TRZ of the engine. Results illustrate that SPI propensity is correlated with fuel retention in the TRZ. Note negative values can occur from measurement uncertainty and non TRZ sources of fuel retention (e.g., piston crown wetting).

2021 U.S. DRIVE Highlight

In situ EPR Spectroscopy Provides Insight on SCR Catalyst Changes under Mild Aging

Monitoring of Cu/CHA with novel in situ electron paramagnetic resonance (EPR) spectroscopy facility explains Cu relocation with mild hydrothermal aging.

Pacific Northwest National Laboratory

Exhaust aftertreatment is facing unprecedented challenges. New combustion technologies require a complement of aftertreatment that functions at lower temperatures, and full useful life (FUL) requirements necessitate catalysts with superior durability and the ability to predict that performance. In response, Pacific Northwest National Laboratory (PNNL) scientists have undertaken multiple research approaches over the past decade to further understand and advance selective catalytic reduction (SCR) catalysts towards enhanced low-temperature activity and superior durability.

The development and efficient prediction of highly efficient industrial catalysts is often hindered by the lack of understanding of how the catalysts function and behave at atomic and molecular levels. Furthermore, FUL requirements necessitate analogous understanding of how catalysts age and/or malfunction at similar resolution. *In situ* (operando) spectroscopic techniques are ideally suited to this and have been developed by PNNL researchers to closely monitor the active sites of Cu/CHA SCR catalysts 'in-action', including their interaction with their local environments and SCR reactants.

Using this *in situ* EPR spectroscopy tool, PNNL researchers have shed light on important catalyst changes where there has long since been a general lack of understanding. Following minor hydrothermal aging, coper (Cu)/CHA catalysts moderately lose low temperature activity with no evidence of previously reported catalyst degradation such as zeolite damage or Cu active site loss.

With *in situ* EPR, the nature of the changes to Cu/CHA during this mild hydrothermal aging has been directly observed and explained for the first time. As depicted in Figure 1, the Cu active sites reposition and align with two Cu(II) cations positioned in a double six-membered ring prism. This repositioning is also associated with ZCuOH conversion to Z_2Cu resulting in increased Cu and zeolite interactions. Although the ZCuOH to Z_2Cu transition strengthens the catalyst's hydrothermal stability, the Cu re-repositioning lowers the catalyst's activity.

This insight is vitally important for understanding the catalyst changes with in-field use including contaminant interaction and aggressive thermal aging. Furthermore, this brings industry one step closer to accurate FUL modeling of these complex catalysts.

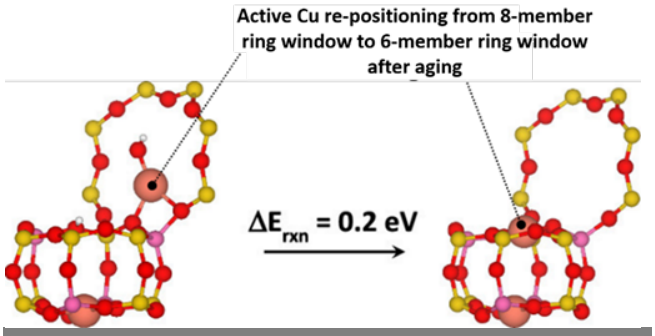

Figure 1. The effect of mild hydrothermal aging on increasing Cu-zeolite interactions and decreased activity. Cover Art from: *ACS Catalysis, 2020, 10, 9410-9419*. https://doi.org/10.1021/acscatal.0c01590.

2021 U.S. DRIVE Highlight

$Rh1/CeO_2$ Single Atom Catalysts Show Ability to Use Significantly Less Rh Compared to Current TWCs

A catalyst with low Rh loading (~0.1 wt%) and maximized interface between Rh(I) and ceria is very active for nitrogen oxide reduction by carbon monoxide.

Pacific Northwest National Laboratory

To decrease tailpipe pollutant emissions, cars and trucks are equipped with catalytic converters that contain platinum-group metals such as rhodium, palladium, and platinum. However, the demand for these precious metals is mounting as countries around the world seek to lower vehicle emissions to curb climate change and poor air quality. Furthermore, the price of rhodium (Rh), the key PGM in three-way catalysts (TWCs), is highly volatile and often in excess of $20,000 per troy ounce.

The work at Pacific Northwest National Laboratory (PNNL) relates to TWCs, named for their ability to simultaneously reduce carbon monoxide (CO), nitrogen oxide (NO), and hydrocarbons. It is currently well accepted in the literature that extended metal surface with contiguous Rh-Rh-Rh sites are responsible for NO reduction on TWCs. NO molecules uniquely adsorb on these Rh structures and dissociate into N and O before the former combines into nitrogen and the latter is scrubbed by CO to form carbon dioxide (CO_2).

In contrast to this belief, PNNL researchers successfully produced thermally stable and atomically dispersed $Rh1/CeO_2$ catalysts with maximized interface between Rh and CeO_2, i.e., Rh-O-Ce. Synthesis of this material is based on recent advances in the atom trapping approach and the ability of ceria to provide O-Ce bonds to stabilize the interface between Rh and ceria.

PNNL researchers discovered that these Rh catalysts are significantly more active as single atoms per molecule of Rh than higher concentrations of Rh. As low as 0.1 wt% Rh of these catalysts exhibit sufficiently high NO_x reduction activity (Figure 1), achieving full NO conversion at 125°C under simulated exhaust conditions. Furthermore, the presence of water vapor is not detrimental for NO reduction performance. Water is not detrimental; rather, it enables the formation of significant amounts of ammonia via water-gas-shift activity on these catalysts.

This work has uncovered a pathway to TWC formulations with significantly reduced Rh content (present as single atoms) versus metal-intensive contiguous Rh nanoparticles. This is facilitated by maximized metal-support interface enabled by the unique nature of ceria.

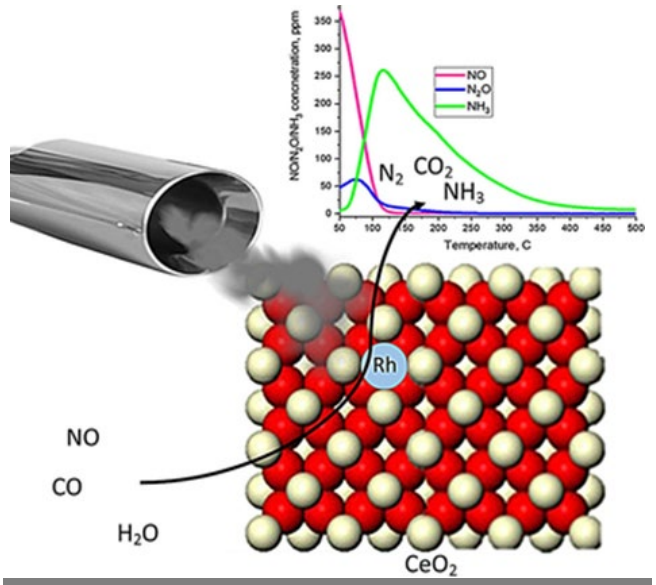

Figure 1. 0.1 wt% $Rh1/CeO_2$ calcined at 800°C for 24 hours shows 100% NO reduction by CO at 125°C (feed gas: 460 ppm NO, 1750 ppm CO, ~3% water balanced with N_2. GHSV ~ 150 L/g*hr).

2021 U.S. DRIVE Highlight

Small Pore Zeolite Supported Palladium as Water-Resistant Methane Combustion Catalyst

Pd/SSZ-13 with tailored palladium structure and location on SSZ-13 with a high Si/Al ratio exhibits superior methane oxidation activity for use in eliminating methane slip from natural gas engines.

Pacific Northwest National Laboratory

Combustion engines will remain indispensable in transportation and off-road applications for the foreseeable future. Among these, natural gas (NG) engines will continue to have important shares due to the abundance of NG, higher fuel efficiency of these engines, and reduced carbon dioxide (CO_2), nitrogen oxide (NO_x), and sulfur oxide (SO_x) particulate matter emissions. However, emissions remain a challenge for NG engines including unburned methane (CH_4), which has a greenhouse gas effect ~25 times that of CO_2. Therefore, catalytic combustion of unburned CH_4 in NG engine exhaust is critical.

Two main challenges exist for catalytic abatement of CH_4 from NG engine exhaust: low temperature activity, and water (H_2O) poisoning. Alumina supported palladium (Pd/Al_2O_3) is by far the most active catalyst for this application, which, unfortunately, suffers from H_2O inhibition. This is currently combated by adding platinum (Pt) but at the expense of substantially reduced activity of the catalyst. Thus, developing catalysts that are active but without susceptibility to H_2O poisoning is extremely important.

Pacific Northwest National Laboratory (PNNL) researchers have discovered that Pd/SSZ-13 catalysts with a high silicon (Si)/aluminum (Al) ratio facilitates Pd as externally decorated PdO nanoparticles that exhibit very high activity comparable to Pd/Al_2O_3 but without deactivation by H_2O. Three distinctly different active sites are achievable in these catalysts: finely dispersed Pd cations inside zeolite, PdO nanoparticles embedded in zeolite, and PdO nanoparticles deposited on zeolite external surface. Finely dispersed Pd cations are less active than PdO nanoparticles due to their inability to activate C-H bonds and O_2. Embedded and external surface PdO nanoparticles display markedly different deactivation rates in the presence of H_2O (Figure 1), which is also affected by Si/Al ratio of the SSZ-13.

Using atom probe tomography, researchers show that embedded PdO nanoparticles are decorated with an Al_2O_3-rich layer and suffer deactivation from H_2O similar to industrial Pd/Al_2O_3 catalysts. In contrast, external PdO nanoparticles supported on SSZ-13 supports with high Si/Al ratios do not suffer deactivation from H_2O, enabling their rational design towards a superior class of CH_4 oxidation catalysts.

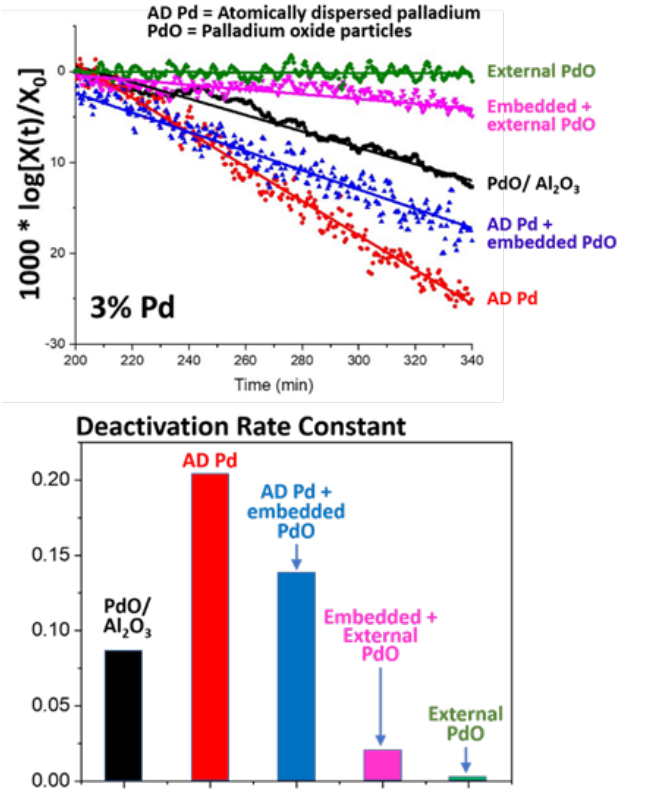

Figure 1. Significantly reduced deactivation rate constant on CH_4 combustion catalysts containing externally decorated PdO nanoparticles.

2021 U.S. DRIVE Highlight

Low-Temperature Gasoline Combustion Exceeds Diesel Efficiencies with Vastly Lower NO_x and Soot Emissions

LTGC engine achieve higher brake thermal efficiencies than those of a comparable diesel engine over the operating map. NO_x emissions are more than two orders of magnitude lower, and soot is near zero.

Sandia and Argonne National Laboratories

Low-temperature gasoline combustion (LTGC) using a unique additive-mixing fuel injection control and operating technique has been demonstrated to provide brake thermal efficiencies (BTEs) that are 10%–25% higher than those of comparable diesel engines over a typical medium-duty (MD) operating map, as evident by a comparison of Figures 1a and 1b. Nitrogen oxide (NO_x) emissions for LTGC are extremely low as shown in Figure 1c, and the composition and temperature of the exhaust gases are suitable for a non-urea HC-selective catalytic reduction (SCR) system (i.e., diesel exhaust fluid would not be required), but a urea-SCR system could also be used. Transients are not expected to influence NO_x since exhaust gas recirculation (EGR)is not used for NO_x control. Turbine-out exhaust temperatures are sufficiently high for oxidation catalysts for hydrocarbon and carbon monoxide (CO) emissions, as shown in Figure 1d. LTGC operates well from idle to high loads and has been demonstrated over most of the MD operating map as shown by the red squares in Figures 1a, 1c and 1d.

Autonomie simulations over the GEM ARB Transient and the GEM 55 mph Cruise driving cycles of a Class 6 MD truck using this technology show a fuel economy of 8.1 and 11.4 mpg-gasoline equivalent, respectively, a 25% and 20% improvement over a similar-size diesel engine. Engine-out NO_x emissions are 0.024 & 0.01 g/bhp-h, respectively, more than two orders of magnitude below those of a diesel engine.

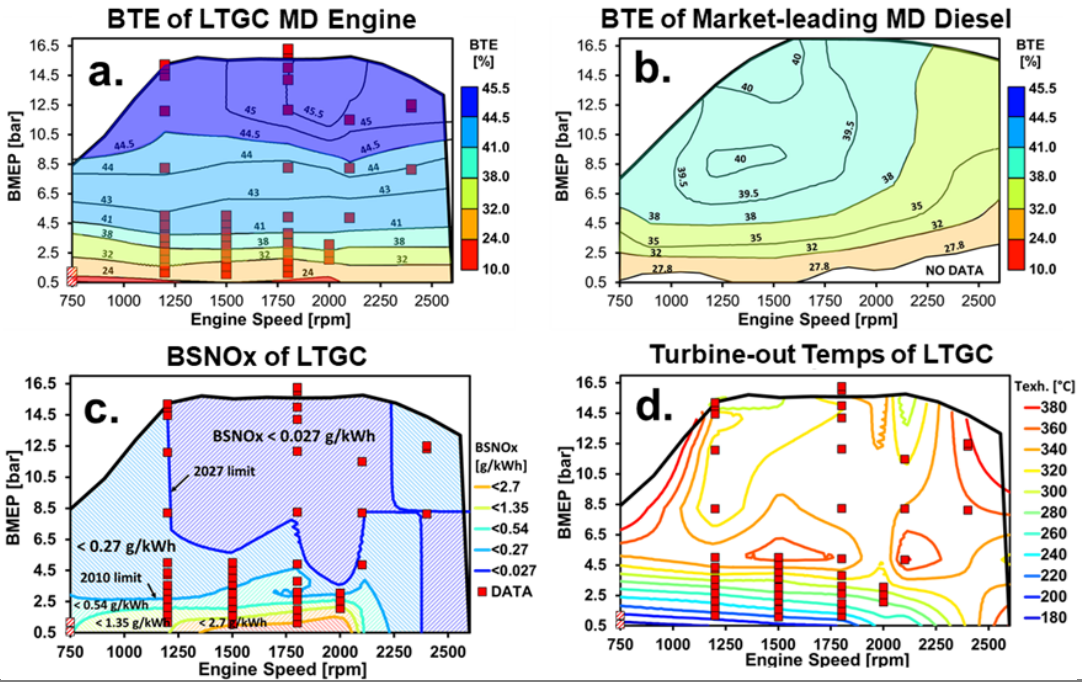

Figure 1. Contour maps over the load-speed range of a typical MD engine showing: a.) BTE for a MD LTGC engine compared to b.) BTE of a market-leading MD diesel engine, c.) Brake-specific NO_x for LTGC, and d.) Turbine-out exhaust temperatures for LTGC. The red squares show the operating points where LTGC data have been acquired.

2021 U.S. DRIVE Highlight

Advanced Optical Diagnostics Provide Understanding of Fuel Film Formation and Evaporation in GDI Engines

Results show strong spray dynamics and complex spray-surface interactions, and provide quantitative validation data to advance wall-film modeling and improve soot predictions under cold-start conditions.

Sandia National Laboratories within PACE Consortium

Gasoline direct-injection (GDI) engine soot emissions are dominated by the cold-start period due to significant wall and piston wetting caused by a combination of low surface temperatures and excess fueling. The leading hypothesis is that the soot is mostly formed via pyrolysis of vapor from surface fuel films. Consequently, accurate knowledge of fuel film thickness and rate of vaporization, and a predictive CFD modeling capability, is necessary to optimize combustion system geometries and operating strategies to minimize soot emissions. To date, this objective has been limited by inaccurate and unreliable measurements of engine films under realistic conditions.

We measured the 2-D thickness distribution, overall film mass, and evaporation rate of spray-generated wall-films via complementary time-resolved diagnostics including laser-induced fluorescence (LIF) for 2-D fuel film distribution, and a new high-speed low-coherence interferometry (LCI) technique. While the LCI technique is 1-D only, it is nearly insensitive to film composition, temperature, and ambient conditions, making it an ideal tool to calibrate and validate the 2-D measurements. Together, these diagnostics provide reliable film measurements under conditions with varying fuel type, surface and fuel temperature, in inert or reacting environments.

The pair of images in Figure 1 present film thickness maps for two injection cases: a single (10 mg) and a double (2 x 10 mg), obtained from the calibrated LIF experiments. The results show clear differences in footprint, film distribution and morphology between single and double injections. The time-resolved fuel film mass measurements shown in the bottom plot of Figure 1 reveal close to a factor two difference between the single and double injection tests, as expected. They also show a 95% wetting reduction when wall temperature is increased from 20° to 90°C. These quantitative measurements greatly enhance our understanding of film formation and distribution over previously applied techniques. The experimental observations are being used to refine modeling practices to better predict the fluid dynamics related to film formation for single- and multiple-injection strategies under relevant engine conditions.

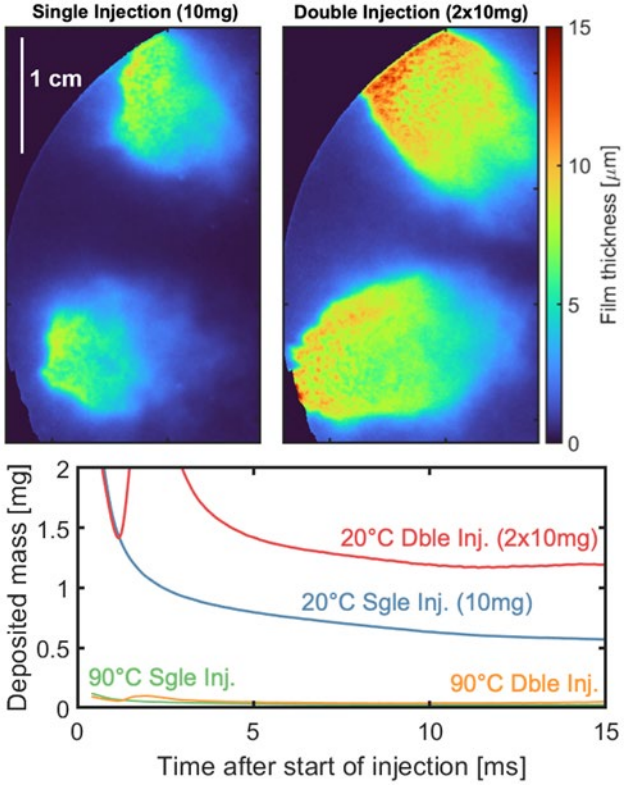

Figure 1. Film thickness distributions for single (top left) and double (top right) injection cases measured via high-speed LIF with the fuel and wall at 20°C. The bottom plot shows the mass of liquid fuel in the film for both injection strategies under two injector and wall temperature conditions.

Electrical and Electronics

2021 U.S. DRIVE Highlight

Enabling the Fine-Grain Approach to Eliminating Heavy Rare Earths in Nd-Fe-B-Based Permanent Magnets

Demonstrated technique to protect ultrafine milled powders from oxidization, enabling a fine-grain microstructure approach to eliminating heavy rare earths in stabilizing magnets at high temperatures.

Ames Laboratory

Currently, up to 6 wt.% dysprosium (Dy), a critical heavy rare earth (HRE), is added to neodymium (Nd)-iron (Fe)-boron (B) magnets for drive motor use at elevated temperatures (180°C). Reducing or eliminating the use of Dy in Nd-Fe-B magnets is a priority of electric vehicle manufacturers. A Nd-Fe-B magnet with smaller grains may exhibit the same high coercivity at high temperature as a magnet containing HRE elements. However, such a fine-grain magnet uses ultra-fine powders as the sintering feedstock. Unfortunately, Nd-Fe-B powders become more sensitive to oxygen when their particle sizes decrease. Once oxidized, these particles become less coercive. They may form centers for early magnetic domain reversal and cause dramatic deterioration of magnet properties. To use the ultra-fine powders in the existing magnet manufacturing process without adding excessive oxygen control, the ultra-fine Nd-Fe-B powders must be properly passivated. The challenge is to ensure the passivation layer has the optimum thickness so that adding passivation materials does not affect the magnetic properties.

Ames Laboratory (AMES) researchers have developed a novel passivation technique that preserves Nd-Fe-B fine powders from oxidization during the magnet fabrication process, enabling use of the fine-grain microstructure approach while maintaining coercivity at elevated temperatures.

AMES researchers are developing an *in situ* NF_3 coating for passivating ultra-fine Nd-Fe-B powders. AMES has demonstrated the proof of process using a high-energy SPEX™ mill to produce fresh new particle surfaces, which are exposed to NF_3 at elevated temperatures and promote a fluorination reaction to form a rare earth (RE) fluoride coating, thus passivating the fine powders. AMES researchers control the extent of passivation by controlling the time–temperature–gas content in the reaction vessel based on the following chemical reaction: $2NF_3 + 2RE = 2REF_3 + N_2$.

AMES tested passivated powders in a thermogravimetric analyzer (TGA) with temperature ramping from room temperature to 300°C (dry air). As shown in Figure 1 (top), the non-passivated powder experienced a sudden weight gain at 260°C due to oxidization, while the weight gain for the passivated powder is gradual and relatively slow. As shown in Figure 1 (bottom), the non-passivated powder gained weight faster than the passivated powder at 150°C and 200°C.

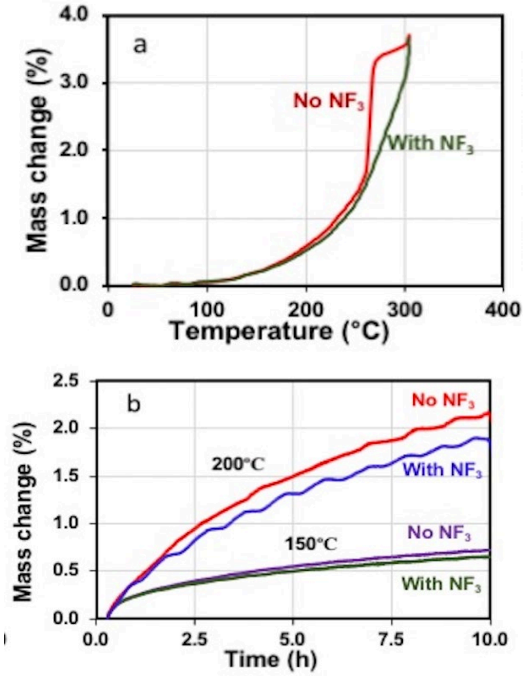

Figure 1. TGA curves of non-passivated powders in dry air: (top) ramping temperature from room temperature to 300°C (10°C/minute); (botttom) maintaining temperature at 150°C for 10 hours.

2021 U.S. DRIVE Highlight

Wound Field and Hybrid Synchronous Machines for Electric Vehicle Traction with Brushless Capacitive Rotor Field Excitation

High-performance traction motors free of permanent magnets.

Illinois Institute of Technology

The wound field synchronous machine (WFSM) is a potentially attractive electric vehicle traction motor topology. WFSMs are free of permanent magnets and have a controllable field excitation. The latter is especially attractive, as it allows for easy field weakening, reduced iron losses at high speed, and a high power factor that enables a lower stator inverter volt-ampere rating. Over the years, a number of approaches have been developed to provide direct current (DC) to the rotating field winding, including brushes and slip rings, brushless exciters, and high-frequency rotary transformers and rectifiers. Our collaborators at the University of Wisconsin-Madison developed an alternative: brushless capacitive couplers to pass a high-frequency current across a rotating airgap, which is then rectified.

A third-generation high-power-density WFSM was optimized, prototyped, and dynamometer-tested. The WFSM was designed using a drive-cycle-based, meta-modeling optimization technique. A hairpin stator from a GM Chevy Volt Gen 1 motor was reused and a custom salient pole wound field rotor constructed. The rotor was designed to be compatible with three high-slot-fill winding technologies: square conductors, twisted square conductors, and die-compressed. The predicted peak volumetric power densities are listed in Table 1 for the rated stator current.

	4000 RPM Base Speed	6000 RPM Base Speed
Active volume	37.7 kW/l	57.6 kW/l
Volume including end turns	24.0 kW/l	36 kW/l

Table 1. Predicted volumetric power densities at rated stator current.

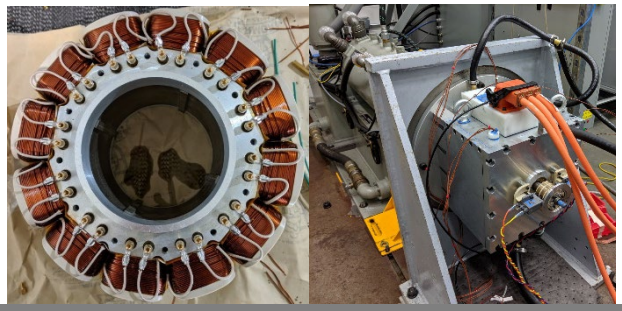

Figure 1. Square WFSM rotor (left) and overall WFSM rotor with brushes and slip rings mounted on the dynamometer for testing (right).

The square conductor and twisted square conductor versions (Figure 1) were fully prototyped and the square conductor version dynamometer-tested. The testing was carried out with brushes and slip rings and with a large gap printed circuit board (PCB)-based capacitive power transfer system. The WFSM prototype was tested to the limit of the available stator inverter current rating. WFSM performance agreed closely with finite-element-predicted performance. Two high-frequency inverter designs were tested with the PCB capacitive power coupler (Figure 2).

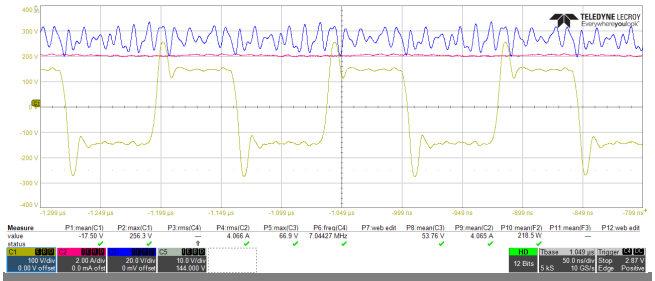

Figure 2. Power delivery to the WFSM using a capacitive power transfer system with an excitation frequency of ~7.1 MHz and 4 A field current. The yellow trace is the inverter output voltage, and the pink trace is the field current.

2021 U.S. DRIVE Highlight

Lifetime Model of Sintered Silver to Guide Wide Bandgap Power Module Design

A lifetime prediction model of sintered silver based on thermomechanical modeling and experimental reliability results.

National Renewable Energy Laboratory

Wide bandgap devices offer a transformational opportunity to reduce cost and improve efficiency and power density of automotive power inverters. Bonding materials such as sintered silver are essential in enabling high-temperature operation of the power electronics module, along with the devices; however, the reliability and failure mechanisms of these materials must be understood and quantified. To this end, we collaborated with Virginia Tech to evaluate the reliability of sintered silver and developed a lifetime prediction model.

We conducted thermal cycling experiments on sintered silver samples and periodically monitored the degradation behavior of the material through C-mode scanning acoustic microscope (C-SAM) images. Figure 1 shows these images of sintered silver before and after 50 thermal cycles. We performed image analysis and observed the high rate of crack growth for various bonding configurations of sintered silver included in the experiments. To identify the failure mechanisms, we cross-sectioned and obtained scanning electron microscope (SEM) images of the sintered silver samples after thermal cycling (Figure 2). We observed predominantly adhesive fracture, along with short cohesive cracks that connected minor voids present in the bond.

We also computed strain energy density values for the different bonding configurations through non-linear finite element analysis. Finally, we correlated the crack growth rates with the strain energy density results to formulate a lifetime prediction model (Equation 1; Figure 3)—the first in the literature that incorporates degradation behavior of sintered silver at 200°C. The model will be a valuable tool for researchers and engineers designing high-temperature power electronics packages.

$$Lifetime\ model, \frac{dA}{dN} = 0.76\ \Delta W^{0.431} \qquad (1)$$

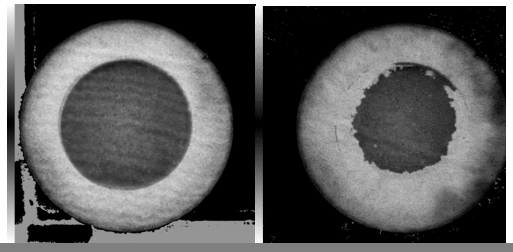

Figure 1. C-SAM images of sintered silver before (left) and after (right) 50 thermal cycles. Experiments conducted at -40°C to 200°C, >25°C/minute ramp rate, 3-minute dwell.

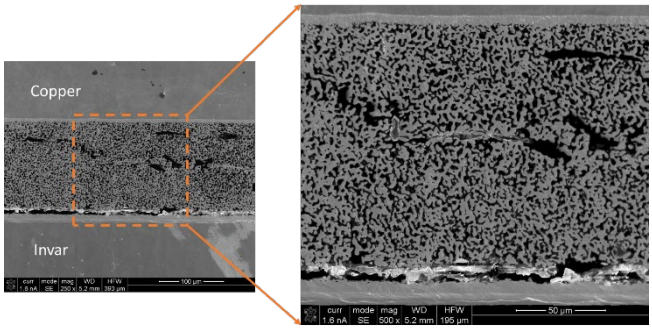

Figure 2. SEM image of failure mechanisms within sintered silver.

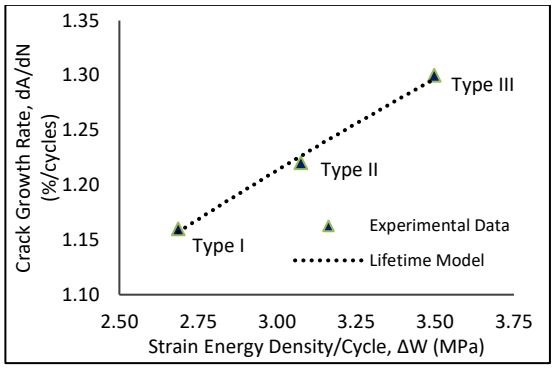

Figure 3. Lifetime prediction model of sintered silver.

2021 U.S. DRIVE Highlight

Automated Heat Sink Design Tool for Wide-Bandgap Power Modules Based on Multi-Objective Optimization

Compact design tool that can develop high-performance heat sink designs for wide-bandgap power modules based on evolutionary algortihms, multiphysics simulation, and multi-objective optimization.

Oak Ridge National Laboratory

Researchers have developed a design optimization method for liquid-cooled heat sinks. The approach uses a Fourier analysis-based tool and an evolutionary algorithm to optimize the heat sink geometry for specified objectives. The resulting heat sink was compared with state-of-the-art solutions in the literature based on finite element analysis of different designs. The proposed methodology can develop complex geometries that outperform conventional heat sink geometries. Using the proposed method, optimized heat sink design was fabricated and tested in an experimental setup under representative operating conditions. The setup was also modeled in the finite element model that was used for the proposed heat sink optimization method. The experimental results show that finite element models can predict the complex design's thermal and flow performance with high fidelity, and the results validate the proposed design approach.

Figure 1 presents the design tool's overall structure. Design variables and power module specifications are used as inputs to develop the initial population of heat sink designs. Each design is simulated in a multiphysics-based finite element analysis tool; the results (e.g., junction temperature, coolant pressure drop) are extracted to determine the simulated design's performance in terms of design constraints and optimization objectives. The fitness of each design that satisfies the constraints is calculated and fed to a genetic algorithm engine, generating populations of designs over multiple generations. At the end of optimization, a pareto-front of designs is plotted, allowing the user to select the optimum design with respect to optimization objectives.

Figure 2 shows the optimized heat sink design for a silicon carbide MOSFET-based power module. The figure shows a significant heat sink volume reduction, increasing the power density by 30% compared with the pin-fin heat sink. The optimized heat sink also achieves up to 50% increased thermal performance in small form factor at high-flow-rate conditions. These cooling performance improvements will help create high-power-density wide-bandgap power modules.

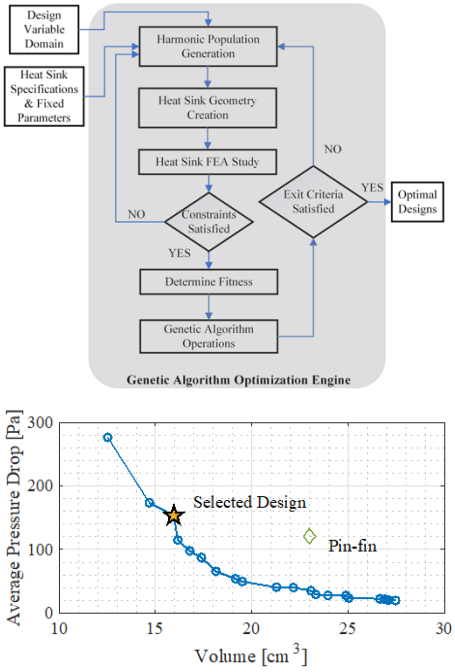

Figure 1. Heat sink multi-objective design optimization (top); parato-front of design with respect to pin-fin design (bottom).

Figure 2. Prototype of the optimized heat sink design (right) in comparison to pin-fin heat sink (left).

2021 U.S. DRIVE Highlight

Capacitor Technologies: Selection, Characterization, and Packaging for Next-Generation Inverter Application

A symmetric capacitor package with a lead lanthanum zirconate titanate (PLZT)-based capacitor with reduced capacitor volume and better electrical and thermal performance.

Oak Ridge National Laboratory

Direct current (DC) bus capacitors take up substantial space in an electric vehicle traction inverter, limiting the traction drive's volumetric power density. Typically, film capacitors are used; however, other capacitor technologies with higher energy densities can help reduce the overall size. This highlight discusses analysis of two types of ceramic capacitor technologies: Class II ceramic and PLZT ceramic, along with the widely accepted film capacitor. The results show that the PLZT-based capacitor will drastically reduce the capacitor volume compared to a film capacitor technology.

The PLZT material is produced in small sizes since it is brittle; therefore, hundreds of capacitors made of PLZT will be paralleled for traction inverter applications. Traditional PCB-based flat packages are simple to design, but they introduce additional layout inductances and show asymmetrical current distribution among the parallel capacitor branches. The layout inductance of the capacitor bank, which is in series with the inverters' commutation loop, causes inverters' switching performance to deteriorate.

A symmetric layout package (circular package) is proposed to address these challenges. The exploded diagram and the assembled symmetric package are shown in Figures 1 and 2, respectively. In this package, 45 capacitors were paralleled such that all the capacitors were equidistant from the termination point. Moreover, the currents going into and coming out of the capacitors overlap, thus minimizing the track inductances. The assembled package is then characterized to evaluate electrical and thermal performance.

The results (Table 1) show that using PLZT capacitors can reduce capacitor volume by 60% compared to BMW-i3s. Moreover, compared to a traditional flat design, symmetric packaging shows 40% less layout inductance for the total package and 80% lower temperature among the parallel capacitor branches.

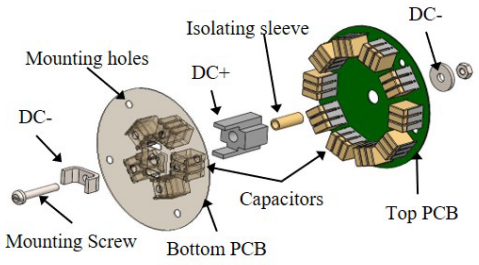

Figure 1. Exploded diagram of the proposed symmetrical (circular) package.

Figure 2. Assembled capacitor package: top view (left), bottom view (right).

1. Parameters	2. Values	3. Comments
Volume	4. 0.028 L	5. 0.168 L (0.6 L for BMW-i3)
Capacitance	4.2 $\mu F - 6\ \mu F$	@100 kHz
Current	100 A	@85 kHz
ESR	2.37 mΩ	100 kHz, 100°C
ESL – circular	3 nH	10 MHz
ESL – flat1	4.9 nH	10 MHz
ESL – flat2	5.3 nH	10 MHz
ΔT	1.8°C	9.5°C–11°C for flat design @100 kHz

Table 1. Designed circular capacitor parameters. ESR = equivalent series resistance; ESL = equivalent series inductance.

2021 U.S. DRIVE Highlight

Vertical Gallium Nitride MOSFETs for Electric Drivetrains

Vertical gallium nitride power devices that increase efficiency and power density compared to conventional solutions, supporting next-generation electric drivetrains.

Sandia National Laboratories

Vertical gallium nitride (GaN)-based power electronic devices are gaining traction for high-power applications. These devices promise better performance and power density than conventional silicon (Si), or even silicon-carbide (SiC)-based, systems. For electric drivetrains, vertical GaN devices translate to more miles driven per charge and more compact charging solutions. A vertical topology (versus a lateral GaN device) promotes more efficient scaling toward high-power applications that demand both high voltage and high current.

A Sandia team has developed a process to fabricate vertical GaN-based trench MOSFETs (metal–oxide–semiconductor field-effect transistors) for use in electric drivetrains. Sandia's first-generation device demonstrator provides milestones along the path of producing devices rated at 1200 volt (V) and 100 ampere (A) operation.

The vertical GaN trench MOSFET (Figure 1) differs from Si or SiC alternatives in that the doped layers comprising the source and body regions are grown by epitaxy rather than formed by ion implantation. In addition, GaN lacks a high-quality native oxide, so the gate dielectric must be deposited rather than thermally grown. The devices produced at Sandia rely on atomic layer deposited thin films for the gate dielectric (primarily Al_2O_3 or SiO_2).

As shown in Figures 2 and 3, the first-generation devices demonstrate capabilities of 400 mA/mm drain current, a 10^8 on/off ratio, and a positive threshold voltage near 8V. This work provides a foundational platform for development of next-generation power electronics that employ wide-bandgap GaN semiconductors.

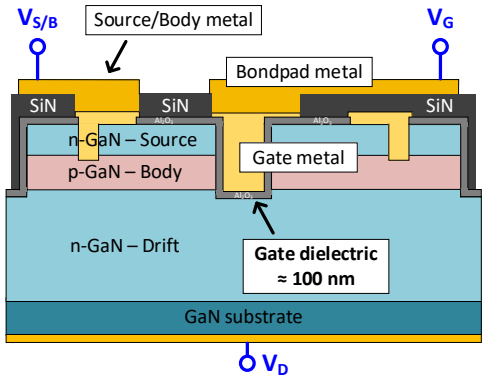

Figure 1. Representative structure of the vertical GaN trench MOSFETs fabricated at Sandia.

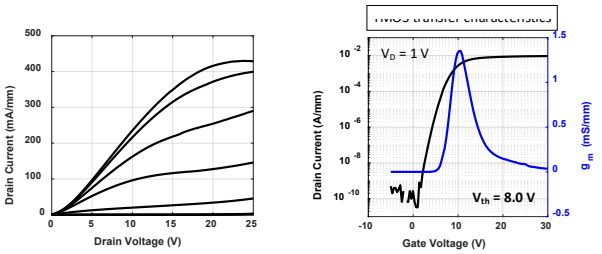

Figure 2. Results from a single-finger MOSFET with an ALD-SiO_2 gate dielectric: I_DV_D results for V_G = 0:30 V in steps of 5 V (left); transfer characteristics (I_DV_G) and transconductance curves demonstrating a positive threshold voltage (right).

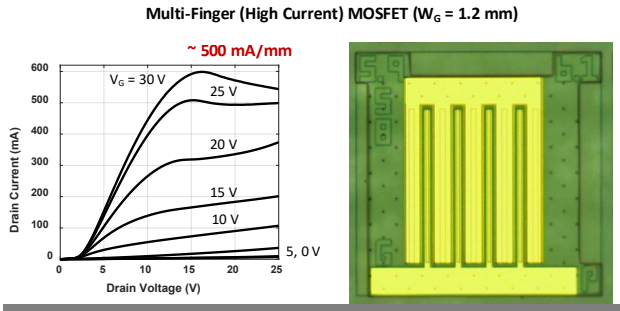

Figure 3. Results from a multi-finger MOSFET with an ALD-SiO_2 gate dielectric: I_DV_D results for V_G = 0:30 V in steps of 5 V (left); optical microscope image of the fabricated device (right).

Electrochemical Energy Storage

2021 U.S. DRIVE Highlight

A New Class of Cobalt-Free Cathodes: Order, Disorder, and the Versatility of Manganese

Controlling atomic disorder within an ordered, lithiated, manganese-spinel framework provides new insights into the design of high-capacity, cobalt-free oxide cathodes.

Argonne National Laboratory

Due to the wide range of structures and electrochemical properties of manganese (Mn)-oxides, as well as its earth-abundance, Mn has a long history in battery technologies, and new discoveries are showing that Mn may have an important role to play in next-generation cathodes. At Argonne National Laboratory, a team of researchers has recently described a novel concept related to lithiated, Mn-spinel oxides as lithium (Li)-ion cathode materials and demonstrated a high voltage material which delivers a specific energy higher than most NMC811 materials.

The spinel framework offers a robust platform to reversibly cycle Li in and out of its 3D tunneled-structure. However, low capacities (e.g., 130mAh/g for $LiMn_2O_4$) and/or untenable voltages (e.g., 5 volt [V] operation in $LiMn_{1.5}Ni_{0.5}O_4$) have hindered the ability of spinel materials to meet practical demands. The Materials Research Group at Argonne has recently revisited the intriguing concept of lithiated spinels, (e.g., $Li_2Mn_2O_4$), as both stabilizing components of Li-excess cathodes as well as stand-alone, high-capacity electrodes.

In short, the study reveals the dramatic influence that local atomic arrangements within the new materials have over macroscopic electrode properties. Starting with a lithiated Co-oxide spinel, the team showed that substituting cobalt (Co) with Al, accompanied by low amounts of disorder among certain crystallographic sites, changed the two-phase Li insertion/extraction mechanisms of known spinels to a single-phase reaction for the new oxides. In addition, electrodes showed a zero-strain behavior with virtually no expansion/contraction on cycling; this is an intriguing result regarding the development of solid-state cells and advantageous for traditional Li-ion cells as it removes mechanical strain.

Using the knowledge from these discoveries, a high-capacity, Co-free composition was targeted utilizing a 50/50 mix of Mn and nickel (Ni). Again, by controlling atomic-level disorder, within an ordered lithiated spinel framework, the team was able to realize a remarkably stable, high-capacity material. Figure 1 shows charge/discharge profiles between 5.0-2.5V of the MnNi electrode, 5mg/cm^2. Of note is that the electrode behaves differently than the high-voltage MnNi spinel, revealing substantial capacity delivered throughout the voltage window (as opposed to the high-voltage material in which a large percentage of the capacity is delivered at 5V). In addition, the new material showed very low expansion/contraction (less than 3%) during cycling, giving a stable ~225 mAh/g with little structural fatigue.

These new findings, along with the large space of relevant parameters (composition/synthesis/site-order/disorder) reveal exciting new opportunities in the design of next-generation, sustainable cathodes.

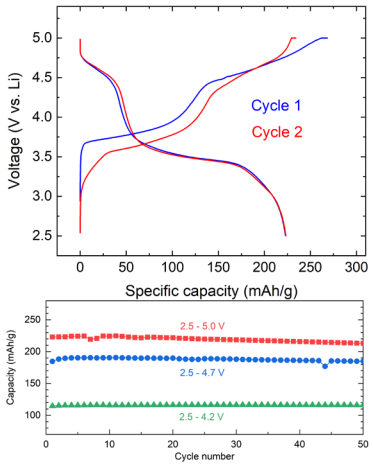

Figure 1. Top. Unique charge/discharge profiles of the novel, lithiated spinel between 5.0-2.5V. Bottom. Cycling capacity at three upper cutoff voltages highlighting the stability of the cathode material, electrolyte is 1.2M $LiPF_6$ EC/EMC 3/7 wt%.

2021 U.S. DRIVE Highlight

Low-Temperature Lithium-Ion Battery Enabled by a Fluorinated Ester-Based Electrolyte

A fluorinated ester-based electrolyte was developed for improved low temperature performance in lithium-ion batteries.

Argonne National Laboratory

Lithium-ion batteries (LIBs) generally have relatively poor power at low temperatures (less than 10°C) due to poor kinetics at interfaces and in the bulk electrolyte. The sluggish ion transport at the electrode interface causes high impedance and results in a large cell overpotential and rapid degradation in cell performance.

Argonne scientists have developed a new electrolyte based on fluorinated ester solvents, EA-f/FEC. The new electrolyte, in graphite/NMC622 cells, exhibits similar room temperature performance as Gen 2 electrolyte (1.2 M LiPF6 EC/EMC (30/70 wt %) as shown in Figure 1a, but superior low temperature performance (-20°C) as shown in Figure 1b and 1c. The conductivity of the bulk electrolyte is not the dictating factor; instead, the low charge transfer impedance at the graphite/electrolyte interface dominates the low temperature performance as revealed by an electrochemical impedance spectroscopy (EIS) study (not shown).

The solid-electrolyte-interface (SEI) formed by the new electrolyte shows low resistance and low charge transfer impedance compared to the baseline electrolyte. This lower impedance enables the fast-charging capability at both low temperatures and room temperature (Figure 1).

Often, electrolytes that have improved low temperature performance have inferior higher temperature performance. Thus, the next phase of this work, currently underway, is to perform testing at 40° and 50°C. In addition, the cost of this electrolyte is currently higher than that of the Gen 2 electrolyte, which will need to be addressed if high temperature performance is adequate.

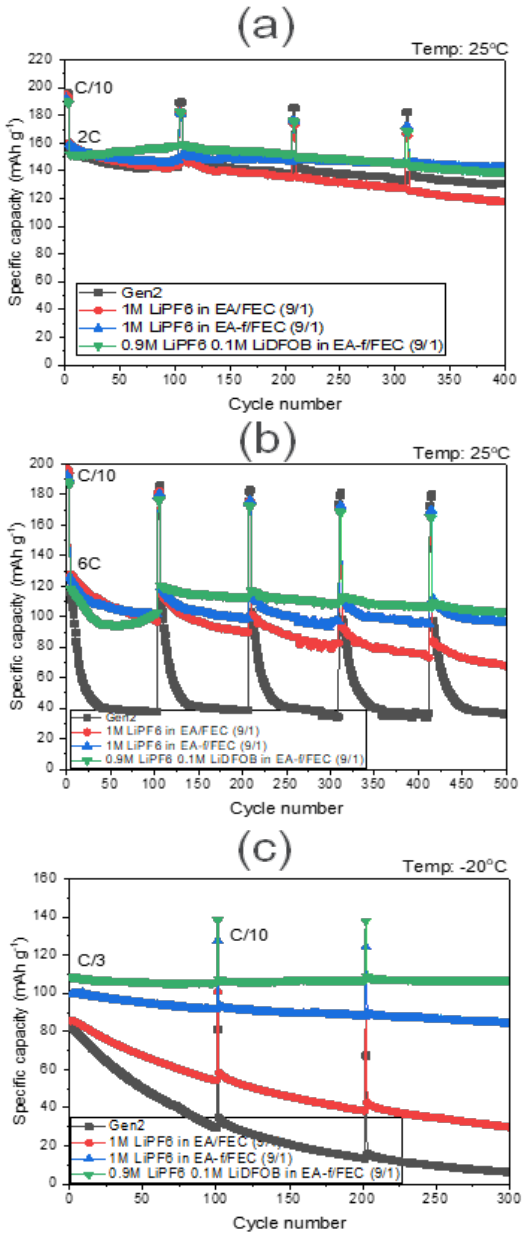

Figure 1. NMC622/graphite cells performance at various temperatures. (a) cycling performance at RT, (b) High rate cycling data and (c) cycling performance at -20°C.

2021 U.S. DRIVE Highlight

Silicon Anodes with Improved Calendar Life Enabled by Multivalent Electrolyte Additives

The resulting solid electrolyte interphase is robust and dense, which more effectively protects the silicon core from side reactions, leading to lower capacity decay after calendar aging at high voltage.

Argonne National Laboratory

Silicon (Si) is widely recognized as the most promising next-generation anode due to its much higher theoretical capacity (~3,000mAh/g for Si vs 300mAh/g for graphite), natural abundance, and ability to be used in the slurry-based, roll-to-roll production lines in use today. However, Si anodes suffer from inferior calendar life, which is particularly important for real-life application. Unlike cycling, which involves volume change and repeated formation of a new solid-electrolyte interphase (SEI); calendar life is more related to the stability of the original SEI and its underlying core. Unfortunately, the SEI of Si electrodes is notoriously unstable due to the high reactivity of charged Si_2^{-2} and/or Si^{-4} anions that react to reduce the binders and electrolyte components. Until now, strategies to effectively improve the calendar life by tailored SEIs remain largely unclear, especially in high-Si content, zero-graphite anodes.

In this work, researchers developed Si anodes with improved calendar life by adding small concentrations of multivalent salts into the baseline electrolyte. The addition of calcium (Ca^{+2}) in the form of as $Ca(TFSI)_2$ co-salt not only stabilizes Si anions via the formation of lithium (Li)-Ca-Si ternary phases electrochemically, but also rigorously reacts with F ions in the electrolyte forming a thick, robust, and dense CaF_2 containing inorganic SEI layer around silicon particles. Transmission electron microscopy (TEM) and nuclear magnetic resonance (NMR) characterizations showed that electrodes with Ca additive have a dense and stable CaF_2 layer with a thickness around 100 nm consisting of nanocrystals embedded in an amorphous matrix, and consisted of inorganic compounds in the SEI, such as LiF and CaF2 as well as the formation of poly-FEC. Because of the high stability of CaF_2 as well as other inorganic compounds, the new SEI is more stable and able to protect the Si core from side reactions that may occur during calendar aging. On average, the Si/NMC532/GenFC (GenF + 0.1 M $Ca(TFSI)_2$) cells lost only 6.98% of capacity after 3-month calendar aging at room temperature (25°C) and 4.1 volt (V) (100% state of charge), which is better than baseline GenF (1.2 M $LiPF_6$ in a 3:7 EC: EMC+10% FEC) cells (13.71 %) and the GenFM (GenF + 0.1 M $Mg(TFSI)_2$) cells (14.86 %). More importantly, the improvement of the calendar life due to the Ca additive can be achieved in all tested commercial silicon or SiO sources with different cathodes.

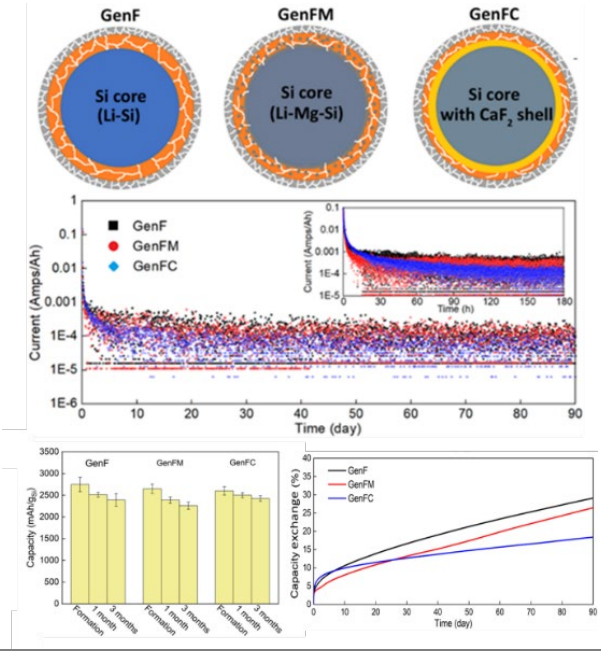

Figure 1. Schematic illustration of SEIs in GenF, GenFM, and GenFC cells. Current leakage of GenF, GenFM, and GenFC cells during three-month holds at 4.1V (1/3000 data points shown). [inset: close inspection of current decay during the first 180 hours (all data points shown]). Capacity exchange percentage (percentage capacity lost during hold) of GenF, GenFM, and GenFC cells during calendar aging. Comparative bar chart of the discharge capacity of the third formation cycle and the second diagnostic cycle

2021 U.S. DRIVE Highlight

Balancing Interfacial Reactions To Achieve Long Cycle Life in High-Energy Lithium Metal Batteries

Battery500 Consortium researchers discovered that thin lithium metal foil as the anode extends lifespan of lithium metal pouch cells compared to thicker lithium metal foil.

Battery500 Consortium

Lithium (Li) metal cells could enable energy densities significantly higher than today's Li-ion cells. The Battery500 Consortium developed a novel and high-performance electrolyte, an optimized electrode architecture and cell design to balance the electrochemical and chemical (side) reactions in high energy Li metal cells, achieving more than 600 cycles in prototype 350 Wh/kg pouch cells (2 Ah) (Figure 1). Commercial EV cells achieve 220-280Wh/kg.

Recently, they discovered that by reducing the thickness of Li metal foil anodes to 20 µm from 100 µm in 350Wh/kg pouch cells (Figure 1b-1d), not only is cycle life improved, but the steep capacity drop towards the end of cycle life, due to electrolyte dry out, is also mitigated.

When Li metal contacts electrolyte, a passivation film or solid electrolyte interphase (SEI) layer forms due to the high reactivity of Li metal with electrolyte. Ideally, the insulating SEI layer stops further reactions or "corrosion" of Li metal in the electrolyte while still allowing Li^+ transport. However, the formation of SEI layers consumes electrolyte which is very lean in high-energy cells.

To explain this result, the team has theorized that there are two different SEI layers formed within cycled Li anodes, wet and dry. "Wet SEI" (Figure 1a) is formed inside shallow channels or pores of Li metal where contact is retained between the liquid electrolyte and the Li. This wet SEI supports cell cycling. "Dry SEI" (Figure 1a) forms when no liquid electrolyte is left, which is often in the deep and very narrow pores of SEI-covered Li present in thicker strips. These dried out regions subsequently smother further electrochemical reactions, leading to cell death. The thicker the Li metal, the deeper the pores/channels formed. The amount of electrolyte is extremely limited in realistic batteries (20-30 times less than in coin cells) and easily depleted in forming dry SEI layers in those deep pores abundant in thick Li strips.

Thus, optimization of Li metal thickness is critical to extend lifespan of Li metal batteries. The team is planning to use ultrasonic imaging to observe the two regions of SEI growth.

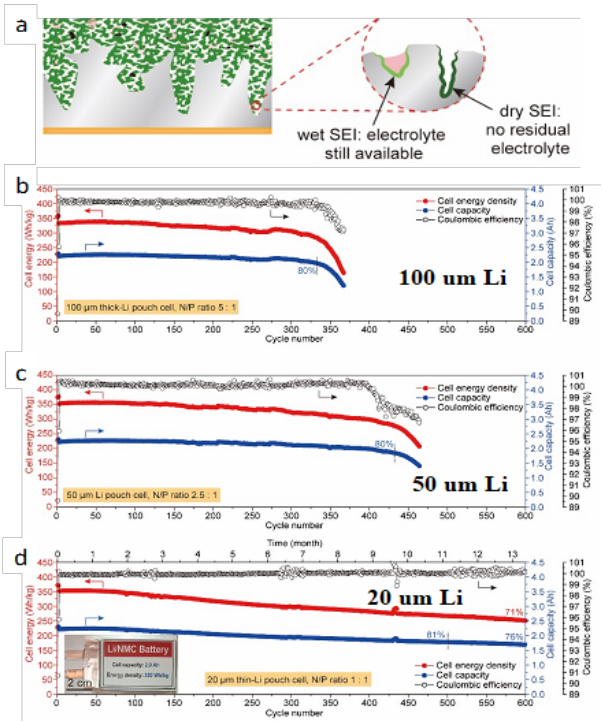

Figure 1. 350 Wh/kg pouch cells achieve more than 600 cycles in research from the Battery500 Consortium. (a) Illustration of wet and dry SEI layers in Li metal anode. (b)-(d) Cycling performances of 350 Wh/kg Li metal pouch cells using 100, 50 and 20 µm Li foils as the anodes, respectively. Cathode: $LiNi_{0.6}Mn_{0.2}Co_{0.2}O_2$; Electrolyte: 1.54 M lithium bis(fluorosulfonyl)imide (LiFSI) in 1,2-dimethoxyethane (DME) and 1,1,2,2-tetrafluoroethyl-2,2,3,3-tetrafluoropropyl ether (TTE).

2021 U.S. DRIVE Highlight

High-Energy Lateral Mapping Studies of Inhomogeneity and Failure Mechanisms in Pouch Cells

New synchrotron diffraction methods were developed to quantify lateral inhomogeneity in cathode films which explained failure mechanisms for high energy density Li metal pouch cell batteries.

Brookhaven National Laboratory

Lithium (Li) metal batteries offer the potential for significant increases in energy density that could enable larger scale adoption of electric vehicles. However, it is not yet possible to build high energy density Li metal batteries with long lifetimes (more than 1,000 cycles) due to the reactivity of Li metal with electrolytes. If specific failure mechanisms of Li metal batteries can be identified, this will help in efforts to mitigate them and potentially increase the lifetime of Li metal batteries.

While traditional electrochemical testing methods are used for determining when batteries fail, these methods cannot determine what the failure mode is, or where it is occurring. To better understand failure mechanisms, researchers developed new X-ray diffraction methods using the National Synchrotron Light Source II to map position-dependent variations in an end-of-life battery cathode. The high-energy X-rays readily penetrate cells, allowing industrially relevant pouch cells to be studied.

For this work, researchers extracted a single cathode layer from a high-energy density Li metal pouch cell which was subjected to ~ 200 cycles (Figure 1a) and then fully discharged. The cell energy dropped below 80% of its starting value after ~175 cycles (corresponding to nominal cell failure), though much of the lost capacity could be recovered by cycling at a lower rate. In mapping experiments (Figure 1b), three hot spots were found in which the cathode state of charge (SOC) was much higher than average, indicating that these three regions were electrochemically isolated. The non-edge spots formed where the cathode amount was about 5% lower than average, indicating that very small manufacturing problems in cathode films can lead to early cell failure.

Based on the spot sizes, the multi-phase mixtures observed in diffraction patterns, and comparisons with cells designed to fail in a specific manner, it was conclusively determined that cells failed due to depletion of the electrolyte (which can occur through reaction with Li metal) needed to transport ions between the anode and cathode. Further mapping studies on a series of coin cell cathodes allowed the electrochemical signatures of this and two other failure modes (loss of Li inventory and impedance rise), providing a new and facile method to determine how a cell is failing.

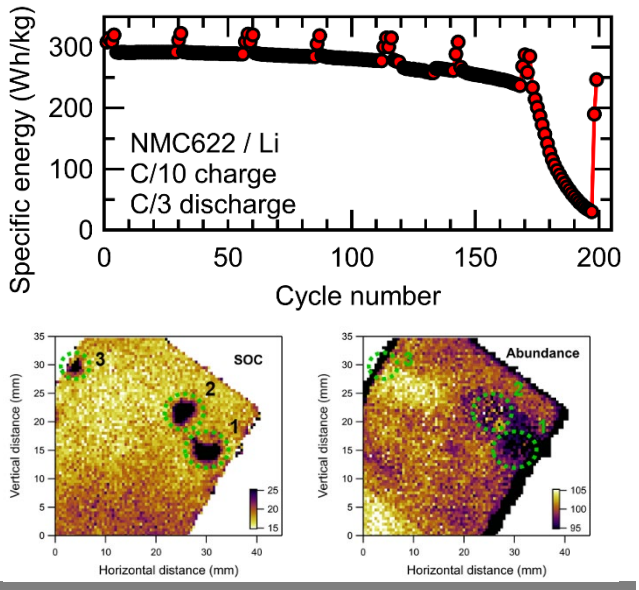

Figure 1. (a) Decay of cell energy during cycling. After every 25 cycles, cell was tested at a very slow rate (C/25) producing spikes of higher capacity. For this cell cycled to failure, maps of (b) the local state of charge and (c) the relative abundance of the NMC cathode were collected, allowing three hot spots (1 – **3**) with poor performance to be identified.

2021 U.S. DRIVE Highlight

Advanced Electrolytes that Enable Fast-Charging

XCEL Program labs have developed improved electrolytes for extreme fast-charge applications through a synergistic combination of modeling, formulation, and laboratory testing and validation.

Extreme Fast Charge (XCEL) Program

Extreme Fast Charge (XCEL) Program researchers are working to advance lithium (Li)-ion cell design (appropriate for electric vehicle applications) to accomplish a fast-charge (XFC) in 10-minutes or less. Electrolytes are a key component for achieving XFC in Li-ion batteries, while meeting other technical and life goals.

Preemptive electrolyte research was conducted using the Idaho National Laboratory (INL) Advanced Electrolyte Model (AEM) to investigate electrolyte metrics that influence cell performance during fast charge, most notably viscosity, conductivity, diffusivity, Li transference number, Li desolvation energies, activation energies, and other terms related to concentration polarization (which alters local transport properties near electrode surfaces). This led to identifying a suite of XFC electrolyte candidates for use in XCEL-designed cells having NMC cathodes and graphitic anodes. The electrolytes are designed to achieve improved transport properties (versus the baseline electrolyte) to mitigate concentration polarization effects, decrease Li plating at the anode, improve permeation of electrolytes through the electrode materials, and stable, low-impedance solid-electrolyte interphase (SEI) films. Based on AEM prescreening, National Renewable Energy Laboratory (NREL) cell modeling determined critical cell performance metrics, concentration polarization profiles, and whether conditions developed during XFC would likely result in Li plating. Best electrolyte candidates from this synergistic set of modeling then proceeded to testing cells.

Figure 1 (a,b) compares electrolyte B26 (EC: DMC: DEC: EP: PN (20: 40: 10: 15: 15, mass) w/ (3%VC, 3%FEC) + $LiPF_6$) with the baseline Gen2 (EC-EMC + $LiPF_6$). B26 sustains a greater fraction of the 6C (10-minute) charge at a constant-current (CC) condition. B26 also produces more consistent cycling performance, indicating less aging compared to Gen2. B26 has also shown less Li metal plating.

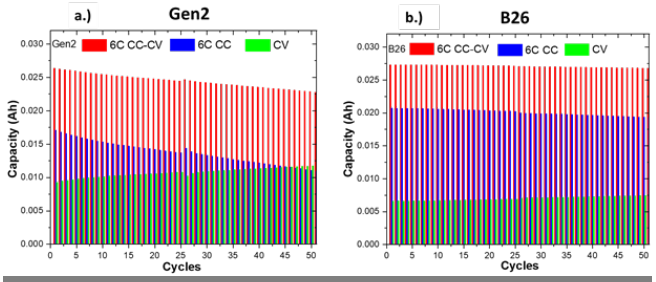

Figure 1. Comparison of Gen2 (a) versus B26 (b) electrolytes in cells with NMC 532 cathodes and graphitic anodes (Argonne National Laboratory Cell Analysis, Modeling, and Prototyping Facility pouch cells).

2021 U.S. DRIVE Highlight

Machine Learning Enabled Rapid Detection of Lithium Plating During Extreme Fast Charging

A machine learning enabled decision tree has been developed, which can rapidly identify lithium plating during extreme fast charging and other use conditions.

Idaho National Laboratory

Extreme fast charging (XFC) is a critical advancement for faster adoption of electric vehicles (EVs). For cells undergoing XFC, a critical failure mode is lithium (Li) plating on the negative electrode. When plating occurs, it can shorten the life of a cell, increase the likelihood of cell failure and also increases cell-to-cell variability, which makes battery management and control more difficult. Recently a team at Idaho National Laboratory (INL) developed a rapid, machine learning-based classification framework that allows researchers, EV manufacturers, and cell developers to rapidly classify if a cell is experiencing Li plating during XFC.

The INL team used a combination of electrochemical (EC) signatures obtained from graphite/NMC532 cells during each cycle, including coulombic efficiency, capacity loss, voltage at the end of the rest period after charging, and the differential voltage (dV/dt) signature at rest after charging. Using data collected from the suite of EC signatures made it possible to identify Li plating 4x earlier than a human user. To facilitate the rapid identification of Li plating for multiple charging protocols, the team constructed a decision tree, based on logistic elastic net analysis that could identify Li plating for different charging conditions and then verified the presence of Li plating using 30 optical images.

Key advantages from this work are that early identification of plated Li shortens several key development and deployment aspects. First by identifying plating in the first 25 cycles it is possible to evaluate different cell designs and charge protocols more quickly. The framework also allows a streamlined approach that can be used to differentiate between Li plating and more standard solid electrolyte interphase (SEI) growth. The ability to make this distinction early might allow manufacturers to build battery packs with less cell-to-cell variation, which enhances overall pack performance. Lastly, early identification of Li plating serves as a key safety feature which can notify consumers or manufacturers early if problems within the battery pack are emerging.

This method will be applied to the newly built graphite/NMC811 cells to be studied in the next phase of the fast charge lab program.

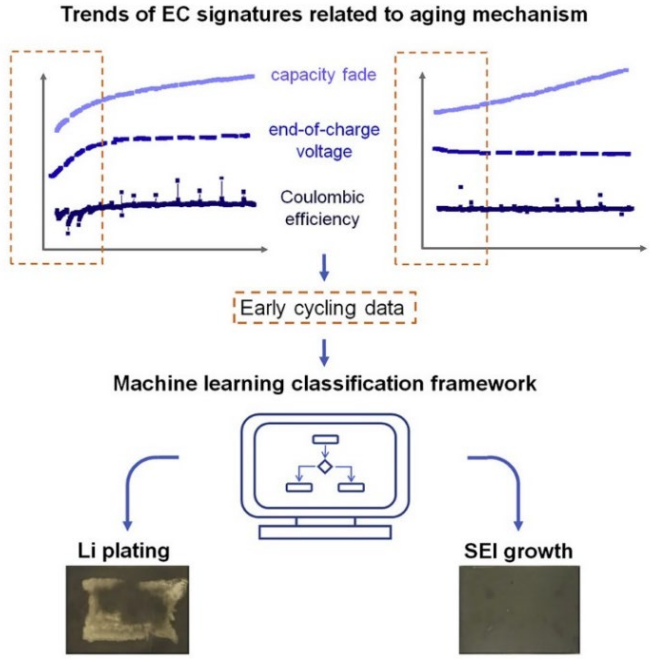

Figure 1. Example of different EC signatures that can be fed into the machine learning classification framework for the early detection of Li plating.

2021 U.S. DRIVE Highlight

Improved Cycling of Cobalt-Free Disordered Rock-Salt Cathodes Via Fluorination

A highly fluorinated disordered rock-salt cathode based on cost-effective and earth-abundant manganese and titanium exhibits excellent energy and cycling performance.

Lawrence Berkeley National Laboratory

Development of new cathode materials with higher performance and lower cost is needed to further enable the commercialization of electric vehicles. Conventional layered oxides are the dominant cathode in commercial lithium (Li)-ion batteries for high-energy applications. However, layered cathodes contain a large amount of expensive and scarce transition metals (TM) (i.e., cobalt [Co], nickel [Ni]), presenting a challenge to their commercdialization.

The recently developed Li-excess cation-disordered rock-salts (DRXs) have received significant interest as they are Co/Ni-free and can be made from cost-effective and earth-abundant TMs. The structural flexibility of DRXs substantially lessens the elemental constraints and enables the incorporation of a wide range of TMs as well as fluorine anions (considered enabling for high voltage operation) in the crystal lattice (Figure 1a). Such a large chemical space opens up the opportunities to search for improved and less expensive cathode materials.

Researchers at Lawrence Berkeley National Laboratory have synthesized a fluoridated manganese (Mn)-titanium (Ti) DRX cathode, $Li_{1.2}Mn_{0.6}Ti_{0.2}O_{1.8}F_{0.2}$, via a solid-state reaction. These Mn and Ti TMs present distinct advantages in cost and resource sustainability compared to their counterparts (e.g., Co, Ni) in conventional layered and other DRX analogs (Figure 1b). As shown in Figure 1c, $Li_{1.2}Mn_{0.6}Ti_{0.2}O_{1.8}F_{0.2}$ delivers an initial capacity of 233 mAh/g (754 Wh/kg, comparable to NMC 811) when cycled between 4.8 and 1.5 volt (V), using 1M $LiPF_6$ EC:DMC. Moreover, this material exhibits stable cycling with over 90% capacity retention after 200 cycles. The excellent cycling stability of this DRX cathode is attributed to the partial fluorination of the oxygen lattice, which increases the content of redox-active Mn and facilitates the utilization of more reversible Mn redox during electrochemical cycling. This material experiences a local structural rearrangement during early cycles before exhibiting a stable voltage upon extended cycling (Figure 1d, e). This early change in voltage profile may present an implementation challenge and researchers will investigate this in future studies. These recent advancements demonstrate a great promise to develop cost-effective DRX cathodes with enhanced capacity and retention for high-energy Li-ion batteries.

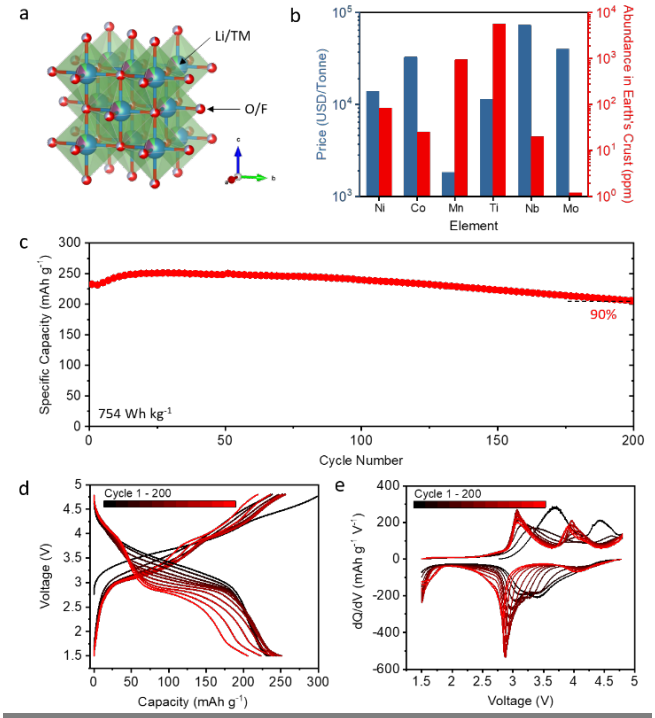

Figure 1. Battery performance of a highly fluorinated DRX, $Li_{1.2}Mn_{0.6}Ti_{0.2}O_{1.8}F_{0.2}$. (a) Crystal structure, (b) price and abundance of selected transition metals, (c) specific capacity, (d) voltage profiles, and (e) differential capacity plot. DRX cell is cycled at 16 mA g^{-1} within 4.8 and 1.5V.

2021 U.S. DRIVE Highlight

Optimizing High-Energy Electrodes

High loading, commercially relevant cathodes were fabricated with just 1.2% binder and 0.8% conductive carbon that cycle as well as electrodes with 3x the amount of those inactives. The electrodes with lower amounts of inactive components require less solvent and hence less drying energy.

Lawrence Berkeley National Laboratory

Researchers at Lawrence Berkeley National Laboratory (LBNL) are studying the manufacturing processes of today's lithium (Li)-ion battery industry by translating them to a bench scale to understand how the processing steps impact cell performance. They hope to reveal how the processing steps dictate exactly where the inactive components (i.e., binder and conductive carbon, needed to hold the electrode together and provide electronic conduction, but these do not store Li ions) are needed to make an electrode that performs as well as electrodes fabricated with excess levels of inactive components. With this detailed information, U.S.-based companies can introduce faster and cheaper methods of Li-ion battery production.

First, the researchers investigated the impact of lowering the total carbon and binder content from a total of 7.2% to 2%. The viscosity of the slurry is critically important to the quality of the cast films and the viscosity is strongly dependent on the carbon content (Figure 1.) In other words, less carbon requires less solvent for a given viscosity. Thus, reductions in carbon result in less solvent and hence less energy needed for drying the electrode slurry. With lower amounts of inactive materials, the importance of the mixing order becomes even greater. One needs to mix the carbon and active material together first, otherwise, the active material can be ground down to a non-optimum small particle size in the absence of the carbon.

Through optimized processing steps, the investigators produced electrodes of different active material contents starting from 92.8 % up to 98 % actives, and tested them in half cell coin cells, Figure 2. The cathode—loading was 5 mAh/cm², approximately 20% higher than commercial cell electrodes.

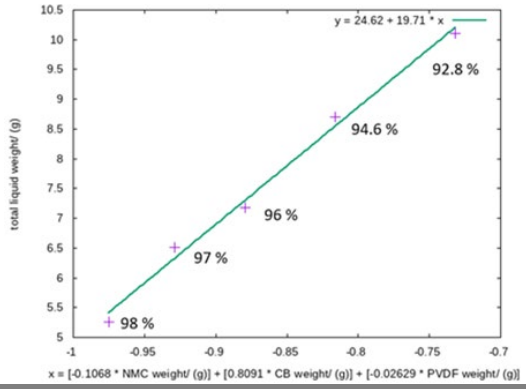

Figure 1. Plot of the weight of solvent in a slurry versus a correlation of the weights of the three solid components of active material (NMC), carbon, and polymer binder as indicated on the abscissa (obtained via ML). There is a strong positive correlation to carbon, weak negative correlations to NMC, and almost no correlation to binder content. Crosses indicate solutions that result in laminates of the highest quality.

The low carbon and binder content leads to very compact electrodes (i.e., higher energy density) that require half the solvent content and hence half the energy for drying the low active material electrodes.

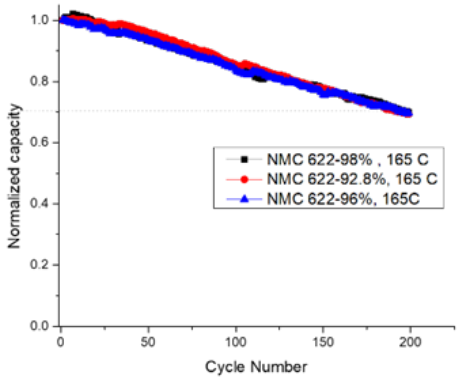

Figure 2. Cycling data of three cells of the same loading prepared with three different levels of inactive materials (active material content indicated in legend). All three electrodes were dried at 165°C.

2021 U.S. DRIVE Highlight

Stable Nickel-Rich Single Crystal Cathode Materials Synthesized with Fast-Charge Capability

In this work, we developed synthetic approaches to produce morphology-controlled NMC single-crystals for superior cycling performance under fast-charge conditions.

Lawrence Berkeley National Laboratory

Nickel (Ni)-rich LiNixMnyCo1-x-yO_2 (NMCs, x ≥ 0.8) are currently the most promising cathode materials for high-energy lithium (Li)-ion batteries. Conventional NMCs are polycrystalline (PC) aggregated particles consisting of a large number of grains in random orientations. As both Li+ diffusion and volume expansion/contraction occur anisotropically upon charge/discharge, this causes torturous Li+ diffusion pathways and nonuniform Li concentration inside the particle, leading to stress and strain and the eventual cracking of the particles. In addition, the newly exposed surface area from cracking can cause parasitic reactions with the electrolyte. These issues are greatly exacerbated with increasing current density, resulting in rapid capacity fade and impedance rise under fast-charge conditions. Hence, design and development of Ni-rich NMC particles with morphology optimized for the fast-charge application is essential.

Our previous studies established fundamental relationships between particle surface properties, particularly surface facets, and cycling stability. This led to the development of single-crystal (SC) NMC cathodes with reduced oxygen release and minimized side reactions under high-voltage operations, enabling excellent performance in high-energy cells. In this work, we prepare Ni-rich NMC single-crystals with morphology and surface orientation optimized for Li transport properties. As an example, studies carried out on $LiNi_{0.8}Mn_{0.1}Co_{0.1}O_2$ (NMC811) single crystals (referred to as SC811) with ~1 µm size and predominately (104)- surface are shown in Figure 1, along with the comparison with a commercial polycrystalline sample (referred to as PC811). After 100 cycles, extensive cracking along the internal grain boundaries is clearly visible in the PC sample, whereas the SC particles remained nearly unchanged morphologically after cycling at 1C or even 6C rate. At the same rate, better cycling stability is achieved on the SC sample. Moreover, while both cathodes delivered similar charge and discharge capacities at 0.1C, the SC cathode significantly outperformed the PC counterpart at higher rates such as 10C. The performance improvement is attributed to the more desirable (104) surface facets for Li transport and better cracking resistance in the SC sample. Although the SC particles are much smaller than the PC, which can in itself provide significantly better high rate performance for the SC particles, the same cracking issue has been seen in multiple smaller PC samples and preferentially using the faster 104 facets results in better rate.

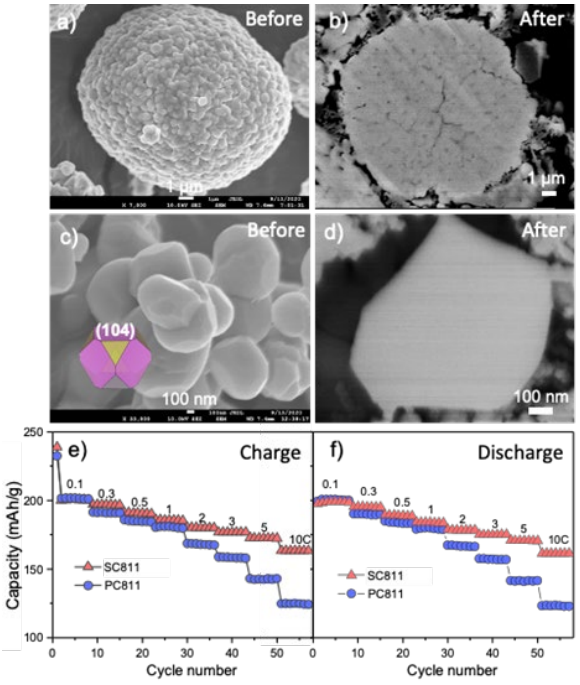

Figure 1. a-d) scanning electron microscopy images of PC (a, b) and SC (c, d) NMC811 before (a, c) and after (b, d) cycling. Enhanced cracking resistance in SC is clearly shown. e-f) Electochemical testing confirms superior charge and discharge rate capability of SC.

2021 U.S. DRIVE Highlight

Model-Based Optimization Improves Fast-Charging

Electrochemical models inform enhanced design for thick-electrode lithium-ion batteries that support extreme fast charge.

National Renewable Energy Laboratory, Argonne and Idaho National Laboratories

Electric vehicles (EV) should 'refuel' in 10-15 minutes to help increase market adoption. Today's thin-electrode lithium-ion (Li-ion) batteries can be charged in less than 15 minutes; however, those cells are 20% less energy-dense and may cost more than thick-electrode cells in $/kWh terms. Thicker electrode cells, appropriate for EVs, usually struggle to support fast charge and often suffer reduced life when fast charged. DOE's eXtreme Fast Charge Cell Evaluation of Li-ion Batteries (XCEL) program aims to improve the fast-charge performance and cycle life of low-cost thick-electrode EV cells.

The XCEL team used a combination of prototyping, characterization, diagnostics, and modeling to understand the performance limits and degradation of graphite/nickel-manganese-cobalt cells under fast-charging conditions. Multi-scale electrochemical models coupled with testing and diagnostics suggested design improvements.

For faster transport of Li^+ ions through the electrode, the team prototyped a dual-layer-anode. Graphite active material is tightly packed into the back of the electrode (near the current collector) to improve energy density. The front of the electrode is more porous, allowing for fast transport, and uses high-surface-area particles to delay Li plating. The team used microstructure models to optimize the amount of binder and electronic-conductive (CBD) additives in the electrode to provide enough electron conduction without blocking the electrolyte pores.

Electrochemical models also guided the selection of a new separator that, despite being thicker, achieved faster electrolyte transport due to its higher porosity. First, the team tested a baseline thin-electrode cell. With low energy density, this cell charges quickly, accepting 79% of its capacity in a 10-minute charge before hitting a 4.1 volt (V) limit. Next, the team tested a moderately thick electrode cell. This cell exhibited a 30% higher energy density, but its 10-minute charge acceptance dropped to 38%. With the optimized carbon/binder recipe, new separator, and an improved electrolyte formulation developed through a separate modeling effort (B26), the modified cell's charge acceptance increased from 38% to 73% and still maintained 230 Wh/kg, appropriate for EV cells (Figure 1). Finally, the baseline cells plated Li in the first 10 cycles, while the final optimized cell has shown no sign of Li plating after 175 cycles to date.

In addition, models optimized the charge protocol by replacing slow-rate constant voltage with a ramped-voltage step that charges faster and avoids Li plating.

The physics-based models used here enable fast use of knowledge with different cell designs, chemistries, and protocol constraints. Next, the XCEL team is applying these methods to achieve 10-minute charge acceptance and 1000-cycle lifetime with thick electrode (255 Wh/kg) cells.

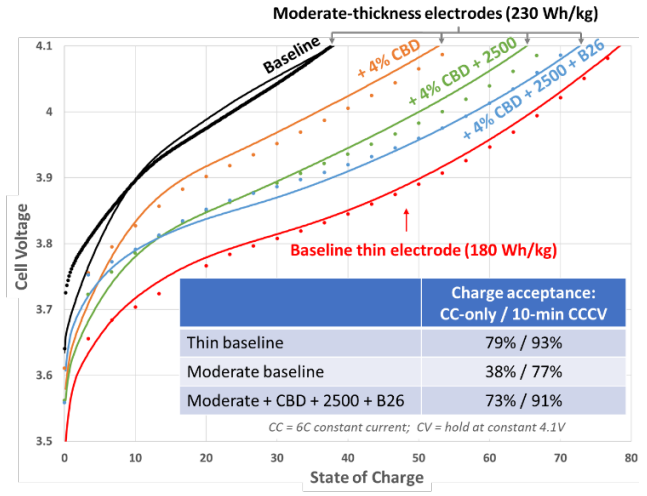

Figure 1. Fast-charge results of prototype single-layer pouch cells (symbols) compared with model predictions (lines).

2021 U.S. DRIVE Highlight

Aqueous Sequential Separation of Electrodes from Used Lithium-Ion Batteries

An aqueous sequential separation process has been developed to recover both electrode materials and current collectors using buffer solutions and surfactant additives in a single pot.

Oak Ridge National Laboratory

Direct recycling of lithium-ion (Li-ion) batteries aims to recover the valuable components in a lithium-ion cell, including black mass (e.g., active cathode materials and graphite), copper (Cu) foils, and aluminum (Al) foil current collectors. Electrode materials are tightly adhered to metal current collectors through binders, increasing the challenge of recovery. The separation challenge is further increased because cathode and anode are mixed after shredding. To reclaim the most valuable active cathode materials with high purity for subsequent regeneration, separation of electrode materials from their current collectors, as well as of anode from cathode, is required.

Scientists at Oak Ridge National Laboratory (ORNL), as part of the ReCell program, have developed a low-cost and selective two-step process to recover electrode materials and current collectors from spent Li-ion batteries. During the first step, a solution containing an aqueous potassium phosphate buffer solution with a constant pH at 5.0 is selected to delaminate anode films from copper foils at room temperature and prevent Al from dissolution (Figure 1). At this stage, the graphite is separated while the cathode films stay intact due to the strong adhesion of the binder to the Al foil. In the second step, a surfactant (sodium dodecyl sulfate, Triton™ X-100) is added to the mix of copper foils and cathode electrodes in the presence of the buffer solution to peel off the cathode films from the Al foil by both reducing the surface energy and weakening the adhesion (Figure 1). Thereafter, the cathode films and current collectors (Al and Cu) are separated due to the difference of density.

By avoiding use of complex separation processes, the aqueous sequential separation method alone could fulfill the goal of reclaiming higher-purity materials, making recycling more profitable. Techno-economic analysis with EverBatt modeling developed by Argonne National Laboratory shows that selling recovered metal foils alone could recoup all recycling processing expenses, including those of the developed sequential separation method, suggesting attractive profit motive. After direct regeneration, the cost of recovered cathode materials is about 50% less than that of virgin cathode production. Additionally, this novel process reduces greenhouse gas emissions by 60% compared with traditional recycling processes. Overall, the aqueous sequential separation is a potential sustainable electrode recovery process that may advance battery recycling and secures the domestic battery supply chain.

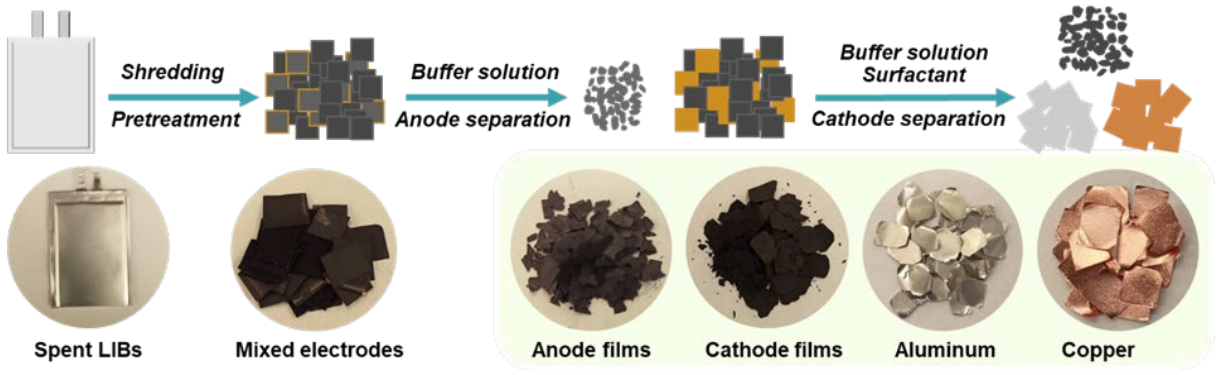

Figure 1. Flowchart of the aqueous sequential separation process to recover cathode films, anode films, copper, and aluminum foils.

2021 U.S. DRIVE Highlight

Scalable Method to Resolve Materials Joining in Solid-State Batteries

Electrochemical pulsing overcomes contact impedance and could enable a breakthrough in solid-state batteries.

Oak Ridge National Laboratory

Scientists at Oak Ridge National Laboratory (ORNL) have developed a scalable, low-cost method to improve the joining of materials in lithium (Li) metal-based solid-state batteries, potentially resolving one of the major challenges in this energy storage technology.

Solid-state batteries use a safer architecture featuring a solid-state electrolyte instead of the flammable organic solvent-based liquid electrolytes in today's Li-ion batteries. A successful solid-state battery, if it uses a Li metal anode, could provide a large increase in energy density relative to Li-ion batteries, enabling electric vehicles with improved driving range, for instance.

One of the challenges in manufacturing solid-state batteries is the difficulty of getting materials to properly join and remain stable during repeated cycles of charging and discharging. Scientists studying this characteristic, known as contact impedance growth, have so far focused on applying high pressures and other mechanical methods.

In contrast, ORNL researchers used an electrochemical pulse to reduce contact impedance, eliminating the voids that form when joining layers of Li metal with a solid electrolyte material: in this case the ceramic garnet-type electrolyte LALZO ($Li_{6.25}Al_{0.25}La_3Zr_2O_{12}$) (Figure 1). Applying short, high-voltage pulses both during formation and following cycling led to increased contact at the interface of the materials while resulting in no detrimental effects.

This work complements earlier work carried out by scientists at ORNL that leveraged similar electrochemical principles to reduce dendrite formation and partially recover degraded solid-state batteries, leading to extended battery life. The non-destructive, low-cost pulsing method results in a local heat-generating current that surrounds the Li metal-encased voids and causes them to dissipate. The team repeated experiments and advanced characterization of the materials, which revealed the battery components did not degrade after applying the pulsing method (Figure 1). This approach could be scaled to allow the solid-state battery to be removed and refreshed, potentially restoring significant accessible capacity.

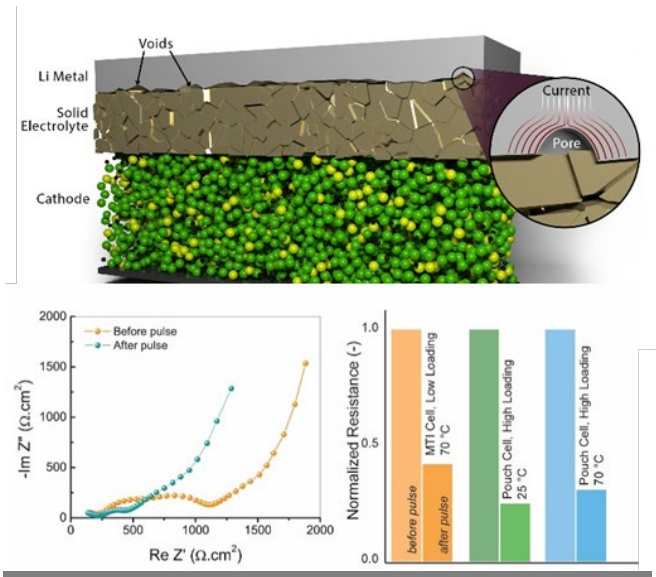

Figure 1. Principle and results of electrochemical pulse method to improve the contact between layers of materials in solid-state batteries.

2021 U.S. DRIVE Highlight

Charge Protocol for Reactivating Isolated Lithium Metal for Extended Life and Fast Charging

Developed a method to reactivate isolated Li metal filaments in Li-metal batteries under normal usage and further found benefits to lithium-ion batteries under fast charge usage using a similar protocol.

Stanford University and SLAC National Accelerator Laboratory

The increasing demand for high-energy batteries has encouraged the development of lithium-(Li) metal batteries. Unfortunately, the current Li anode batteries often exhibit short cycle life due to the continuous generation of solid electrolyte interface and isolated Li (i-Li). The formation of i-Li during cycling leads to a significant capacity loss in Li batteries. Since i-Li loses electrical connection with the current collector, it has been considered electrochemically inactive or "dead" in batteries. Contradictory to this presumption, we discover that i-Li is highly responsive to battery operations because of their dynamic polarization to the electric field in the electrolyte (Figure 1a). Simultaneous Li deposition and dissolution occur on two ends of the i-Li, leading to its spatial progressions toward cathode (anode) during charge (discharge). In the meantime, the migration rate of i-Li is faster under high current densities.

To promote the reactivation of i-Li during battery operations (that is, to reconnect it to an electrode), we incorporated a short fast-discharging step after the conventional charging protocol (Figure 1b). During this step, i-Li grows toward Li anode, and some of it can re-establish electrical connection with the electrode, participating in the subsequent electrochemical processes. The benefit of this activation step in Li-metal batteries becomes more pronounced after 30 cycles when the cell without activation starts to exhibit fast capacity fade (Figure 1c). In sharp contrast, the cell with activation maintains stable cycling for more than 40 cycles (versus 30 cycles) and a much slower degradation process afterward, attributed to the partial recovery of "dead Li." Moreover, the formation of i-Li also occurs in Li-ion batteries, especially during fast-charging. Graphite/NMC532 cells were charged at 4C, followed by a constant voltage charge until the current decreased to 1C, and discharged at 0.5C at 25˚C. The depth of discharge is 84%. With the modified protocol, the cell can charge to 80% capacity in 15 minutes while losing only 5% of its capacity after 300 cycles (Figure 1d). In comparison, the control cell loses 20% capacity after 300 cycles.

In this study, we discovered a mechanism of isolated Li metal filaments in Li-metal batteries and developed a protocol to reactivate them. We achieved an extended lifetime in Li-metal batteries and found that a similar protocol could also provide fast charging improvement in Li-ion batteries.

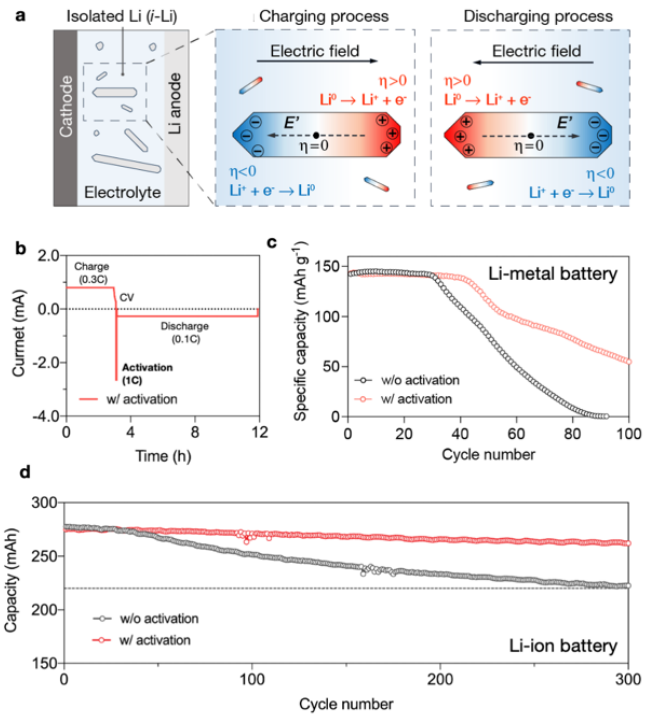

Figure 1. a. Illustration of the dynamic polarization of i-Li under the electric field. b. Modified charging protocol for Li-metal battery. Specific capacity of c. Li-metal batteries and d. Li-ion batteries with/without activation steps.

Fuel Cells

2021 U.S. DRIVE Highlight

Advanced Electrode Ionomer Leads to Increased Performance and Durability

Improved understanding of high-oxygen-permeability ionomer and how it could enhance efficiency and life of fuel cells will lead to future advancements.

Carnegie Mellon University

In a proton exchange membrane fuel cell (PEMFC), polymer electrolyte, or ionomer, is blended with the catalyst in the electrode to transport protons to electrochemical reaction sites on platinum (Pt) nanoparticles throughout the electrode. At high load operation where high oxygen and proton local flux to the Pt surface is required, noticeable voltage loss has been observed. It was shown that replacing the flexible tetrafluoroethylene backbone of a conventional perfluorosulfonic acid (PFSA) ionomer with a more rigid backbone, using a steric hindrance group, could mitigate this voltage loss. This novel ionomer was termed high-oxygen-permeability ionomer (HOPI) (Figure 1a).

Carnegie Mellon University, with team partners Chemours and Ballard Power, performed a comprehensive investigation of the HOPI structure and how it could improve the fuel cell efficiency and durability.

Water uptake and grazing incidence small-angle X-ray scattering measurements indicated that the HOPI forms a more amorphous film with a structure that is less sensitive to water content. Molecular dynamics simulations also suggested reduced compaction of the ionomer at the Pt surface than the conventional ionomer. The more open HOPI structure has a measured oxygen permeability three times higher than the conventional ionomer, ensuring higher oxygen access to the Pt catalyst particles, which leads to higher oxygen reduction reaction activity. Once optimized, cathodes with HOPI showed >50% increased activity and noticeably better high-current-density voltage at low Pt loading. Diagnostics revealed 40% lower local oxygen transport resistance. Lower local oxygen transport resistance is particularly beneficial for extending fuel cell life as the Pt surface area degrades and the local oxygen flux elevates. Evident in Figure 1b, the fuel cell performance of the HOPI cathode is noticeably better after the accelerated stability test than catalysts with the conventional ionomer. This is despite both having a similar level of catalyst degradation.

The project mainly used pure Pt supported on low-surface-area carbon chosen for high durability to demonstrate the benefits of the approach. The team demonstrated key fundamental characteristics of HOP in higher-performing state-of-the-art PtCo alloy supported on high-surface-area carbon, albeit to a lesser degree. HOPI has been shown to improve both performance and durability for Pt catalysts, and further development on alloy catalysts will continue to improve understanding of the HOPI structure and Pt-electrolyte interface.

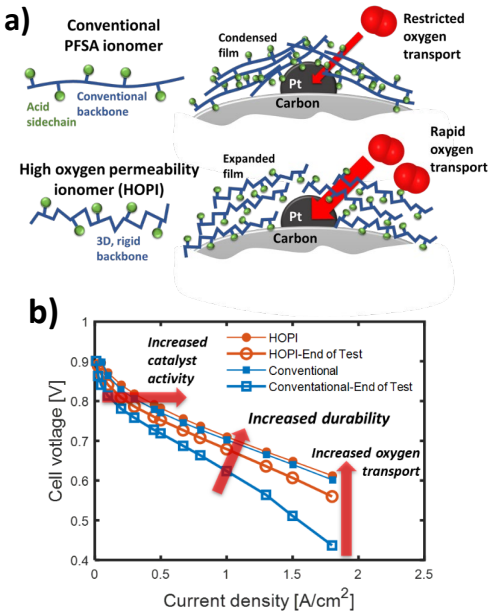

Figure 1. (a) Illustration of Pt and ionomer interface. (b) Fuel cell performance of cathode with HOPI and conventional ionomers at the beginning and end of accelerated stability testing.

2021 U.S. DRIVE Highlight

Ionic Liquid-Based Polymers Improve High Current Density PEMFC Performance

Sulfonated polymerized ionic liquid block co-polymer – Nafion composite ionomers are a replacement for standard Nafion ionomers in the PEMFC cathode.

Drexel University

In a proton exchange membrane fuel cell (PEMFC) cathode, the Nafion polymer electrolyte, an ionomer, is blended with a catalyst to shuttle protons from the membrane to the catalyst surface where they react with oxygen to form water. The Nafion ionomer decreases the catalyst activity and restricts oxygen transport to the catalyst, resulting in significant performance loss, especially at high load. The addition of ionic liquids, which have high oxygen solubility, to the interface between the catalyst and the ionomer can mitigate these losses. However, difficulties associated with integration and homogeneous dispersion of ionic liquids throughout a PEMFC cathode and issues with their wash out from the cathode have limited their application in PEMFCs.

Drexel University, Texas A&M University, and the National Renewable Energy Laboratory have developed a new ionomer that draws on the benefits of ionic liquids and improves on their proton conductivity while preventing wash out. They accomplished this in a block co-polymer with one block providing the proton conductivity, a sulfonated hydrocarbon, and the other block providing the high oxygen solubility, a polymerized form of an ionic liquid (Figure 1). PEMFCs using a composite of the co-polymer ionomer and Nafion show performance far surpassing that of PEMFCs using either the incumbent Nafion or the co-polymer ionomer in the cathode (Figure 2). This performance enhancement has been attributed to reduced blockage of catalyst by the Nafion ionomer, suppressed oxide formation, and enhanced oxygen transport.

An additional benefit of the hydrocarbon-based co-polymer over traditional Nafion, is that it minimizes environmental concerns associated with a fluorinated polymer. Further development of these co-polymer ionomers to improve oxygen permeability and dispersibility, using new ionic liquid chemistries, can eliminate the need for Nafion in the cathode catalyst layer and bring this technology one step closer to commercialization.

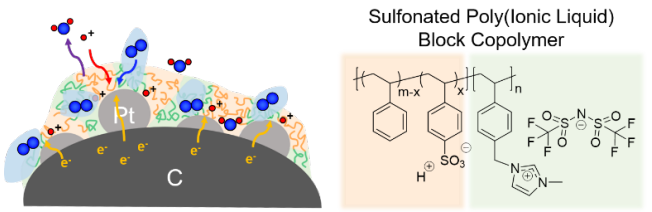

Figure 1. Left. Schematic representation of the interface between the sulfonated poly(ionic liquid) block copolymer (S-PILBCP) and a Pt/C catalyst. Right. Structure of S-PILBCP.

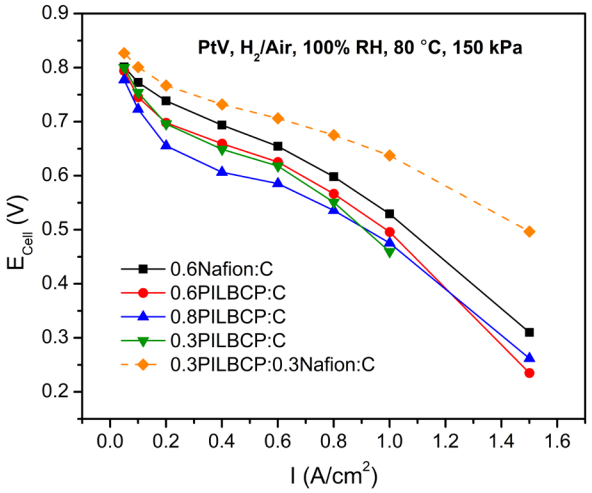

Figure 2. Hydrogen (H_2)/Air polarization curves for MEAs with Nafion, S-PILBCP, and mixed S-PILBCP/Nafion-containing cathode catalyst layers.

2021 U.S. DRIVE Highlight

Durable Catalyst and Membrane Materials for Fuel Cell Electric Vehicles

Durable fuel cell membrane electrode assemblies through immobilization of catalysts and membrane chemical stabilizers.

General Motors

The application of proton exchange membrane fuel cells (PEMFCs) for power generation in medium- and heavy-duty trucks requires highly durable and efficient membrane electrode assemblies to meet the long lifetime requirements (~30,000 hours of runtime or 1 million mile driving distance). This project uses a two-pronged approach to improve the durability of cathode catalysts and membranes used in PEMFCs. These approaches include i) stabilizing platinum (Pt) catalysts via annealing and using metal-oxide anchoring agents on the carbon support, and ii) immobilizing radical scavenging additives within the perfluorosulfonic acid (PFSA) polymer membrane to extend its lifetime.

In 2021, the project team (GM, Pajarito Powder, 3M, and Cornell) demonstrated that annealed Pt shows exceptional durability even after being subjected to extended accelerated stress tests consisting of 90,000 voltage cycles (Figure 1). The non-annealed Pt catalyst features a smaller particle size of ~2 nm that enables better efficiency (i.e., high voltage performance) but poor durability due to rapid loss of surface area. Annealing the Pt catalyst increases the particle size to ~4.5 nm, which enables higher resistance to surface area losses and longer durability. Further, the team developed advanced carbon supports incorporating ZrO_2 nanoclusters to stabilize 2 nm Pt nanoparticle catalysts that show 25% improvement in surface area and kinetic activity retention.

State-of-the-art PFSA membranes utilize soluble cerium-based salts (Ce3+/Ce4+) as radical scavenging agents that impart chemical stability to the membrane. While highly efficient, these cerium salt-based additives are prone to migration during fuel cell operation, leaving Ce-depleted areas of the membrane vulnerable to early failure. To combat this issue, the team developed PFSA membranes with heteropoly acid (HPA) radical scavengers immobilized through direct attachment to the membrane backbone. Durability tests shown in Figure 2 confirm that the HPA immobilized membranes enable improved durability as compared to a membrane without radical scavenging additives.

Ongoing studies focus on integrating the newly developed catalyst and membrane materials to deliver highly durable and efficient membrane electrode assemblies for heavy-duty fuel cell electric truck applications.

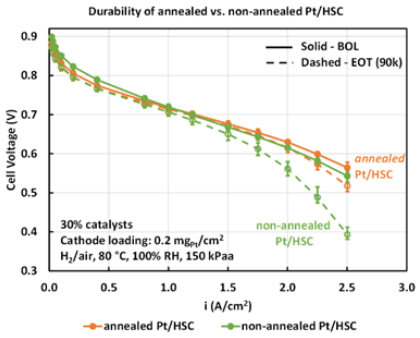

Figure 1. Hydrogen (H_2)/air fuel cell polarization curves showing the high stability of annealed Pt-based catalysts after extended cycling.

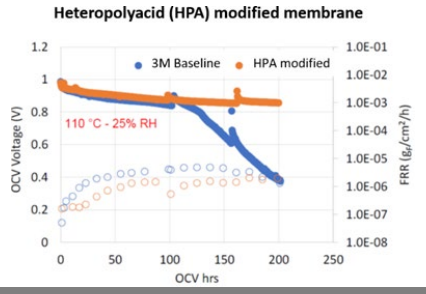

Figure 2. OCV durability tests showing the improved durability of HPA modified membrane.

2021 U.S. DRIVE Highlight

Plant-Based Gas Diffusion Layers for Lower-Cost Fuel Cell Stacks

Low-cost materials and treatments for durable, high performance PEM fuel cells.

Los Alamos National Laboratory

Fuel cell stack cost reduction is needed to enable widespread use of fuel cells in transportation. High-cost materials and processes used in gas diffusion layer (GDL) manufacturing cause GDLs to contribute from 3% to 15% of heavy-duty vehicle stack cost, depending on production volume Strategic Analysis (2021 Hydrogen Program Annual Merit Review, FC163.) The Los Alamos National Laboratory (LANL) team has made progress toward developing lower cost materials and processes, as well as simplifying the GDL manufacturing process.

Substituting traditional polyacrylonitrile (PAN) fibers with plant-based materials allows for lower cost fibers and can reduce or eliminate binder requirements. LANL tested 5 different fiber sources that produced 2 useable GDL papers and 1 GDL fabric. Plant-based fibers enable the use of relatively low (less than 1500°C) carbonization temperatures during processing. These changes could reduce processing and materials costs by 50% and 25%, respectively, according to LANL estimates, leading to an overall stack cost reduction of up to 7%, depending on production volume.

LANL's paper and fabric GDLs achieved equivalent electrical conductivity compared to commercial materials. Subsequent testing of LANL's plant-based GDL (Figure 1) showed similar performance to a commercially prepared GDL. LANL also examined new methods of hydrophobic treatment to improve water management and performance. Rather than using traditional Teflon™ treatment, which can aggregate and reduce porosity, LANL implemented a gas phase hydrophobic treatment that applies an atomic-scale layer of a hydrophobic chemical (Figure 2). The resulting GDL achieved the same level of hydrophobicity as a Teflon™-treated GDL, based on contact angle measurements. Additionally, this gas-phase treatment proved durable, showing minimal change in contact angle after 1000 h of fuel cell operation.

This project has shown the potential for low-cost materials and less expensive processing techniques to yield high performance and durable GDLs. Further development work is required to optimize performance for deployment in vehicle applications.

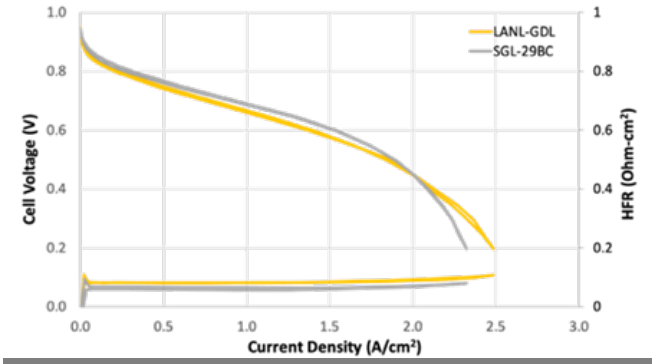

Figure 1. Fuel cell polarization curve comparing the performance of the plant-based LANL GDL to commercially available PAN-based 29BC manufactured by SGL Carbon.

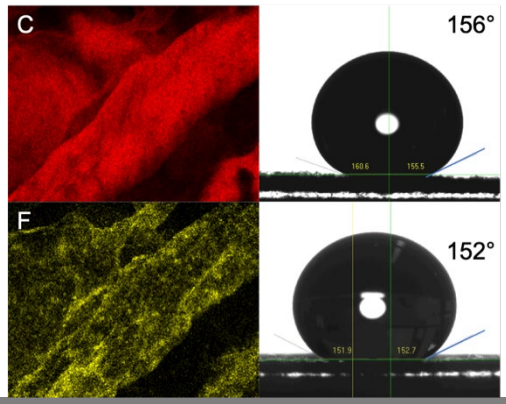

Figure 2. Elemental mapping of LANL GDL showing carbon and fluorine on hydrophobic fibers (top and bottom left). Contact angle measurements on GDL before and after 1000 h of operation in a fuel cell (top and bottom right).

2021 U.S. DRIVE Highlight

Durable and Active Fuel Cell Cathode Catalysts

Nitrogen-doped ordered-intermetallic platinum nickel catalysts demonstrate improved durability while providing the performance benefits of alloys compared to commercially available platinum catalysts.

Million Mile Fuel Cell Truck Consortium

The application of proton exchange membrane fuel cells (PEMFCs) for power generation in medium- and heavy-duty trucks requires highly durable and active electrocatalysts to meet the efficiency and long lifetime targets (~30,000 hours, 1 million mile driving distance). As part of the Million Mile Fuel Cell Truck consortium (M2FCT), Brookhaven National Laboratory (BNL), in collaboration with Los Alamos National Laboratory, has developed and demonstrated a PEMFC cathode catalyst with fuel cell performance and durability exceeding that of a benchmark commercial catalyst.

Platinum is typically alloyed with other transition metals, such as cobalt and nickel, to enhance its performance as a PEMFC cathode catalyst. While traditional platinum alloy catalysts show excellent initial performance, they quickly lose performance due to leaching of the transition metal from the alloy. BNL has developed approaches and synthetic methods to prevent this leaching: formation of a highly-ordered intra-particle arrangement of platinum and nickel (PtNi) (an "intermetallic" rather than random alloy) and doping the PtNi alloy with nitrogen (Figure 1). They have also developed a one-step synthesis procedure that is amenable to manufacturing scales.

Two variations of the BNL nitrogen-doped PtNi catalyst have shown high initial performance and excellent durability in fuel cell tests (Figure 2). The beginning-of-life current density at application-relevant cell voltages (0.8 volt [volt]) of fuel cells using these two cathode catalysts are approximately 55% and 80% higher than those containing a baseline commercial platinum catalyst (Umicore Elyst Pt50 0550), at the same platinum loading.

Maintaining high performance at high cell voltages is of paramount importance for maintaining efficiency and minimizing hydrogen fuel cost over the million mile lifetime of the vehicle. Importantly, the newly-developed catalysts maintained their initial performance better than either a commercial platinum alloy catalyst or the baseline catalyst. After subjecting the fuel cells to accelerated stress tests (AST) designed to simulate the lifetime requirements for the heavy-duty application, the fuel cells containing these two catalysts achieved 79% and 93% higher current densities at 0.8V after the AST versus the fuel cell containing the benchmark Pt catalyst.

Next steps are to further enhance the performance and durability of these catalysts by increasing the nitrogen content and nitriding the catalyst support.

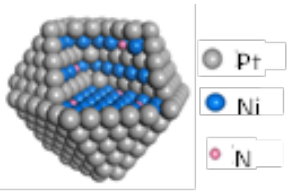

Figure 1. Atomic structure of nitrogen-doped intermetallic PtNi fuel cell cathode catalyst.

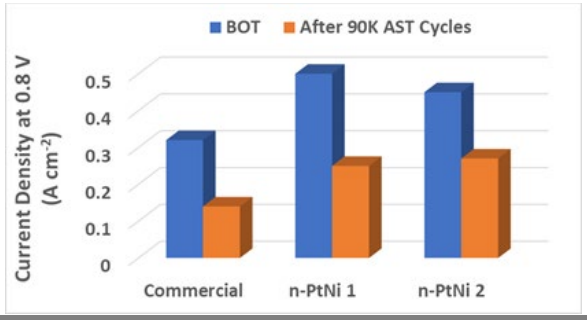

Figure 2. Hydrogen/air fuel cell performance at 0.8V showing the high performance and durability of nitrogen-doped intermetallic PtNi fuel cell cathode catalysts.

New Catalyst Shows Improved Durability and Potential to Meet Heavy-Duty Vehicle Targets

Platinum catalyst with novel support has minimal degradation after 90,000 voltage cycles.

pH Matter

Increasing catalyst durability without requiring large increases in the amount of platinum (Pt) metal is critical to ensuring cost-competitiveness of fuel cell vehicles with incumbent internal combustion engine technology. pH Matter has developed a new catalyst with a support that greatly improves catalyst durability without negatively impacting performance and cost. The catalyst shows potential to achieve the performance and durability targets for the Million Mile Fuel Cell Truck Consortium (M2FCT).

Commercial fuel cell catalysts are supported on carbon particles. pH Matter has developed an in-house carbon support with tailored porosity to restrict movement of the Pt on the surface, decreasing degradation while still allowing the Pt to be accessible to the reactants. In their latest development, they have increased the porosity of these supports from 100-250 m^2/g to 650-750 m^2/g, while keeping most of the pore diameter in the desired range of 50-150 Å.

Catalysts utilizing the pH Matter supports have been integrated into MEAs and subjected to voltage cycling accelerated stress tests. After 90,000 voltage cycles the pH Matter catalyst performance dropped only slightly (20 m volt [mV] at 0.8 A/cm^2), and experienced smaller decreases in performance than a commercial standard (Figure 1). The pH Matter catalyst performance came very close to meeting the preliminary targets for performance and durability established by the DOE, achieving 99% of the high-power performance target at 0.7V after the accelerated stress test, while losing 60% less mass activity and 33% less electrochemical surface area than a commercial catalyst, all with lower Pt content than the DOE target for fuel cells for heavy-duty vehicles. This work suggests that with further electrode optimization, catalysts using pH Matter's support will meet the M2FCT targets.

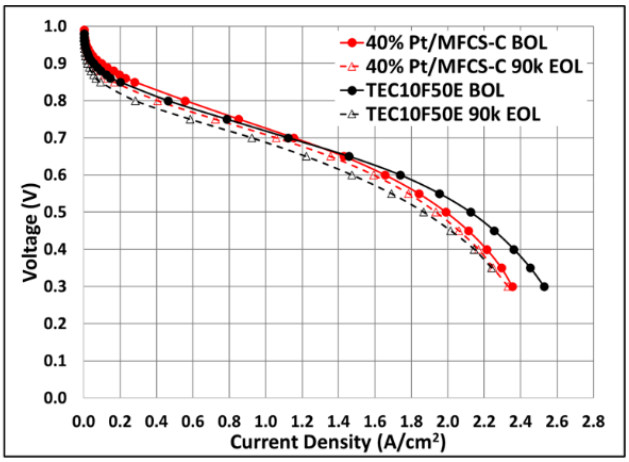

	Loading (mg/cm^2)	BOL Mass Activity (mA/mg)	% Mass Activity Loss	ECSA Loss	ΔV @ 0.8 A/cm^2 (250 kPa, 100%RH)	EOL A/cm^2 @ 0.7V (250 kPa, 100%RH)
Project Targets		440	<40%	<40%	<30 mV	1.07
MFCS-C	0.2	609	44%	38%	20mV	1.06
TEC10F50E	0.2	384	74%	61%	30 mV	0.92

Figure 1. Performance comparison of commercial catalyst (TEC10F50E) and pH Matter catalyst (40%Pt/MFCS-C) at BOL and after 90,000 potential cycles from 0.6 to 0.95V.

Materials

2021 U.S. DRIVE Highlight

Laser Powder Bed Fusion Parameter Development for Novel Steel and Aluminum Powders Using *In-Situ* Synchrotron Imaging and Diffraction

Enabling the use of lower cost, high performance, lightweight alloys for additive manufacturing.

Argonne National Laboratory and General Motors

Weight-reduction requirements in the automotive industry have led to an increased interest in the use of metal additive manufacturing (AM) in vehicle-body structures and powertrain components. Metal AM processes using laser powder-bed fusion (LPBF) and direct energy deposition have been demonstrated as viable methods for producing these metallic components. Establishing the optimized AM printing parameters (laser power, speed, etc.) for specific materials is a long and costly process that typically relies on trial-and-error approaches. This uncertainty translates to increased process-parameter development time and a barrier to introducing new alloys for use in additive manufacturing.

Argonne National Laboratory has developed advanced *in-situ* characterization techniques (Figure 1) to observe metal AM process in 'real-time' utilizing high-energy X-ray synchrotron capabilities, which enables a unique combination of *in-situ* x-ray imaging, temperature measurement, and microstructural phase-transformation diffraction monitoring during the laser additive process. This provides a rapid pathway for relating printing parameters to resulting print quality, and greatly reduces the time and cost for material conception to printing fully dense components in a manufacturing process.

General Motors (GM) has teamed with Argonne, through a LightMAT consortium project, to utilize this capability to establish printing parameters for advanced steel- and aluminum-based alloys. These high performance and lower cost alloys, developed by GM, are suitable for powertrain components and have demonstrated up to 45% weight reduction for specified components. So far, the project team has successfully completed *in-situ* characterization of four alloys including an ultra-high strength low alloy steel, a copper precipitation strengthened non-stainless steel, a high-temperature aluminum alloy, and high-conductivity aluminum alloy. This includes a parametric study of printing parameters with *in-situ* measurements of top surface temperature profiles and related X-ray images showing sub-surface defect formation, such as porosity. Parameter sets observed to exhibit stable gaussian vapor cavities using *in-situ* X-ray imaging have translated to high-print densities using commercial additive manufacturing systems. The high-fidelity temperature measurements along with the measured melt pool geometries have led to the development of a simplified laser-material model that GM can use to detect and predict defect formation during component manufacturing.

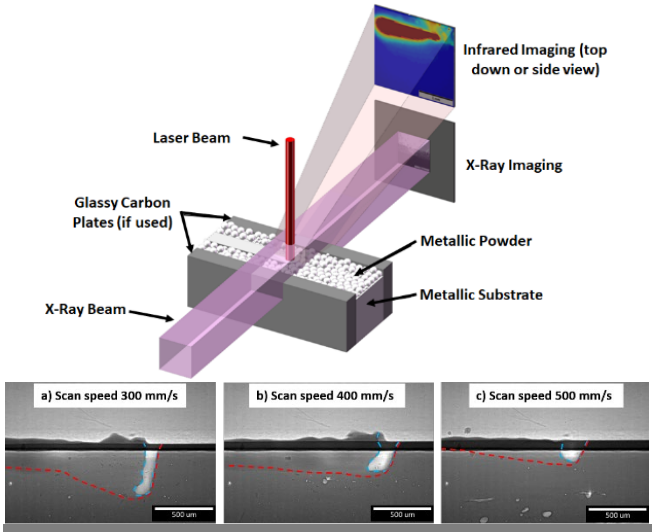

Figure 1. Top. Schematic of experimental setup for *in-situ* x-ray and IR observation of the LPBF experiments. Bottom. Sideview X-ray images of the melt pool and vapor depression in iron/copper alloy processes at 350W laser power and different scan speeds (a) 300 mm/s, (b) 400mm/s and (c) 500 mm/s. Red dashed line outlines melt pool, blue dashed line outlines vapor depression; laser translates left to right.

2021 U.S. DRIVE Highlight

Functionally Designed Ultra-Lightweight Carbon Fiber Reinforced Thermoplastic Composites Door Assembly

Manufacturing the world's first thermoplastic composites door.

Clemson University

One of the most promising ways of increasing fuel economy/range is by decreasing vehicle weight by using lightweight composites.

Researchers at Clemson University are manufacturing the world's first thermoplastic composites door to replace a current baseline steel door (Figure 1). This approach differs from existing thermoset-based composites that are used in industry as it is more sustainable, requires lesser capital costs, and has reduced cycle times. The thermoplastic door was designed to meet the following objectives when compared to the baseline steel door:

- 42.5 % Reduction in weight
- Meet all baseline crash targets of baseline steel door
- 100 % recyclable
- Manufacturing technology must be scalable to 20,000 vehicles per year.

Researchers utilized a forming process using match metal dies to reduce capital costs for automakers, as the infrastructure required overlaps with existing stamping lines. This achievement was made possible by the creation of a simulation pathway that uses proprietary user defined subroutines and commercial finite element analysis (FEA) software to couple manufacturing process and mechanical performance. The pathway is designed to predict changes in composites microstructure such as thickness variation, fiber orientations, and residual stresses and couple these to mechanical simulation to help predict mechanical performance. The pathway was able to capture these changes with less than ~ 4% error.

The pathway was experimentally validated at a subcomponent level with quasi static and dynamic experiments. Subsequently, full scale vehicle crash simulations were carried out and will be validated this year.

Lastly researchers developed a comprehensive parametric cost model and factory layout simulations using commercial software for this process to help predict the cost of manufacturing these thermoplastic composites doors to accelerate industrial adoption.

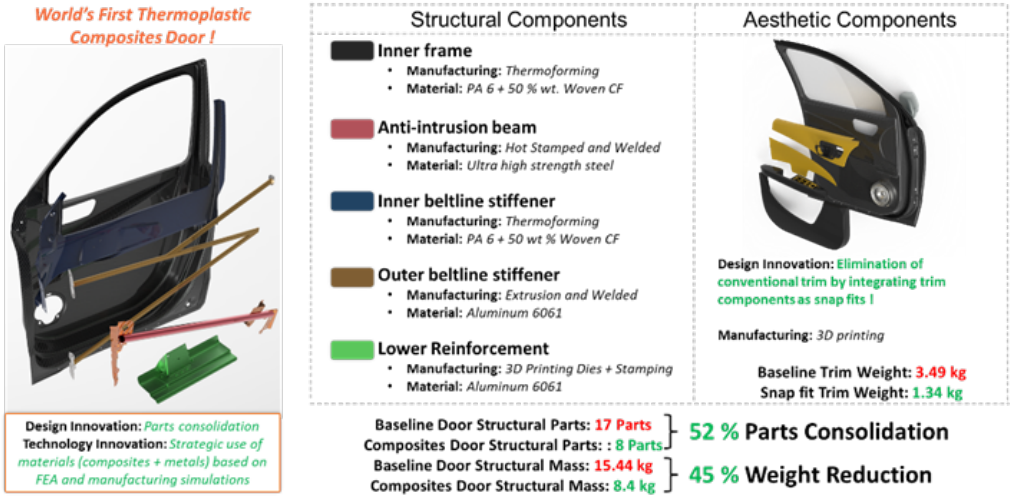

Figure 1. Overview of structural and aesthetic components of world's first thermoplastic composites door assembly.

2021 U.S. DRIVE Highlight

Development of a Novel Magnesium Alloy for Thixomolding of Automotive Components

New alloy improves strength, ductility, and manufacturability for high quality lightweight cast components.

Stellantis, Oak Ridge National Laboratory, and Leggera Technologies

Magnesium alloy die-castings are being increasingly used in the automobile industry as a means of providing cost-effective mass reduction, especially in systems where multiple components can be integrated into a single thin-wall die-casting. However, Mg die-castings suffer from quality issues including variability in dimensional accuracy, part-to-part variation in mechanical properties, and porosity in the final part, which has limited the continued growth of die-cast components in the automobile industry.

An alternative to die-casting is thixomolding. While the die-casting process fills the mold at high speeds with the alloy in the completely molten state, the thixomolding process fills a mold with a thixotropic alloy in a semi-solid slurry state at a temperature between the liquidus and solidus temperatures. Advantages of the thixomolding process include a finer grain structure; lower porosity; improved dimensional accuracy; improved part-to-part consistency; improved mechanical properties, particularly ductility in the component; the ability to reduce wall thickness for mass savings; and longer tool life due to lower process temperatures.

Although thixomolding offers improved mechanical properties over die-cast Mg components, the mechanical properties obtained in the thixomolded parts are still not sufficient to broadly enable application in components where both strength and ductility are key requirements (e.g., crash critical components exposed to high-impact velocities and powertrain or chassis components subjected to high levels of cyclic loading) since the alloys used in the process are optimized for die-casting.

The project team aimed at the development of new alloys for use in the thixomolding process with the potential to balance three major characteristics—ease of processing, strength, and ductility. Using computational modeling, the team identified an initial set of alloys with targeted liquidus and solidus temperatures and the solid-liquid range (Figure 1). Selected alloys have been cast in laboratory scale heats and liquidus, solidus, and the solid-liquid range, and tensile properties were measured and found to meet the targeted values. The team is now scaling up two down-selected alloys to produce larger industrial scale heats which will be used to fabricate prototype thixomolded tire carriers (Figure 2).

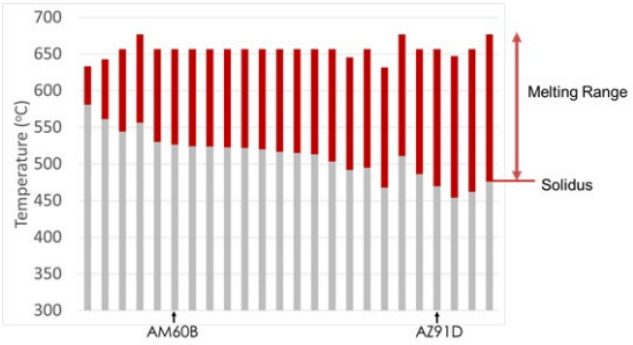

Figure 1. Schematic showing calculated values for liquidus, solidus, and melting range of candidate alloys AM60B, AZ91D, and selected developmental alloys.

Figure 2. Image of spare tire carrier to be fabricated by Leggera Technologies using two scaled up, developmental alloys.

2021 U.S. DRIVE Highlight

Evaluation of Lightweighting Cost Targets to Provide Affordable, Efficient, and Clean Advanced Light-Duty Vehicles

Vehicle lightweighting target setting support analysis using the ADOPT Model.

National Renewable Energy Laboratory

Advanced lightweighting materials help provide affordable, efficient, and clean advanced light-duty vehicles. The National Renewable Energy Laboratory worked with the U.S. Department of Energy and the U.S. DRIVE Materials Technical Team to help estimate the lightweighting cost targets needed to achieve low-cost energy and emission benefits.

NREL's Automotive Deployment Options Projection Tool (ADOPT) estimated the uptake and benefits of lightweighting. ADOPT is a consumer choice and stock model. It starts simulations with over 700 existing vehicle makes, models, and options to provide realism, captures the outlying characteristics of the best-selling advanced vehicles, and estimates the influence of regulations and incentives. The tool has been extensively validated with historical sales data to ensure confidence in the results. During the simulation, ADOPT optimizes the amount of lightweighting applied to each vehicle to achieve the combination of vehicle price, fuel cost per mile, acceleration, and range that achieves the greatest estimated sales. This analysis evaluated three different lightweighting cost target scenarios including a no program (NP) scenario, technology success – version 1 (TS-1) scenario, and technology success – version 2 (TS-2) scenario. Figure 1 shows the final scenario which provided the greatest benefits.

Figure 2 shows the resulting sales weighted average lightweighting of the three scenarios. The TS-2 scenario achieved the greatest level of lightweighting due to the large amount of lightweighting that stays below $5/kg. It reduces carbon emissions by about 4% compared to the NP scenario from an additional 10% glider mass reduction. The benefit came largely from lightweighting being implemented in the large market segment of lower-price ($20K-$40K) vehicles. For high-price vehicles ($100K-120K), there are little differences due to the low-price sensitivity of those consumers.

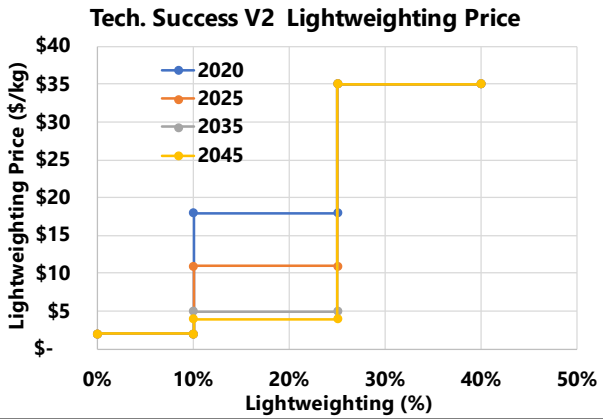

Figure 1. Final lightweighting cost targets by year.

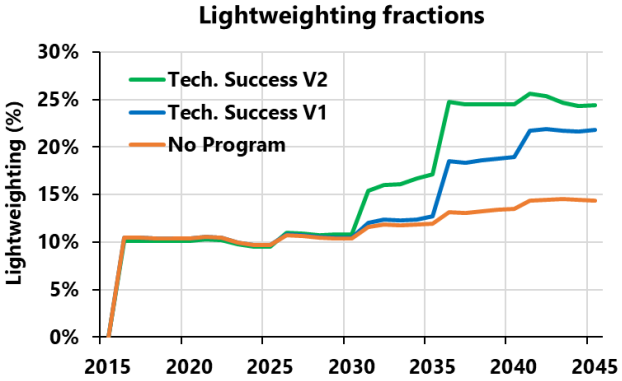

Figure 2. Sales weighted average lightweighting adoption estimates by lightweighting cost target scenario.

2021 U.S. DRIVE Highlight

Machine Learning for Automated Weld Quality Monitoring and Control

Machine-learning based tool to analyze in-line and post-welding data for resistance spot weld quality monitoring and control.

Oak Ridge National Laboratory and Pacific Northwest National Laboratory

Dissimilar material joints made of lightweight materials are in high demand for manufacturing automotive structures due to higher fuel efficiency. However, it is challenging to identify manufacturing conditions needed to synthesize joints with desired performance due to complex interactions between process conditions and material features. It is also difficult to transfer the know-how of joining one set of materials to another set (with different features like plate thicknesses, coatings etc.) due to the many hidden factors that may not be trackable during process development. Adding to the complexity are the several independent process variables that are responsible for developing joint attributes in the material microstructures that lead to joint properties. Machine-learning (ML) methods offer a pathway to identifying the process-structure-property relationships at an accelerated pace. They are helpful in reconciling large streams of data, generated by original equipment manufacturers, in the form of material, process, environment, equipment, microstructural, and performance information. It is desirable for vehicle manufacturers to develop a framework by which the know-how associated with manufacturing one stack-up can be used to reduce the development time for another stack up, instead of starting afresh every time.

This project is demonstrating the application of a suite of ML tools to analyze in-line and post-processed resistance spot welded (RSW) joint data for weld quality monitoring and control (Figure 1). RSW is the process used primarily for welding two or more metal sheets together using pressure and heat from an electric current. Aluminum and steel RSW joint data, provided by an OEM partner, are used in developing complementary ML approaches, namely Deep Neural Networks (DNN) by Oak Ridge National Laboratory and Random Forest models by Pacific Northwest National Laboratory. High-dimensional correlations have been established through recursive learning for RSW dataset of various combinations of aluminum and steel alloys with over 80% accuracy. Using these approaches in a cohesive model, the research team is identifying important process and material factors, as well as joint attributes, that result in joints with desired performance. The ML models have also been used to identify process conditions responsible for highest joint properties, without requiring physics-based process modeling. In addition, they can aid in transferring the process development from one stack up to another and thereby accelerate the development and deployment of new joints in vehicles compared to current industry standards.

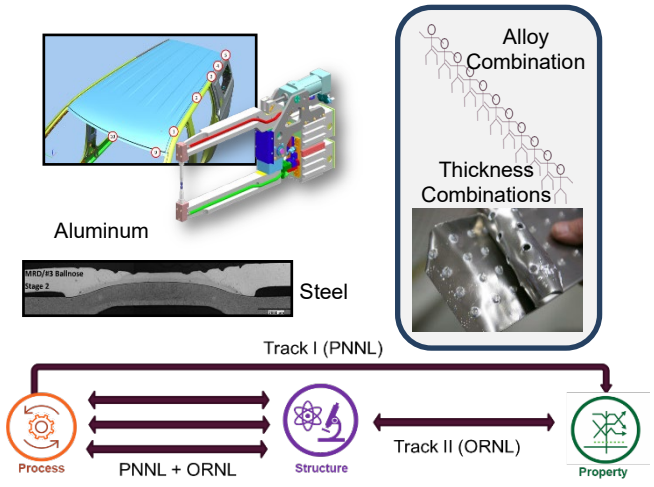

Figure 1. Schematic of process-structure-property correlations made with ML models to identify and transfer RSW manufacturing know-how from one aluminum/steel stack-up to another to reduce new joint development and deployment time.

2021 U.S. DRIVE Highlight

Ultra-Lightweight, Ductile Carbon-Fiber Reinforced Composites

Development of carbon-fiber reinforced lightweight cellular materials for high specific stiffness and damping coefficient.

Oak Ridge National Laboratory and University of California Los Angeles

Traditionally, reducing the mass of structural systems and enhancing the energy dissipation of materials have been the subjects of automotive fields over the years. Carbon fiber reinforced polymer (CFRP) composites are known for their high stiffness-to-weight ratio and hence is of interest in extensive research and industrial uses. Incorporating CFRP in additive manufacturing provides further opportunities for significant weight reduction. However, as with other stiff materials, CFRPs suffer from poor damping and brittleness, limiting their energy dissipation capacity. The aim of the project is to develop a process to produce a novel lightweight cellular CFRP material to achieve simultaneous high stiffness and high damping.

The team is developing a scalable multi-material additive manufacturing technique for carbon fiber reinforced cellular materials with optimized 3D architectures for lightweighting and resilience. The technique can achieve complex 3d topologies with feature sizes smaller than 100 μm while the overall size can be beyond 50 cm, as shown in Figure 1(a). Utilizing this technique, the team developed an ultra-lightweight, ductile, cellular composite composed of a network of complex micro-lattice topologies cells in which a soft material is embedded in stiff CFRP ligaments, as shown in Figure 1(b). The soft phase was embedded within the micro-lattice to increase damping performance—such a new concept allows simultaneously high damping, high stiffness and ultra-lightweight.

The team fabricated composites with various densities and soft phase ratios and tested for mechanical performance evaluation. Figure 1(c) summarizes the mechanical and damping performance of the composites against other existing materials. The orange ellipse highlights the CFRP composites that achieve both high damping performance and specific stiffness compared to other commercial CFRP at an ultra-low density of 50 kg/m^3.

This work demonstrates the feasibility of a novel class of composites printing methods that can be deployed in automotive parts that require lightweight and energy dissipation. Our current work further improves the scalability of parts spanning over three orders of magnitude in feature sizes.

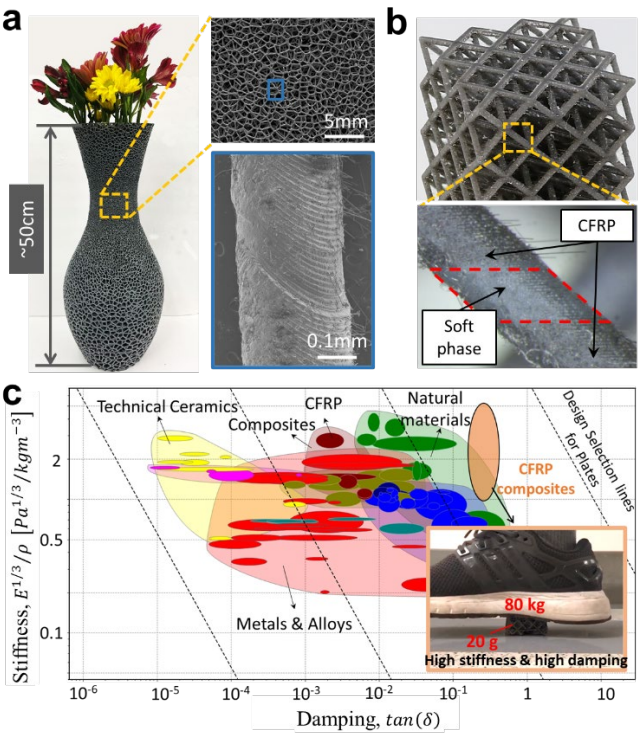

Figure 1. (a) Samples made of CFRP composite. (b) Fabricated ultra-lightweight, ductile CFRP lattices with two phases. (c) Material selection chart for vibration management of plates.

2021 U.S. DRIVE Highlight

A Multi-Scale Computational Platform for Predictive Modeling of Corrosion in Aluminum-Steel Joints

Project to develop modeling techniques using machine learning for prediction of corrosion in multi-material joints.

University of Michigan

The global cost of corrosion was estimated at about 3.4% of the global GDP in 2013. By using available corrosion control practices, it is estimated a saving between 15%-35% of the cost of corrosion. In the U.S., more than $276 billion is spent repairing corrosion damage. Prediction of the corrosion and its impact on performance of the dissimilar material joints is critical for reducing the number of the current corrosion-based recalls for automobiles. Thus, the project goal is to develop models to enable predictive maintenance and end-of-life planning of multi-metal joints with risk of corrosion under different cycling conditions, such as exposure to high temperatures and salt solutions in winter, quantified through its pH.

An academia-industry consortium led by the University of Michigan and including Pennsylvania State University, University of Illinois Urbana-Champaign, University of Georgia, General Motors Company, Livermore Software Technology Corporation, and Optimal Process Technologies, LLC. developed multi-scale models for prediction of corrosion in aluminum-steel joint structures used in vehicle subassemblies such as chassis and transmission systems.

Starting from fundamental calculations, the team developed data-driven mathematical models to predict the inter-metallic phases and micro-constituents formed during joining of two dissimilar materials, for example aluminum and steel—a lightweight multi-material system which is currently used in more than 60% of the vehicles. These models were used for simulating chemical reactions that are produced when the joined metallic components are exposed to high temperatures and different pH values. The team was able to predict how the corrosion nucleates and grows on the metallic components (Figure 1) and how the failure occurs on the car components. The newly developed machine learning algorithms combining Science, Technology, Engineering and Math disciplines, advanced finite element simulation and experimental validations have been integrated in a platform for prediction of the corrosion evolution and prediction the failure of joints under mechanical loadings and fatigue (Figure 2). Moreover, based on machine learning and inverse analysis, the team proposed solutions for designing new metallic alloys less susceptible to corrosion when used in multi-material joints for vehicle assembles.

The team achieved an average of 4% error compared with experiments for the most common joints currently used in vehicle subassemblies.

Figure 1. Machine learning is used for corrosion prediction.

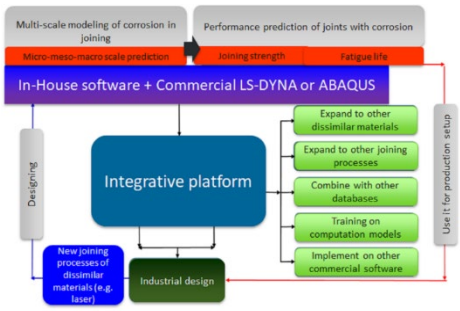

Figure 2. Integrated platform for corrosion prediction and its impact on joining performance over time. In-house software is publicly available.

2021 U.S. DRIVE Highlight

Integrated Computational Materials Engineering (ICME) Predictive Tools for Low-Cost Carbon Fiber

Develop predictive models for low-cost carbon fibers (CF) from molecular fingerprints of feedstocks derived from abundant natural carbon sources, feedstock processing, CF fabrication, and CF properties.

Western Research Institute, Oak Ridge National Laboratory, Massachusetts Institute of Technology, University of Wyoming, Ramaco Carbon, Solvay Composites, and Southern Research Institute

To increase electric vehicle (EV) driving distances and fully realize their environmental and societal benefits, it is necessary to reduce their weight, which can be done by incorporating more lightweight composites for traditional steel body and load bearing components.

This program studied readily available large volume feedstocks from biomass, coal, and petroleum to produce precursors of appropriate qualities that lend themselves to the production of carbon fiber (CF) with the appropriate physical properties and cost to be used in the automotive industry (strength: 250 Ksi, modulus: 25 Msi, strain: 1%, cost: $5/lb). The project developed predictive ICME models that can be used to guide the development of CF from new or blended feedstocks to remove risk from this process. The team integrated feedstock chemical fingerprints, precursor chemical and physical properties, CF fabrication conditions, and CF characterization and properties using machine learning and neural networks to build predictive ICME models. The models were bidirectional from the molecular fingerprint to single filament CF and to tow-level CF properties. Figure 1 shows the developed ICME approach. Mesophase pitch CF precursor and bio-based precursor polyacrylonitrile were converted into CF. Single filament CF and CF tows were characterized and evaluated for their mechanical properties. Scaled-up batches of multi-filament CF from bio-PAN and coal tar pitch mesophase were produced that met the desired DOE goals for strength, modulus, strain, and cost. Predictions of modulus were accurate within the targeted ±15%.

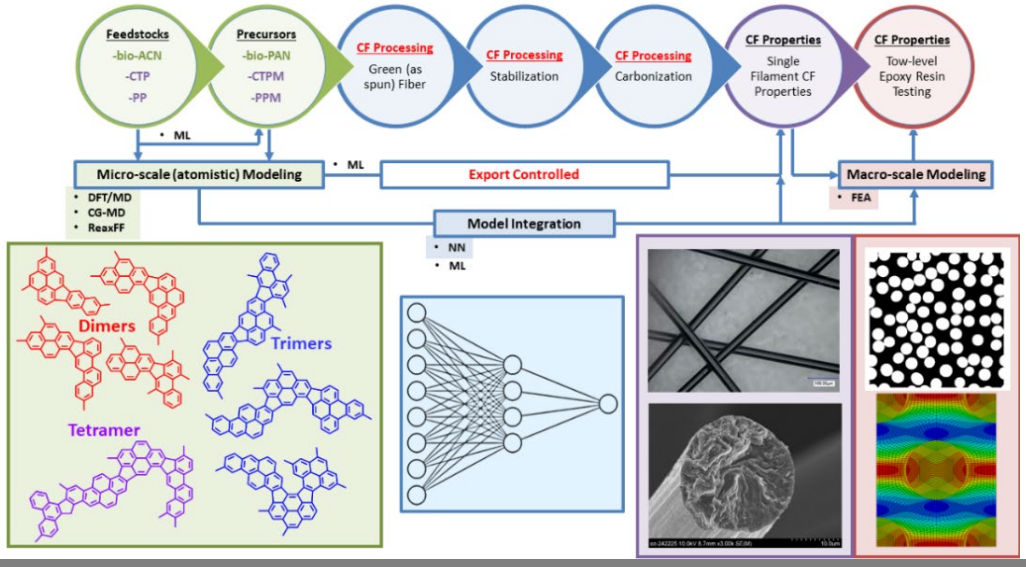

Figure 1. Schematic flow diagram used for generating predictive models for single filament and tow-level CF properties using molecular fingerprints from chemical characterization of feedstocks. The models account for precursor properties and chemistry, CF processing conditions, single filament morphology, and crystalline alignment.

Vehicle and Mobility Systems Analysis

2021 U.S. DRIVE Highlight

Energy Efficient Control of Connected and Automated Vehicles

Energy savings up to 22% demonstrated under real world driving conditions using a custom connected and automated vehicle control system.

Argonne National Laboratory

Connected and automated vehicles (CAVs) use information from on-board sensors and from communications with infrastructure (V2I) and other vehicles (V2V) to calculate their trajectory and speed in a safe and comfortable way. By adding energy efficiency as an objective, we demonstrated an energy consumption reduction of up to 22% in simulation, lab-testing, and track-testing. Researchers implemented control algorithms in vehicles tested on a chassis dynamometer at Argonne National Lab and on track at the American Center for Mobility (ACM). In both cases, the experiments were performed using an XIL ("Anything-in-the-loop") framework, which combines physical systems (e.g., a vehicle under test) with virtual assets (e.g., other vehicles, traffic infrastructure, etc.) in a closed-loop environment. The newly-developed dynamometer-based XIL workflow allows quick and robust transfer of control algorithms from model-based simulation using RoadRunner (ANL's powertrain and driving dynamics system simulator) to XIL experiments. The controls were implemented in an electric vehicle and a conventional internal combustion engine vehicle, in a variety of scenarios (e.g., empty road, car-following, and traffic signal phase and timing [SPaT] communicated via V2I). Figure 1 shows results for empty road scenarios, featuring five different routes with different arrangements of speed limits, traffic lights, and traffic light timing. Results demonstrate that, when SPaT information is communicated via V2I (indicated by "V2I ON"), the CAV saves approximately 10% more energy than in the case with no V2I. The communication range for the SPaT was set to 250m from the signalized intersection.

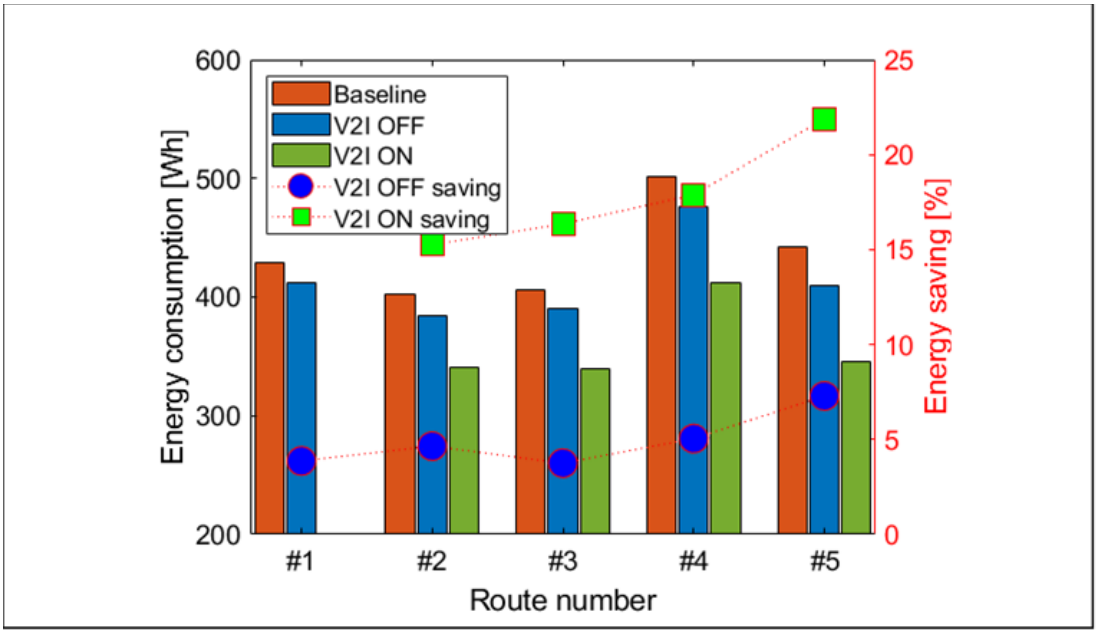

Figure 1. Energy savings for a lead vehicle (GM Bolt) with Argonne-developed eco-driving CAV controls and V2I-enabled eco-approach.

2021 U.S. DRIVE Highlight

Impact of Cooperative Adaptive Cruise Control (CACC)

Quantified the impact of CACC on mobility, energy, emissions, and travel behavior at the transportation system level under multiple market penetration scenarios.

Argonne National Laboratory

Advanced technologies such as connectivity and automation have the ability to not only impact individual vehicle energy consumption but also result in outcomes at the transportation system-level. Indeed, while technologies such as cooperative adaptive cruise control (CACC) may offer smoother acceleration and deceleration, they may also impact overall traffic flow and influence travel behavior.

Researchers considered scenarios with different CACC market penetrations over different timeframes. POLARIS, a high-performance agent-based transportation system simulation framework, was combined with the Autonomie vehicle system simulation tool to estimate the technology impact across multiple metrics including mobility, energy, and emissions.

When only considering the impact of CACC technology itself, average vehicle speed increased due to improved highway throughput while vehicle miles traveled (VMT) was constant, with minimal energy consumption impact. However, when also considering changes in the value of travel time (VOTT), increased VMT leads to more congestion, negatively impacting vehicle fuel economy.

Overall findings:

- Deployment of CACC, even at high penetrations, has only moderate system-wide impact, with average highway travel speeds increasing by 1%-2%
- When considering changes in VOTT due to more productive travel, per capita VMT increases by 4%-6%, leading to an increase in congestion which reduces travel speeds by up to 8% and increases vehicle energy consumption by 6%
- CACC can increase the capacity of the road network, limiting the congestion increase at very high penetrations.

Future research will focus on including additional vehicle and mobility technologies (e.g., considering U.S. DRIVE Tech Targets).

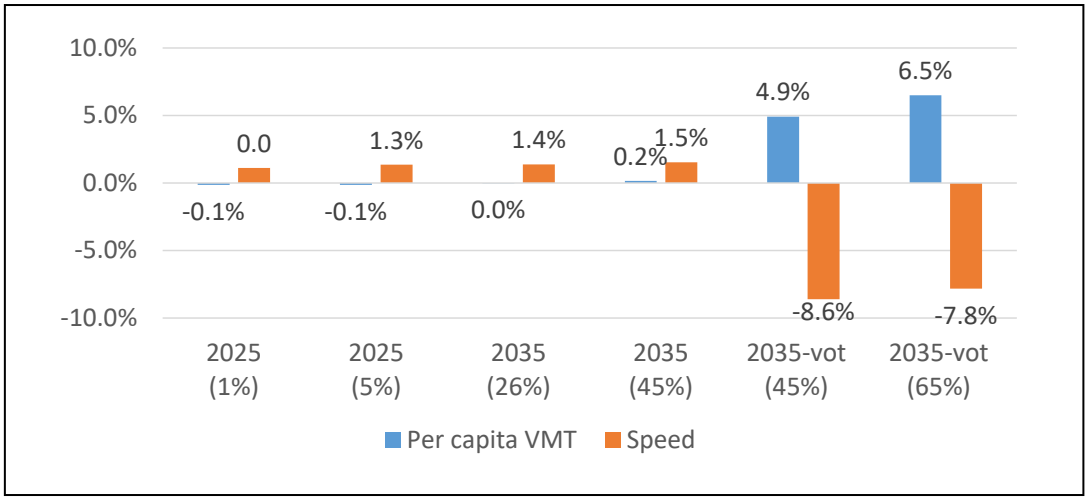

Figure 1. CACC impact on main mobility metrics.

INFRASTRUCTURE AND INTEGRATION

Grid Integration

2021 U.S. DRIVE Highlight

Consequence-Driven Cybersecurity of High-Power EV Charging Prioritizes Mitigation Solutions and Strategies

Evaluating high-consequence events caused by cybersecurity exploits provides a prioritized pathway for developing mitigation solutions to ensure safe and secure high-power EV charging.

Idaho National Laboratory

Cyber-physical security of high-power charging infrastructure for electric vehicles (EVs) is critical to safety, reliability, and consumer confidence in this publicly accessible technology. Cybersecurity vulnerabilities in high-power EV charging infrastructure may present risks to broader transportation and energy-infrastructure systems.

Idaho National Laboratory (INL), Oak Ridge National Laboratory (ORNL), and the National Renewable Energy Laboratory (NREL) in collaboration with ABB Ltd., Tritium Inc., and Electrify America conceptualized, analyzed, prioritized, and evaluated potentially disruptive events caused by cybersecurity exploits of high-power EV charging infrastructure vulnerabilities. The consequence-based framework analysis categorized and prioritized the disruptive events into five categories:

- Safety: injury or loss of life
- Adverse impacts to the electric grid
- Hardware damage
- Denial of service or reduced capacity
- Data theft or alteration.

The team evaluated the 15 highest prioritized events to verify both the impact severity and cybersecurity manipulation complexity of each event in the laboratory using a state-of-the-art extreme fast charger (XFC). The most notable results of the highest prioritized events include:

1. XFC load shed when caused by cybersecurity exploit is very abrupt (4 msec.) as shown in Figure 1. Simulation of the concurrent load shed of fifteen 350kW-XFCs results in electric-grid distribution feeder instability.
2. Cybersecurity manipulation of the CCS liquid-cooled cable thermal management system results in unsafe charge cable temperature.
3. XFC power electronic controls cybersecurity manipulation results in power transfer oscillations to the EV and poor AC power quality at the grid connection.
4. Wireless 'sniffing' data theft from the CCS communications between the EV and the EVSE is possible.

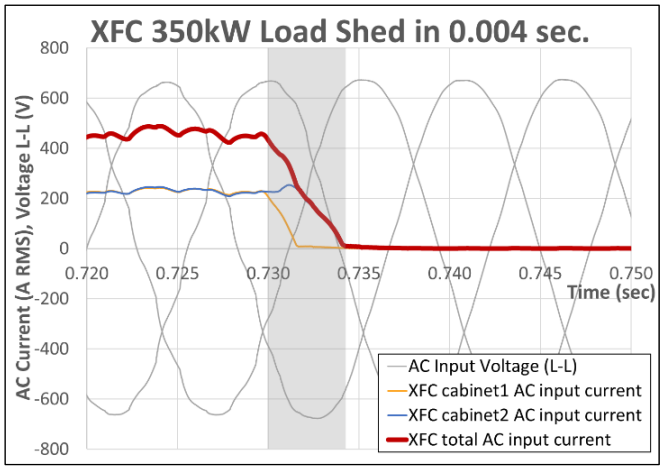

Figure 1. Reduced electric grid feeder stability due to 5MW concurrent load shed of 15 350kW-XFCs at the grid connection initiated by a remote access cybersecurity exploit.

The project team developed mitigation strategies and solutions to identify, protect, and detect the vulnerability cybersecurity exploits resulting in high-consequence events. Recommended mitigation solutions include using secure network communication (examples: SSH, TLS, OCPP2.0), implementing a zero-trust network, and utilizing a stand-alone monitoring safety system to identify anomalies in electrical performance, component temperature, and communication protocols.

An EV Future: Navigating the Transition—DOE Voices of Experience

A DOE initiative to explore and discuss the transition to wide-scale adoption of electric vehicles from different stakeholder perspectives.

Vehicle Technologies Office; and Advanced Grid R&D Division, Office of Electricity

With millions of personal and commercial electric vehicles (EVs) set to hit U.S. roads in the coming decade, the increasing overlap of the transportation and electricity sectors must be addressed now. The growing electrification of the transportation sector has the potential to fundamentally transform how customers fuel vehicles and how goods are transported across the country. Conversations about transitioning to EVs have shifted from "Can we do it?" to "How do we do it?" While on the surface it might seem straightforward—replace petroleum fuel with electricity—the reality is not always so simple and it won't happen overnight.

The U.S. Department of Energy (DOE) has researched EV and charging technologies, as well as grid modernization, for decades. DOE has long understood the importance of peer-to-peer dialogue for uncovering fresh perspectives and enhancing learning, and recognizes the magnitude of change that the adoption and integration of EVs will present for utilities, business, and other stakeholders. In response, the Office of Electricity's Advanced Grid Research and Development (AGR&D) Division, in partnership with the Office of Energy Efficiency and Renewable Energy's Vehicle Technologies Office (VTO), launched *An EV Future: Navigating the Transition* in July 2020. The initiative utilized the Voices of Experience approach that AGR&D had pioneered over a decade ago. The effort brought together diverse transportation and electrification stakeholders to get their perspectives on what the buildout of the EV charging infrastructure and its integration with the electric grid will mean. DOE hosted a series of 33 two-hour virtual meetings covering 15 topics. An industry steering committee provided feedback and input on the scope and topics to ensure alignment with stakeholder needs. High-level topics discussed in the regional calls are shown in Table 1.

Planning	Operations	Business Case
Forecasting	Managing Load	Infrastructure Design
Service Requests	New Technologies	Infrastructure Deployment
Future Requirements	Resilience	Economic Feasibility

Table 1. Topics discussed in regional calls.

Key takeaways include, but are not limited to, the importance of collaboration and need for robust discussions on challenges, including unpredictable EV loads, criticality of charging networks, changes in the utility-customer relationship, and commercial fleet electrification, all while ensuring social equity. More than 3,500 individuals, representing 700 unique entities, registered for the calls, as shown in Figure 1. Participants included utilities, regulatory commissioners and staff, charging network providers, state and local agencies, advocates, university staff, and vendors from not only the U.S. but from 18 other countries. A public report that includes major themes, conversations, and discussions is now available.

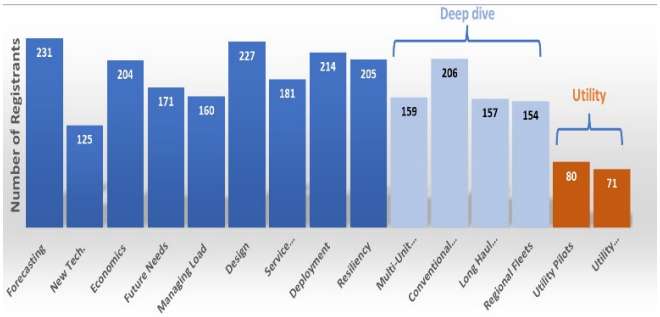

Figure 1. Participation by topic for An EV Future: Navigating the Transition.

2021 U.S. DRIVE Highlight

A DC Meter Benchmark Study to Assess Quality and Availability to Meet Accuracy Compliance of Dispensers

A DOE-Argonne National Laboratory independent assessment of currently available DC meter products that can meet NIST Handbook 44-3.40 accuracy type certification requirements.

Vehicle Technologies Office, Argonne National Laboratory

Argonne National Laboratory (ANL) investigators conducted research to develop and validate a methodology to demonstrate electric vehicle (EV) direct current fast charger (DCFC) compliance with the National Institute of Standards and Technology's (NIST's) Handbook 44 Section 3.40 (HB44-3.40). The primary focus of this research was to determine an accurate approach for equipment manufacturers and charging network operators to comply with HB44-3.40 without incurring unnecessary costs and equipment upgrades. ANL developed a system accuracy calculation method that meets NIST's HB44-3.40 requirements, then conducted benchmark research on components to verify system level accuracy. The study included laboratory testing of representative DC meters and charging cables from low power (non-cooled) to high power (liquid cooled). ANL evaluated DCFC meter accuracy and cable losses to determine the overall accuracy of the energy measurement system and compliance with HB44-3.40.

The benchmarking study included the top 10 candidate meter products that can measure 1,000 volt (V) up to 500A DC at better than 1% tolerance at the point of dispensing (cable end). The comparison of testing results confirmed that electric vehicle supply equipment (EVSE) DCFC manufacturers have sufficient options for meter solutions to meet these criteria. Remote sensing leads in the charging cable can eliminate errors in voltage drop of the charging conductors downstream of the measurement point. Thermal stability and dynamic range accuracy were not in the study scope.

Meters tested in this study are shown in Table 1 and Figure 1. The project team held a web-based meeting with ~100 participants in September 2021 as a forum to disseminate the study results and directly address questions from stakeholders (weights and measures officials, meter and EVSE manufacturers, and charging network operators). The meeting participants reached consensus that there are sufficient manufacturers of DC meters that meet the 1% net accuracy goal, but cost of present models is an issue. Another web-based discussion is planned for 2022 to cover type certification gaps of EVSE including lack of approved certification testing tools.

	Manufacturer	Model
1	AccuEnergy	AcuDC 243
2	EVoke	EUMD6m
3	Isabellenhuette	IEM-DCC
4	LEM	DCMB
5	Lumel	PH30
6	MeasurLogic	DTS DC
7	Porsche Engineering Services	DCEM 100
8	Rish	Alpha EM DC
9	Satec	PM130-PLUS-DC
10	Tritium	integrated DC

Table 1. Benchmarked DC meters in study.

Figure 1. Tested 1000V/350A HB44-3.40 compliant DC meters.

Hydrogen Codes and Standards

2021 U.S. DRIVE Highlight

Empirically Based Design Curves Lead to Increased Design Life of Stationary Hydrogen Pressure Vessels

Design life improved 3 times by using design curves recently published in ASME Code Case 2938.

Sandia National Laboratories

A recently published DOE Hydrogen Program Record[1] demonstrated that using design curves enables approximately three times longer design life of typical hydrogen storage vessels compared to the previous design basis, resulting in reduced costs associated with pressure vessel lifetimes and allowing for a harmonized approach to design life. Fatigue crack growth rate design curves were developed at Sandia National Laboratories and accepted into ASME Section VIII Division 3 Code Case 2938 in December 2018. The design curves are for steels used in high-pressure hydrogen storage vessels (e.g., Type 1 and 2) commonly installed at hydrogen refueling stations (HRS).

The ASME code used for hydrogen pressure vessel design (Article KD-10) requires extensive fatigue crack growth testing in gaseous hydrogen, which is extremely expensive and challenging. Figure 1 shows fatigue crack growth rate curves measured in 103 MPa hydrogen gas for pressure vessel steels commonly used at HRS. Fatigue crack growth rate is defined as the crack growth per cycle (da/dN) and increases as a function of stress intensity factor range (ΔK), which is a fracture mechanics parameter representing stress range, size, and geometry of a crack. ΔK is transferrable between laboratory tests and engineered structures. Typically, ΔK is greater for a larger crack; thus, as a crack grows, ΔK increases, and the rate of fatigue crack growth also increases.

Prior to Code Case 2938, only one steel alloy (SA-372) had publicly accessible design data that satisfied KD-10, and data were limited to ΔK>10 MPa $m^{1/2}$. This resulted in the design basis following the extrapolated (dashed) line in Figure 1. Sandia tested a variety of pressure vessel steels over a broader range of ΔK and found common performance among the tested steels. Additionally, a distinct 'knee' was observed, which represents a transition point to significantly lower crack growth rates than the extrapolated trend. The Code Case 2938 design curve (solid line) was extracted from these results as an upper-bound design basis for pressure vessel design. The newly identified difference between the extrapolated (dashed) curve and the design curve (solid) results in significantly longer design life. Extended design life will depend on specific design and operation of the vessel, but one case study showed nearly 3 times increase in design life. In this case study, the vessels were retired after 7 years due to reaching cycle limit; however, if new design curves were used the vessels could have remained in operation up to 20 years, resulting in lower capital costs for the HRS.

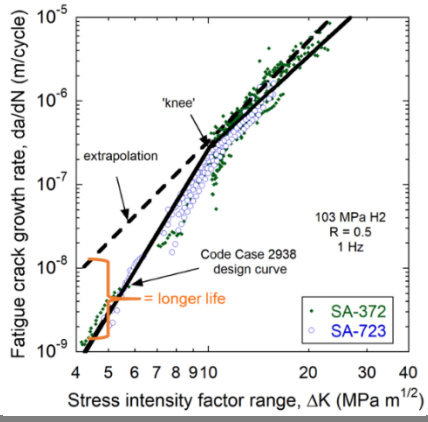

Figure 1. Fatigue crack growth rate curves for pressure vessel steels tested in high-pressure hydrogen gas. Dashed line represents previous design curve which required extrapolation to low DK. Solid line is new Code Case 2938 design curve, which better represents the data and results in lower da/dN values equating to longer pressure vessel life.

[1] https://www.hydrogen.energy.gov/pdfs/21004-increased-life-pressure-vessel-tanks.pdf.

Hydrogen Delivery and Storage

2021 U.S. DRIVE Highlight

Liquid Storage of Hydrogen Extends Range of Heavy-Duty Trucks

Tanks could be 1/3 smaller and 75% lighter than current compressed gas tanks.

Argonne National Laboratory, Sandia National Laboratories, Lawrence Livermore National Laboratory, and Strategic Analysis

Liquid hydrogen (LH_2) storage systems offer 1.3 times higher storage densities, smaller storage footprints, and faster refueling rates compared to gaseous hydrogen storage. A viable system design for LH_2 storage onboard medium- and heavy-duty (MD/HD) trucks has been developed that will enable progress towards DOE's Class 8 truck targets. This is critical because MD/HD trucks require 5 to 10 times more hydrogen be stored onboard compared to light-duty fuel cell electric vehicles on the road today.

A team of analysts from Argonne National Laboratory, Sandia National Laboratories, Lawrence Livermore National Laboratory, and Strategic Analysis established vehicle duty cycles and LH_2 storage system requirements for three types of MD/HD trucks. The team analyzed pivotal characteristics such as the performance and dormancy time without hydrogen boil-off of the Type 1 vacuum-insulated cryogenic vessels for various LH_2 tank design options. Analysis results recommend a dormancy time of 1 to 3 days, with a usable hydrogen density of 45-60 g/L.

The resultant baseline design provides a starting point for LH_2 tank development. It entails two frame-mounted tanks and a low-pressure onboard pump. The onboard pump enables higher usable hydrogen storage densities. Operating pressure is kept low at 5 bar. The storage system has a 1-day, no-loss dormancy with 82 kg of usable hydrogen stored onboard.

Gravimetric and volumetric capacities are 17.7 wt.% and 37.1 g/L, respectively (Figure 1). These capacities clearly outperform those of state-of-the-art 700 bar gaseous hydrogen storage tanks, which currently achieve gravimetric and volumetric capacities of 5.7 wt% and 27.7 g/L, respectively.

Structural and safety analyses identified critical design components within the storage system, such as the tank liner and shell, and pressure relief devices. Additionally, refueling and discharge simulations revealed the amount of hydrogen returned to the station during refueling and the heat supplied during discharge. Main system cost drivers include the balance of plant components and storage tank insulation.

Future work will focus on further improvements to cost and capacities and incorporating analysis of refueling interfaces. This work demonstrates the feasibility of onboard LH_2 storage for MD/HD trucks and provides the foundation for the development of storage systems with capacities that can meet or exceed the DOE storage targets.

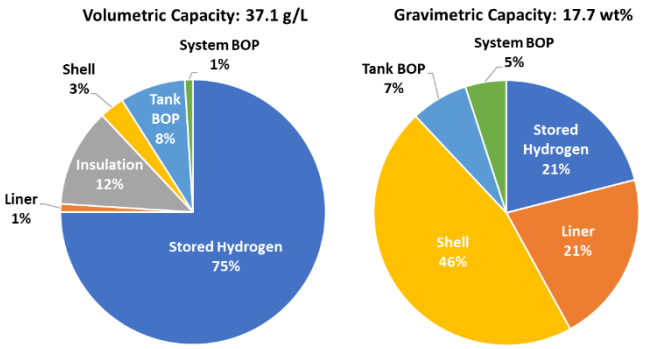

Figure 1. LH_2 storage system volume and weight distributions. System details: Onboard pump, 1-day no loss dormancy, 94.6 kg hydrogen stored, 82 kg usable hydrogen.

2021 U.S. DRIVE Highlight

Innovating High Throughput Hydrogen Stations

Hydrogen testing and research facility for heavy-duty vehicle high-flow fueling evaluations.

National Renewable Energy Laboratory, Air Liquide, Shell, Toyota, and Honda

A high-flow hydrogen fueling testing and research facility has been established at the National Renewable Energy Laboratory (NREL) in Golden, Colorado. High-flow rate hydrogen fueling is essential for enabling the adoption of heavy-duty fuel cell electric trucks, which in turn will contribute to the decarbonization of the on-road vehicle transportation sector.

High-flow fueling data generated at this first-of-its-kind facility will enable timely development of fueling protocols and standards, which currently do not exist. Data gathered will also inform the design of needed technologies as well as help validate publicly available fueling models to drive further advancement in technology development.

A team led by NREL completed construction of the facility, leveraging comprehensive modeling tools (CFD, H2FillS, etc.) and existing hydrogen infrastructure at the site. The station is comprised of a heavy-duty research dispenser, heavy-duty vehicle storage simulator, high-capacity hydrogen chiller system, and 665 kg of bulk gas hydrogen storage. At the design conditions (700 bar at -40°C), the facility can transfer precooled pressurized hydrogen gas at an average flow rate of 10 kg/min (20 kg/min peak), which is sufficient to fill a heavy-duty truck in six minutes for a range of 750 miles. In comparison, light-duty fuel cell electric vehicles typically fuel at an average flow rate of 1 kg/min with five-minute fueling times.

The facility will serve as a test bed for heavy-duty fueling technology and protocols development as well as validation. A key feature of the facility is an environmental chamber for the vehicle storage simulator which enables simulation and study of seasonal and location-related temperature ranges for the filling process. The equipment is configurable to explore a wide range of fueling scenarios through the ability to vary hydrogen pre-cooling temperatures, vehicle storage capacities, hydrogen mass flow rates, and vehicle storage simulator pressure ramp rates. The station also allows for hydrogen gas recirculation which increases system up time and cost savings.

Researchers at NREL will be among the first to demonstrate the viability of high-flow-rate hydrogen fueling. The outcomes of the project will be made publicly available, including tools and data for the benefit of hydrogen stakeholders. The project also established an industry and laboratory partnership for future research needs.

The Innovating High Throughput Hydrogen Stations project is a Cooperative Research and Development Agreement co-funded by the U.S. Department of Energy's Office of Energy Efficiency and Renewable Energy, Hydrogen and Fuel Cell Technologies Office, along with a stakeholder base that informed station development to ensure relevance to industry. Stakeholders include Air Liquide, Honda R&D Americas, Shell, and Toyota.

Figure 1. The new heavy-duty hydrogen station at the NREL Energy Systems and Integration Facility in Golden, Colorado.

Hydrogen Production

2021 U.S. DRIVE Highlight

HydroGEN Benchmarking: Developing Best Practices for Water Splitting Technologies

Project team set to publish 30 protocols for hydrogen production best practices available to stakeholders in early 2022.

Hydrogen and Fuel Cell Technologies Office, and Nel Hydrogen

The HydroGEN Benchmarking project is set to publish over 30 protocols after conducting extensive engagement with stakeholders, making them publicly available to the water splitting community. These protocols detail the best practices for producing hydrogen from the four advanced water splitting pathways.

The goal of this benchmarking work is to create a comprehensive Best Practices framework at the materials, component, device, and system levels for advanced water splitting technologies. All advanced water splitting pathways covered under the HydroGEN Energy Materials Network (EMN) Consortium, which include advanced high-temperature electrolysis, low-temperature electrolysis (LTE), photoelectrochemical water splitting, and solar thermochemical hydrogen, need these best practices to advance materials discovery. This effort will help chart a path to the Hydrogen Energy Earthshot of $1/kg by 2031.

Protocol	Component
Compressibility of GDLs for Water Electrolyzers	GDL
PEM Ion Exchange Capacity	PEM
PEM Thermal Stability	PEM
AEM Conductivity	AEM
AEM Ion Exchange Capacity	AEM
Gas Permeability	AEM/PEM
Rotating Disk Electrode	PGM
3-Electrode Cell for Screening OER/HER Electrocatalysts Activity	Non-PGM
Electrical Conductivity of PGM-free OER Catalysts	Non-PGM
Resistance measurements and water properties	PTL
Comparison Metrics and Terms for LTE	General
Water Uptake Measurement	PEM/AEM
Develop standard post mortem analysis	General
Alkaline Stabililty of AEM	AEM
AEM Oxidation resistance protocol	AEM
Sub-Scale Test Protocol	PEM
AEM Creep rate protocol	AEM

Table 1. Protocols for LTE with associated component with completed (green) and draft (white).

Table 1. shows the protocols for LTE and the associated components which covers Alkaline Exchange Membrane (AEM) and Proton Exchange Membrane (PEM). The benchmarking team drove development of the protocols through a series of workshops, with the third workshop held virtually on 3/1/2021 with over 200 attendees from 15 countries. Reports form the workshops are available to the public on the HydroGEN DataHub, https://datahub.h2awsm.org/dataset/2021-water-splitting-technologies-benchmarking-and-protocols-workshop.

Protocols provide clear work instructions and include practical advice to ensure consistent results. This is critical for developing material standards, assessing existing capabilities, and identifying needs to accelerate R&D. Publication of the protocols will be under the Research Topic, Advanced Water Splitting Technologies Development: Best Practices and Protocols in the journal of Frontiers in Energy Research.[2] The community will stay involved even after publication, editing and updating the protocols to stay relevant over time.

In addition to the protocols, the benchmarking team has led the development of a water splitting roadmap across the different technologies, based on the varying maturity levels and challenges of each approach. The roadmaps drive new development, track progress against U.S. Department of Energy targets, and to set global priorities for advanced water splitting hydrogen research.

[2] https://www.frontiersin.org/research-topics/16823.

2021 U.S. DRIVE Highlight

H2NEW Consortium: Hydrogen from Next-Generation Electrolyzers of Water

Nine national laboratories work together in the H2NEW consortium to make large-scale (MW-scale) manufactured electrolyzers more durable, efficient, and affordable.

Lab Leads: National Renewable Energy Laboratory and Idaho National Laboratory

DOE's newly established H2NEW consortium[3] will play a critical role in achieving the DOE Hydrogen Energy Earthshot target for clean hydrogen (H_2) production of $1/kg hydrogen ($H_2$) by 2030.[4] Electrolyzers produce clean H_2 when paired with renewable electricity, and megawatt-scale electrolyzer installations are becoming increasingly commonplace with 3 GW of new capacity projected for 2022.[5] Recent technoeconomic analysis demonstrates that capital cost, system efficiency, and durability remain major hurdles to cost reduction and subsequent widespread adoption.[6]

H2NEW is addressing components, materials integration, and manufacturing R&D hurdles to enable manufacturable electrolyzers that meet capital cost, efficiency, and durability targets simultaneously (Table 1). In conjunction with DOE's Hydrogen and Fuel Cell Technologies Office (HFTO), H2NEW established technical targets for both low- and high-temperature electrolyzers (LTE and HTE) to achieve an interim cost target of $2/kg by 2026. H2NEW collaborates with academic researchers, including those with access to advanced characterization tools, and solicits regular feedback from an advisory board of industrial representatives to ensure the consortia follows the most impactful R&D path.

H2NEW Electrolyzer Stack Goals by 2025		
Metric	LTE	HTE
Capital Cost	$100/kW	$100/kW
Electrical Efficiency (Lower Heating Value)	70% at 3 A/cm^2	98% at 1.5 A/cm^2
Lifetime	80,000 h	60,000 h

Table 1. H2NEW goals for 2025.

The accurate and reproducible characterization of electrolyzer performance within H2NEW as well as within the entire LTE community is essential for accelerating R&D progress. Towards that goal, the consortium is establishing diagnostics tools such as developing methods to quantify the interfacial contact resistance between materials in LTE systems (Figure 1). This specific technique will allow the team to correlate differences in electrolyzer performance with through-plane conductivity.

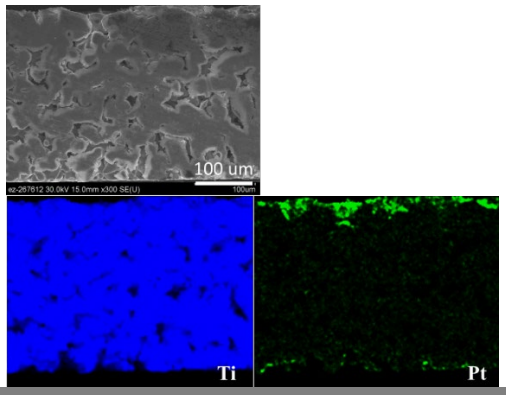

Figure 1. Scanning electron microscopy cross-sectional image of platinum (Pt)-coated porous transport layer (PTL) with titanium (blue) and Pt (green) spectrum resolving depth & distribution of Pt on PTLs.

H2NEW is also leveraging lessons learned from the photovoltaic/semiconductor industry's fabrication development to mitigate electrical contact degradation that can significantly impact the durability of HTE systems. Through extensive collaboration across nine national laboratories, H2NEW is tackling the critical technical RD&D barriers for LTE and HTE technologies that will accelerate commercial deployment.

[3] https://h2new.energy.gov/
[4] https://www.energy.gov/eere/fuelcells/hydrogen-shot
[5] "Global Hydrogen Review 2021." IEA, 2021.
[6] https://www.hydrogen.energy.gov/pdfs/19009_h2_production_cost_pem_electrolysis_2019.pdf

Integrated Systems Analysis

2021 U.S. DRIVE Highlight

Comparative Cost Metric Facilitates Comparison Across Potential Future Advanced Vehicle Technologies

The Comparative Cost Metric combines vehicle cost reduction and efficiency improvement considerations.

Integrated Systems Analysis Technical Team

The U.S. DRIVE portfolio of advanced automotive and infrastructure technologies includes a range of promising pathways, from electrification to hydrogen and net-zero carbon fuels. These advanced technologies are intended eventually to offer American consumers benefits in the form of reduced initial vehicle technology cost at the point of purchase as well as lower operating costs over the vehicle lifetime. To bring these potential benefits together in one straightforward metric, the Integrated Systems Analysis Technical Team (ISATT) defined the Comparative Cost Metric, CCM, as incremental initial vehicle retail price, RPE_{Incr}, equivalent cost plus the net present value of three years of fuel costs, $NPV_3(Fuel)$:

$$CCM = RPE_{Incr} + NPV_3(Fuel)$$

Figure 1 provides an illustrative application of the CCM over time.

In coordination with subject matter technical experts from other tech teams in the U.S. DRIVE Partnership, ISATT coordinated estimates about future potential ranges of component-level vehicle technology cost and performance (for example, batteries, electric-drive systems, fuel cells, hydrogen storage, advanced combustion, and advanced lightweight materials). These estimates, in turn, informed a series of vehicle-level simulations conducted by Argonne National Laboratory that combined ranges of component-level estimates into synthetic future vehicles and possible ranges of vehicle-level costs and efficiencies.

To contextualize modeling and simulation results, Argonne National Laboratory developed the BEAN (BEnefit ANalysis)[7] tool to organize a set of thousands of sensitivity cases on key parameters (for example, oil price scenarios, electricity price scenarios, hydrogen cost scenarios, vehicle miles traveled, consumer expectations regarding payback period, discount rate, and technology progress, among others) meant to inform Partnership-internal discussions about advanced technology trajectories.

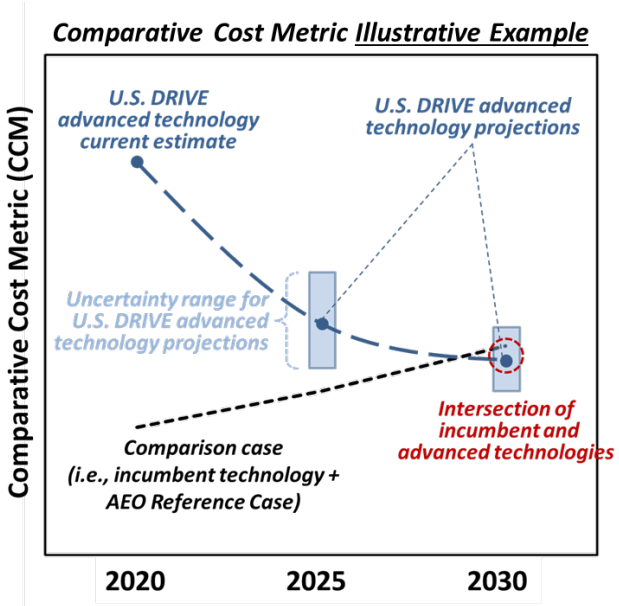

Figure 1. Illustrative example of Comparative Cost Metric application. Advanced technology cost (initial incremental vehicle purchase plus three years of fuel expenditure) estimates, including ranges of uncertainty, declining over time to the point of intersection with incumbent technology in approximately 2030.

7 More information on the BEAN tool is available at https://vms.es.anl.gov/tools/bean/.

2021 U.S. DRIVE Highlight

Electrified Vehicles Deliver Large Reductions in gCO_{2e}/mile Greenhouse Gas Emissions

A cradle-to-grave greenhouse gas emission analysis of conventional and electrified light-duty vehicles.

Integrated Systems Analysis Technical Team

A comprehensive lifecycle analysis (LCA), or cradle-to-grave (C2G) analysis, has been performed of the greenhouse gas (GHG) emissions of a variety of vehicle-fuel pathways. The C2G analysis spans a full portfolio of midsize-sedan and small SUV light-duty vehicles (LDVs), including conventional internal combustion engine vehicles (ICEVs), hybrid electric vehicles (HEVs), plug-in hybrid electric vehicles (PHEVs), battery electric vehicles (BEVs), and fuel cell electric vehicles (FCEVs). In evaluating the vehicle-fuel combinations, the study considered both a "CURRENT TECHNOLOGY" case (nominally 2020) and a high-volume "FUTURE TECHNOLOGY" lower-carbon case (nominally 2030–2035).

The study considered emissions associated with both the fuel cycle and vehicle production cycle. Researchers carried out the C2G GHG emissions assessment by expanding and modifying the GREET® model suite with inputs from industrial experts. The team estimated vehicle fuel economies and component sizes using the Autonomie Model. U.S. grid average generation mixes were taken from the Energy Information Agency's 2021 Annual Energy Outlook.

Four types of plug-in vehicles were included: all-electric vehicles with ranges of 200 mi (BEV200), 300 mi (BEV300) and 400 mi (BEV400), and a plug-in hybrid electric vehicle with a charge-depleting range of 50 mi (PHEV50).

Results for small SUVs are shown in Figure 1. The black lines are the C2G GHG emissions for the CURRENT TECHNOLOGY case. For this case, conventional gasoline ICEVs are modeled to have C2G GHG emissions of about 430 g CO_2e/mile (grams of CO_2 equivalent per mile) while BEV300 have about 210 g CO_2e/mile. The red lines show that lower GHG emissions can be realized in the FUTURE TECHNOLOGY case across all vehicle platforms due to vehicle efficiency gains, such as lightweighting and higher powertrain efficiency. Such improvements lead to C2G GHG emissions of about 320 g CO_2e/mi for gasoline ICEVs and 150 g CO_2e/mi for the BEV300. Combining vehicle efficiency gains with low-carbon fuels, the GHG reductions (grey lines) are generally more than double compared to vehicle efficiency gains alone. The blue bars show emissions from vehicle production.

Comparison of the ICEV data on the left in the figure with the HEV, PHEV, FCEV, and BEV data shows the substantial reductions in GHG emissions delivered by electrified vehicles.

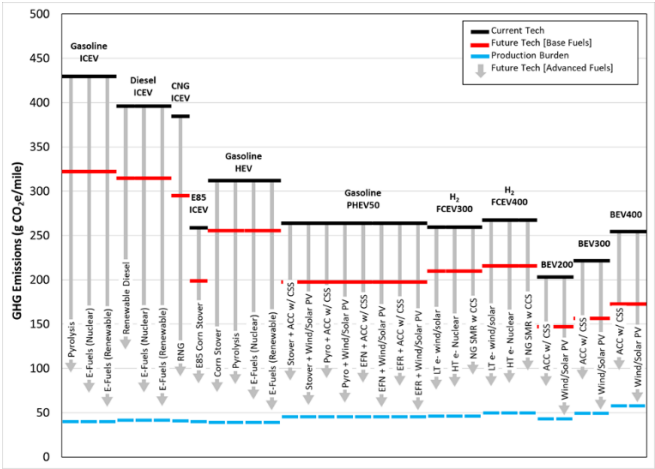

Figure 1. Cradle-to-grave GHG emissions for small SUVs. The horizontal black lines are emissions from current (2020) vehicles. Red lines are emissions assuming future (2030-2035) vehicle efficiency gains. The vertical gray arrows show GHG emissions mitigation for future vehicles and advanced fuels. The blue lines show the vehicle production emissions.

Net-Zero Carbon Fuels

2021 U.S. DRIVE Highlight

Assessing Pathways for Producing Carbon-Neutral Fuels

Understanding the carbon intensity implications of several fuel pathways optimized to minimize GHG production through complimentary life-cycle assessments (LCA) and technoeconomic analyses.

Argonne, Lawrence Livermore, National Renewable Energy, and Pacific Northwest National Laboratory

Researchers at the national labs evaluated several pathways for their potential to produce "net-zero carbon" fuels. These pathways were optimized for reducing carbon intensity (CI) and their economics were assessed to understand the associated cost of carbon mitigation. The team investigated several advanced carbon management strategies for their potential to lower the CI of fuels and to understand their implementation costs. Researchers selected six unique fuel pathways for scrutiny to discern their costs and benefits and their ability to provide net-zero carbon fuels. The results from one pathway are discussed here.

In Year 1, one of the most viable near-term pathways to a net-zero liquid fuel was the conversion of corn starch to ethanol with carbon capture and sequestration (CCS) of the fermentation off-gas while also implementing additional carbon mitigation strategies, such as renewable electricity and renewable natural gas (RNG) for process energy/heat and leveraging fertilizer made with clean hydrogen. In Year 2, this pathway was extended to support the production of drop-in fuels (jet fuel) via alcohol-to-jet (ATJ) conversion, which includes alcohol dehydration, oligomerization, and hydrogenation. In addition to extending the Year 1 pathway via ATJ, the researchers also analyzed the cost/benefit of using clean H_2 for hydrotreating as well as sequestering waste CO_2 versus electrocatalytically converting it to CO for fermentation to ethanol and reentry into the ATJ process.

The figure below represents the LCA of the ATJ process with no mitigation of the fermentation gas (yellow), with CCS (green), and where the carbon is captured and utilized (CCU) to make additional fuel (blue). Each scenario has five separate bars representing additional carbon mitigation strategies in place, with their resulting CI in black and minimum selling fuel price (MFSP) in red. This information provides a first step to quantitatively assess different ways to lower the CI of drop-in fuel. An in-depth analysis of this pathway and several alternatives can be found in the upcoming FY21 Net-Zero Technical Team Analysis Summary Report.

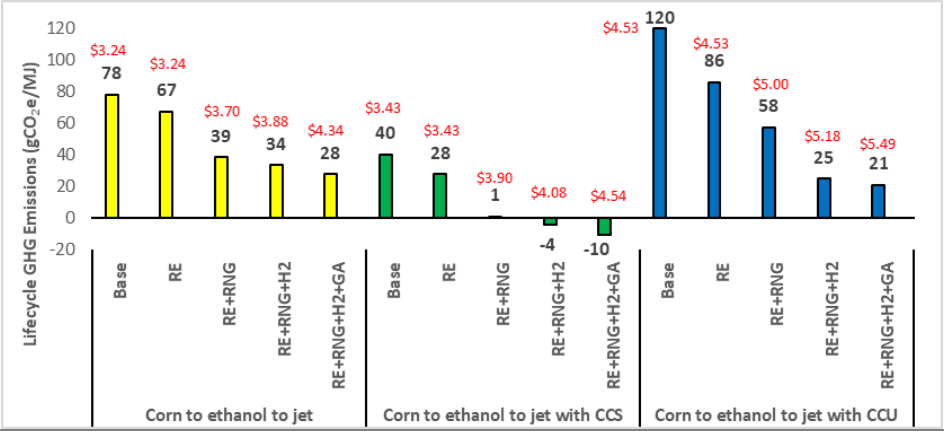

Figure 1. Lifecycle GHG emissions associated with generating fuel with multiple mitigation strategies in place. For reference, fossil jet fuel = 85 gCO2e/MJ. RE = renewable electricity, RNG = renewable natural gas, H2 = clean hydrogen, GA = green ammonia.